

UN

CLASSIFIED

190

ASSIFIED

190

Reproduced

Technical Information Agency

STATION, ARLINGTON 12 VIRGINIA

NOTICE:  
OTHER  
WITH A  
THE U.  
OBLIGAT  
STATE FO  
DRAWING  
IMPERIAL  
OR ANY  
PUBLIS  
THAT H

NT OR OTHER DRAWINGS, SPECIFICATIONS OR  
ANY PURPOSE OTHER THAN IN CONNECTION  
GOVERNMENT PROCUREMENT OPERATION,  
EREDY INCURE NO RESPONSIBILITY, NOR ANY  
AND THE FACT THAT THE GOVERNMENT MAY  
SHED, OR IN ANY WAY SUPPLIED THE SAID  
I, OR OTHER DATA IS NOT TO BE REGARDED BY  
E AS IN ANY MANNER LICENSING THE HOLDER  
CORPORATION, OR CONVEYING ANY RIGHTS OR  
ORE, USE OR SELL ANY PATENTED INVENTION  
RELATED THERETO.

UN

ASSIFIED

AD NO. 561-0

ASTIA FILE COPY

EXPERIMENTAL INVESTIGATION OF THE PRESSURE DISTRIBUTION ON  
XI - SYMMETRIC FLAT - FACE CONE - TYPE BODIES AT SUPERSONIC AND  
HYPERSONIC SPEEDS

1 OCTOBER 1957



**U. S. NAVAL ORDNANCE LABORATORY**  
**WHITE OAK, MARYLAND**

Aerodynamics Research Report 3

EXPERIMENTAL INVESTIGATION OF THE PRESSURE DISTRIBUTION ON  
AXI-SYMMETRIC FLAT-FACE CONE-TYPE BODIES AT SUPERSONIC AND  
HYPERSONIC SPEEDS

Prepared by:

S. M. Hastings  
J. Persh  
E. J. Redman

ABSTRACT: An extensive systematic experimental investigation of the pressure distribution on blunt body shapes at supersonic and hypersonic speeds is in progress ~~at the Naval Ordnance Laboratory~~. This report contains the results obtained from the initial phase of this investigation. The experimental wind tunnel results ~~reported herein~~ are for six variations on a general truncated cone-type body shape. The data cover a Mach number range from about 1.75 to 8.00 for bodies with 2-inch and 5-inch base diameters. Also included ~~herein~~ are typical schlieren and shadow photographs obtained for a number of the body shapes. In addition, shadow graphs and aerodynamic drag data were obtained for a single configuration in the ~~Naval Ordnance~~ Laboratory Pressurized Range.

NCL

U. S. NAVAL ORDNANCE LABORATORY  
WHITE OAK, MARYLAND

1 OCTOBER 1957

For ballistic missile application the axi-symmetric truncated cone-type body configuration is of particular interest because of its attractiveness from the standpoint of heat transfer and aerodynamic stability.

Because of the current deep interest in the above body shapes and because there are no adequate analytical means presently available for accurately predicting the pressure distribution along the contour, the present experimental investigation has been conducted as part of the over-all program on blunt bodies.

This work was sponsored by the U. S. Navy Bureau of Ordnance and the U. S. Air Force and was performed under Task Numbers NO 562-825/51014/01 and NOL-291. The authors are indebted to Mr. I. Korobkin and Dr. R. K. Lobb for their encouragement and continued interest during the course of the investigation.

This project was a joint effort conducted within the Aeroballistic Research Department at the Naval Ordnance Laboratory. The assistance and cooperation of Messrs. W. R. Witt, L. Pasiuk, H. Honecker, A. J. Chones, and Miss A. Chamberlain, is gratefully acknowledged.

WILLIAM W. WILBOURNE  
Captain, USN  
Commander

R. KENNETH LOBB  
By direction

## CONTENTS

	Page
Introduction . . . . .	1
Models and Facilities. . . . .	1
Selection of Model Configuration . . . . .	1
Facilities Used for Tests. . . . .	2
Results and Discussion . . . . .	2
Pressure Distributions, $\epsilon = 0^\circ$ . . . . .	2
Pressure Distributions, $\epsilon \neq 0^\circ$ . . . . .	4
Effect of Roughness. . . . .	5
Pressurized Ballistic Range Results. . . . .	6
Concluding Remarks . . . . .	6
References . . . . .	8
Appendix I . . . . .	9
Table I. . . . .	10

ILLUSTRATIONS

- Figure 1 The variation of  $Re_\theta$  along the contour of Body #1 ( $M = 4.84$ ) as calculated by using both the pressure distribution calculated from the modified Newtonian concept and that determined experimentally.
- Figure 2 The static pressure distribution on Body #1 at  $M = 4.84, \epsilon = 0^\circ$
- Figure 2a Shadowgraph of Body #1 at  $M = 4.84, \epsilon = 0^\circ$
- Figure 3 The static pressure distribution on Body #1 at  $M = 4.12, \epsilon = 0^\circ$
- Figure 3a Shadowgraph of Body #1 at  $M = 4.12, \epsilon = 0^\circ$
- Figure 4 The static pressure distribution on Body #2 at  $M = 4.84, \epsilon = 0^\circ$
- Figure 4a Shadowgraph of Body #2 at  $M = 4.84, \epsilon = 0^\circ$
- Figure 5 The static pressure distribution on Body #2 at  $M = 4.12, \epsilon = 0^\circ$
- Figure 5a Shadowgraph of Body #2 at  $M = 4.12, \epsilon = 0^\circ$
- Figure 6 The static pressure distribution on Body #2 at  $M = 2.88, \epsilon = 0^\circ$
- Figure 6a Shadowgraph of Body #2 at  $M = 2.88, \epsilon = 0^\circ$
- Figure 7 The static pressure distribution on Body #2 at  $M = 1.79, \epsilon = 0^\circ$
- Figure 7a Shadowgraph of Body #2 at  $M = 1.79, \epsilon = 0^\circ$
- Figure 8 The static pressure distribution on Body #3 at  $M = 4.84, \epsilon = 0^\circ$
- Figure 8a Schlieren photograph of Body #3 at  $M = 4.84, \epsilon = 0^\circ$
- Figure 9 The static pressure distribution on Body #3 at  $M = 4.12, \epsilon = 0^\circ$
- Figure 9a Shadowgraph of Body #3 at  $M = 4.12, \epsilon = 0^\circ$
- Figure 10 The static pressure distribution on Body #3 at  $M = 2.88, \epsilon = 0^\circ$
- Figure 10a Shadowgraph of Body #3 at  $M = 2.88, \epsilon = 0^\circ$
- Figure 11 The static pressure distribution on Body #3 at  $M = 1.79, \epsilon = 0^\circ$
- Figure 11a Shadowgraph of Body #3 at  $M = 1.79, \epsilon = 0^\circ$
- Figure 12 The static pressure distribution on Body #4 at  $M = 4.84, \epsilon = 0^\circ$
- Figure 12a Schlieren photograph of Body #4 at  $M = 4.84, \epsilon = 0^\circ$
- Figure 13 The static pressure distribution on Body #4 at  $M = 4.12, \epsilon = 0^\circ$
- Figure 13a Shadowgraph of Body #4 at  $M = 4.12, \epsilon = 0^\circ$
- Figure 14 The static pressure distribution on Body #4 at  $M = 2.88, \epsilon = 0^\circ$
- Figure 14a Shadowgraph of Body #4 at  $M = 2.88, \epsilon = 0^\circ$
- Figure 15 The static pressure distribution on Body #4 at  $M = 1.79, \epsilon = 0^\circ$
- Figure 15a Schlieren photograph of Body #4 at  $M = 1.79, \epsilon = 0^\circ$
- Figure 16 The static pressure distribution on Body #5 at  $M = 4.84, \epsilon = 0^\circ$

- Figure 16a Schlieren photograph of Body #5 at  $M = 4.84$ ,  $\epsilon = 0^\circ$
- Figure 17 The static pressure distribution on Body #5 at  $M = 4.12$ ,  $\epsilon = 0^\circ$
- Figure 17a Schlieren photograph of Body #5 at  $M = 4.12$ ,  $\epsilon = 0^\circ$
- Figure 18 The static pressure distribution on Body #5 at  $M = 2.88$ ,  $\epsilon = 0^\circ$
- Figure 18a Schlieren photograph of Body #5 at  $M = 2.88$ ,  $\epsilon = 0^\circ$
- Figure 19 The static pressure distribution on Body #5 at  $M = 1.79$ ,  $\epsilon = 0^\circ$
- Figure 19a Schlieren photograph of Body #5 at  $M = 1.79$ ,  $\epsilon = 0^\circ$
- Figure 20 The static pressure distribution on Body #6 at  $M = 5.1$ ,  $\epsilon = 0^\circ$
- Figure 21 The static pressure distribution on Body #6 at  $M = 6.4$ ,  $\epsilon = 0^\circ$
- Figure 22 The static pressure distribution on Body #6 at  $M = 7.2$ ,  $\epsilon = 0^\circ$
- Figure 23 The static pressure distribution on Body #6 at  $M = 8.1$ ,  $\epsilon = 0^\circ$
- Figure 24 The effect of Mach number on the pressure distribution on geometrically similar bodies (Body #1 and Body #6),  $\epsilon = 0^\circ$
- Figure 25 The effect of corner radius on pressure distribution at  $M = 4.84$ ,  $\epsilon = 0^\circ$  (Body #1 and Body #2)
- Figure 26 The effect of corner radius on pressure distribution at  $M = 4.84$  (Bodies #3, #4, and #5),  $\epsilon = 0^\circ$
- Figure 27 The effect of model curvature continuity on pressure distribution,  $M = 4.84$  (Body #1 and Body #3),  $\epsilon = 0^\circ$
- Figure 28 The static pressure distribution on Body #6 at  $M = 5.1$ ,  $\epsilon = 3^\circ$
- Figure 29 The static pressure distribution on Body #6 at  $M = 5.1$ ,  $\epsilon = 6^\circ$
- Figure 30 The static pressure distribution on Body #6 at  $M = 5.1$ ,  $\epsilon = 9^\circ$
- Figure 31 The static pressure distribution on Body #6 at  $M = 6.4$ ,  $\epsilon = 3^\circ$
- Figure 32 The static pressure distribution on Body #6 at  $M = 6.4$ ,  $\epsilon = 6^\circ$
- Figure 33 The static pressure distribution on Body #6 at  $M = 6.4$ ,  $\epsilon = 9^\circ$
- Figure 34 The static pressure distribution on Body #6 at  $M = 7.2$ ,  $\epsilon = 3^\circ$
- Figure 35 The static pressure distribution on Body #6 at  $M = 7.2$ ,  $\epsilon = 6^\circ$
- Figure 36 The static pressure distribution on Body #6 at  $M = 8.1$ ,  $\epsilon = 3^\circ$

NAVORD Report 5659

- Figure 37 The static pressure distribution on Body #6 at  $M = 8.1, \epsilon = 6^\circ$
- Figure 38 Pressure contours ( $p/P_0'$ ) on the face and shoulder of Body #6 at  $M = 8.1, \epsilon = 0$  and  $6^\circ$
- Figure 39 The effect of Mach number on the pressure distribution on Body #6 at  $\epsilon = 6^\circ$
- Figure 40 The effect of yaw on the pressure distribution on Body #6 at  $M = 8.1$
- Figure 41 Shadowgraph of Body #3 at  $M = 1.79$  with roughness at stagnation point
- Figure 42 Shadowgraph of Body #7 at  $M = 3.85$
- Figure 43 Shadowgraph of Body #7 at  $M = 3.19$
- Figure 44 Shadowgraph of Body #7 at  $M = 2.92$
- Figure 45 Shadowgraph of Body #7 at  $M = 2.78$
- Figure 46 Shadowgraph of Body #7 at  $M = 2.73$

# NAVORD Report 5659

## SYMBOLS

a	- model flat face radius
$C_D$	- total drag coefficient
$C_M$	- pitching moment coefficient
$C_N$	- normal force coefficient
$(C_{m_q} + C_{m_{\dot{\alpha}}})$	- damping coefficient
h	- model base radius
L	- model axial length
M	- free-stream Mach number
p	- local static pressure
$P_0$	- tunnel supply pressure
$P_0'$	- Pitot pressure for $\epsilon = 0^\circ$
r	- shoulder radius
Re	- free-stream Reynolds number
$Re_\theta$	- Reynolds number based on boundary-layer momentum thickness
S	- contour length measured from the geometric center of the model face along a streamline
$T_0$	- tunnel supply temperature
$\theta$	- cone half angle - degrees
$\epsilon$	- angle of yaw is the angle between the relative wind and the model axis (equivalent to pitch angle set in wind tunnel) - degrees
$\phi$	- angle of roll is the angle measured from the intersection of the windward cone surface with the plane of yaw - degrees

EXPERIMENTAL INVESTIGATION OF THE PRESSURE DISTRIBUTION ON  
AXI-SYMMETRIC FLAT-FACE CONE-TYPE BODIES AT SUPERSONIC AND  
HYPERSONIC SPEEDS

INTRODUCTION

1. In general, missiles designed for hypersonic flight will be required to have blunt nose shapes. This is because prohibitively high heat-transfer rates are encountered on sharp-nosed bodies. In general, the blunt nose is all-important for such applications since manageable heat-transfer rates are obtained. Because of the current deep interest in these shapes the present extensive experimental investigation has been conducted.

2. The present wind tunnel investigation consisted of pressure distribution measurements on a family of blunt-nosed axi-symmetric bodies over a Mach number range from approximately 1.75 to 8. The bodies considered are essentially truncated cones and hyperbolic bodies of similar shape. From the measured pressure distribution the local flow conditions along the contour can be determined by using the isentropic flow tables (reference a). Having the local flow conditions, quantitative calculations of the local heat-transfer rate may be made.

3. Stability and drag data have been determined for one configuration in the NOL Pressurized Ballistic Range.

MODELS AND FACILITIES

Selection of Model Configuration

4. The axi-symmetric flat-face cone-type configuration (see Table I), was chosen for the present experimental study because of its qualitative attractiveness from the standpoint of aerodynamic stability and heat transfer on both the front face and afterbody. The low velocity on the front face and low density on the conical afterbody both contribute to minimizing the over-all heat transfer.

5. In order to investigate the effect of discontinuities in the model contour curvature on the pressure distribution, a family of continuous curvature bodies\* which closely approximated the truncated cones was tested.

---

\*The equations and coordinate system for the continuous curvature body shapes are given in Appendix A.

## NAVORD Report 5659

### Facilities Used for Tests

6. The Aeroballistics Tunnel No. 2 has the following characteristics:

Size and Type	-	40 x 40 cm open jet
Mach Number Range	-	1.2 to 5.0
Blowing Time	-	Continuous; recirculating
Supply Temperature	-	540-580°R
Supply Pressure	-	1 - 3.5 atmospheres absolute

7. The Hypersonic Tunnel No. 4 has the following characteristics:

Size and Type	-	12 x 12 cm closed jet
Mach Number Range	-	5 - 10 with wedge nozzle
Blowing Time	-	continuous, non-recirculating
Supply Temperature	-	490-1390°R
Supply Pressure	-	1 - 40 atmospheres absolute

8. The Pressurized Ballistic Range No. 3 has the following characteristics:

Length	-	319 Feet
Diameter	-	3 Feet (with a usable dispersion area of 1 x 1 foot)
Pressure	-	0.1 - 6 atmospheres absolute
Temperature	-	534±0.5°R
Maximum Projectile	-	Size - 0.133 feet diameter
Velocity Range	-	Dependent on gun, projectile size and charge
Photographic Spark Stations	-	25
Chronograph Stations	-	Any 13 selected stations - 10 megacycle chronographs

### RESULTS AND DISCUSSION

#### Pressure Distribution, $\epsilon = 0^\circ$

9. Figure 1 presents the calculated, laminar  $Re_\theta$  growth on Body #1 for both the experimental pressure distribution and that calculated by the modified Newtonian concept (reference b) as shown in Figure 2. The results shown in Figure 1 indicate that the predicted variation of  $Re_\theta$  along the contour using the modified Newtonian pressure distribution for these body shapes is appreciably different from that obtained using the actual measured pressure distribution. Consequently, the following experimental results were obtained in lieu of an adequate means for predicting the pressure distribution about such blunt bodies.

10. In some of the figures which follow, several comparisons are made in an attempt to demonstrate important effects. These comparisons are not intended to be all inclusive because it is the primary purpose of this report to present the data. The comparisons are intended, however, to indicate significant trends which are currently of interest.

11. The experimentally determined pressure distributions for zero yaw (angle of pitch) are plotted in terms of the ratio of the local pressure on the surface to the model stagnation pressure ( $p / P_0$ ) as a function of the non-dimensional contour length ( $S/h$ ). These data are given in Figures 2-23. For each set of pressure distribution data presented in Figures 2-19 inclusive, there are corresponding shadowgraph photographs. These are given as Figures 2a-19a.

12. In general, for all of the configurations investigated the data indicated a slight increase in velocity along the front flat face as the contour length from the stagnation point increases. Along the circular arc connecting the front face and the conical portion a rapid acceleration occurs which may or may not result in a localized overexpansion at the start of the conical portion. The strongest overexpansion occurs at the lower Mach numbers, ( $M < 3$ ). Examination of the appropriate photographs shows the shock waves resulting from the overexpansion. These may cause boundary layer separation.

13. To demonstrate the influence of Mach number on geometrically similar configurations. (Bodies 1 and 6), the data presented in Figures 2 and 23 [see Table I] are replotted in Figure 24. The data indicate that the pressure distribution over the face and corner is relatively unaffected by Mach number. However, a Mach number effect is evident on the conical portion at the lower Mach numbers.\* In no case was the conical section sufficiently long to achieve that pressure which would exist on a sharp nosed cone of the same apex angle.

14. The data of Figures 2 and 4 have been replotted on Figure 25 to demonstrate the effect on the pressure distribution of doubling the shoulder radius of Body #1 to make it become Body #2 [see Table I]. The increased shoulder radius resulted in an alleviated pressure gradient in the corner region and a smaller overexpansion.

---

\*This is more self-evident if one also plots the intermediate Mach number data of Figures 3, 20, 21, and 22 on Figure 24.

15. Bodies 3, 4, and 5 [see Appendix I and Table I] are hyperbolic bodies whose contours very closely approximate cone-frustrums whose flat-faces are connected to the conical surface by circular arcs. The radius of the flat-face, the base radius and the cone angle have been held constant for each body and the shoulder radius has been varied thus: Body #3,  $r \approx 1/4"$ ; Body #4,  $r \approx 1/2"$ ; and Body #5,  $r \approx 1"$ . To demonstrate the influence of the different corner radii on the pressure distribution the data of Figures 8, 12, and 16 are plotted on Figure 26. The data of Figure 26 indicate that the steep pressure gradient in the corner region is somewhat alleviated by increasing the corner radius. The local overexpansion is eliminated on Body #5.

16. The pressure distribution obtained on a discontinuous curvature body is compared (for equivalent distances measured along the contour from the model stagnation point) to that obtained on a physically similar continuous curvature body in Figure 27. The data presented in this figure were obtained from Figures 2 and 8. There is little or no difference between the two sets of data indicating that for these particular bodies there is no effect due to discontinuities in curvature.

#### Pressure Distribution, $\epsilon \neq 0^\circ$

17. Additional data were taken on Body #6 for angles of yaw ( $\epsilon$ ) of 3, 6, and 9 degrees at  $M = 5.1$  and 6.4, and  $\epsilon = 3$  and 6 degrees at  $M = 7.2$  and 8.1. Figures 28 through 37 give the basic presentation of this data. A limited amount of data (not shown) were taken with orifices located on the circle defined by the tangency of the shoulder and cone. The orifices were offset  $45^\circ$  on either side of the measuring meridian. The data, so obtained, indicated no overexpansion, so that the levels of cone pressure shown on the plots probably can be extended forward to the termination of the shoulder. The apparent waviness of the pressure distribution along the cone is explained as follows: In terms of  $S/h$ , the orifices on the cone surface were alternated along two diametrically opposite meridians of the model and the orifices were in a single meridian plane to facilitate obtaining roll data. An exception to the above occurs for the two orifices at the largest  $S/h$  values, which are on the same meridian of the cone. Therefore, the data demonstrate the existence of two distinct pressure levels on diametrically opposite meridians of the cone when these meridians are brought consecutively into the same orientation of  $\epsilon$  and  $\phi$ . The effect cited is especially strong in the data of Figures 33, 35, and 37, i.e., at the higher Mach numbers and yaw angles.

18. This asymmetry of the data would seem largely to preclude an explanation based on inclinations of the tunnel flow, or on interference between the tunnel and model. After careful checking of the pressure instrumentation and model symmetry, it is thought that the presence of an orifice on the midpoint of the shoulder ( $S/h \approx 0.452$ ) effectively disrupts the symmetry of the model for most of the test conditions represented by the data of Figures 28 through 37. The 0.025 inch diameter orifice subtends approximately 14 degrees of the 60 degree shoulder arc. A direct experimental check of the effects of known disturbances in the shoulder region would be of interest in this regard.

19. Figure 38 shows contours of  $p/P_0'$  over the flat-face and shoulder of the model. The stagnation region has been designated as that region in which  $0.99 \leq p/P_0' \leq 1.00$ . The radial coordinate implied in this plot is  $S/h$  so that the radial extent of the shoulder is shown larger than would appear in a true projection. The angular extent of the shoulder is 60 degrees of arc. If a contour of  $p/P_0' \approx 0.53$  is taken as the locus of the sonic point on the shoulder, then Figure 38 indicates substantial variations in the position of the sonic point around the model for  $\epsilon = 6$  degrees. For  $\phi = 90$  degrees, the contours are not displaced appreciably as a result of the 6-degree yaw shown in the figure. The preceding figures show that a fairly constant cone pressure is maintained at this roll position throughout the range of Mach numbers and yaw angles.

20. Figure 39 shows the Mach number effect on data taken in the meridian plane of yaw ( $\phi = 0, 180$  degrees) with a yaw angle,  $\epsilon$ , of 6 degrees. A substantial difference exists on the shoulder between data taken for the two lower Mach numbers and those obtained for the two higher Mach numbers. In general, the variation of the data with Mach number appears greatest in regions of steep pressure gradient.

21. Figure 40 shows the yaw effect on data taken in the meridian plane of yaw ( $\phi = 0, 180$  degrees) at the highest Mach number tested. The dual pressure-levels at various roll positions on the cone surface were discussed in paragraphs 17 and 18. Over the shoulder and the cone, the pressure increments due to yaw are nearly constant at each  $S/h$  location.

#### Effect of Roughness

22. A limited investigation of the effect of roughness in the stagnation region was made to determine whether sufficient differences in either the inviscid or viscous flow fields could be detected. The roughness consisted of a

1/2" diameter disc of No. 60 grit placed with its center at the model stagnation point. A shadowgraph photograph showing the model with the roughness patch is given as Figure 41. By comparing this photograph with Figure 11a which was taken for the same body shape and comparable tunnel conditions it may be concluded that the roughness patch did not cause transition. If turbulence had been stimulated, the disturbance pattern in the local compression region at the shoulder would have had a different character than that shown in Figure 11a.

#### Pressurized Ballistic Range Results

23. Five models of Body #7 which were geometrically identical to Body #6 and geometrically similar to Body #1, were fired in the Naval Ordnance Laboratory Pressurized Ballistic Range at several Mach numbers and pressures (see Table I). A representative shadowgraph of each of these firings is given in the succeeding five figures (Figures 42, 43, 44, 45, and 46), and a limited amount of numerical data was obtained.\*\*

#### CONCLUDING REMARKS

24. For axi-symmetric, flat-face, cone-type bodies, the predicted growth of the laminar boundary layer, using the modified Newtonian flow concept for determining the pressure distribution, is appreciably different from that obtained when the measured pressure distribution is used.

\*\*

Round	Data		Body #7				$Re_{\theta}$ at Tran. Pt.
	Station	M	CD	CM	CN	$C_{mq} + C_{m_{\infty}}$	
1989	11	3.7	0.736	-.388	-1.070	-.148	
1985	12	3.0	0.792				148
1986	11	2.0	0.949				364
1984	10	2.6	0.831				
1990	5	2.2	0.898				

$Re_{\theta}$  was computed using the method of Cohen and Reshotko (reference c) and the pressure distribution was obtained from the comparable wind tunnel model data. The values of  $Re_{\theta}$  obtained are comparable to those obtained on other blunt bodies (reference d).

25. An extensive experimental investigation of the pressure distribution on axi-symmetric flat-face cone-type bodies has been conducted. The data cover a Mach number range from about 1.75 to 8.00. Results are also given in the form of schlieren and shadowgraph photographs for most of the body shapes investigated. Stability and drag data for a single body shape were also obtained in the NOL Pressurized Ballistic Range.

26. In general, it was found that for all of the configurations investigated a slight increase in velocity occurred along the front face as the distance from the stagnation point increased. Along the circular arc connecting the front face and the conical portion, a rapid acceleration occurs which results in a localized overexpansion at the start of the conical portion. Qualitatively, the amount of overexpansion varies inversely with Mach number. For Mach numbers greater than about 3, the pressure distributions in the frontal regions are essentially unaffected by Mach number.

NAVORD Report 5659

REFERENCES

- (a) Ames Research Staff, "Equations, Tables, and Charts for Compressible Flow," NACA Report 1135, 1953
- (b) Lees, Lester and Kubota, Toshi, "Inviscid Hypersonic Flow Over Blunt-Nosed Slender Bodies," Jour. Aero. Sci., Vol. 24, No. 3, p. 195
- (c) Cohen, Clarence B., and Reshotko, Eli, "The Compressible Laminar Boundary Layer with Heat Transfer and Arbitrary Pressure Gradient," NACA TN 3326, 1955
- (d) Witt, W. R., and Persh, J., "A Correlation of Free-Flight Transition Measurements on Various Blunt Nose Shapes by Use of the Momentum Thickness Reynolds Number," NAVORD Report 4400, December 1956

NAVORD Report 5659

APPENDIX I

1. The equations used to generate the continuous curvature bodies are as follows:

Body No. 3

$$xy = 0.57737 x^2 + 1.1443 x - 0.00129$$

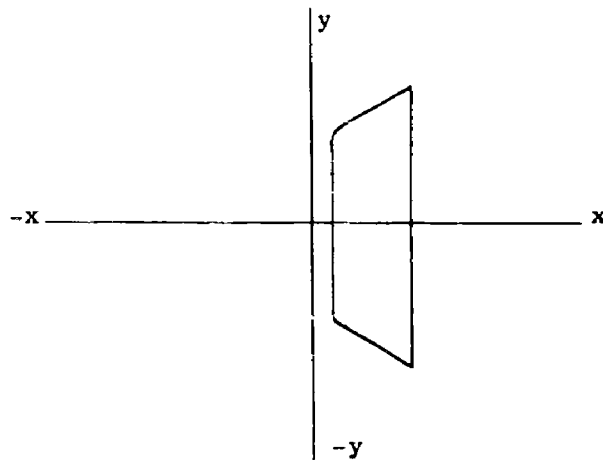
Body No. 4

$$xy = 0.57735 x^2 + 1.28868 x - 0.00518$$

Body No. 5

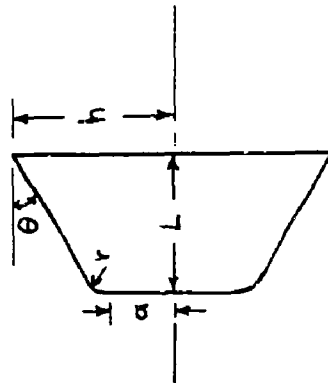
$$xy = 0.57737 x^2 + 1.57737 x - 0.02073$$

In these equations  $x$  and  $y$  are in inches.



Coordinate System

TABLE I  
TABULATION OF CONFIGURATIONS AND TEST CONDITIONS



Config- uration	h inches	L inches	r inches	a inches	$\theta^\circ$	Moo	Po', lbs/ft <sup>2</sup> abs.	To <sup>OR</sup>	Facility	Data Taken	Fig. Nos.	Reco./ft x 10 <sup>-6</sup>
Body#1	2.50	2.35	0.25	1.00	30	4.84	7340	592	Tunnel 2	Pr. Ph.	2	2.88
Body#2	2.50	2.35	0.25	1.00	30	4.12	3480	585	Tunnel 2	Pr. Ph.	3	1.89
	2.50	2.35	0.50	0.86	30	4.84	7360	589	Tunnel 2	Pr. Ph.	4	2.92
Body#3*	2.50	2.35	0.50	0.86	30	4.12	3454	574	Tunnel 2	Pr. Ph.	5	1.94
	2.50	2.35	0.50	0.86	30	2.88	3370	595	Tunnel 2	Pr. Ph.	6	3.35
	2.50	2.35	0.50	0.86	30	1.79	2592	584	Tunnel 2	Pr. Ph.	7	4.52
	2.50	2.35	0.25	1.00	30	4.84	5680	562	Tunnel 2	Pr. Ph.	8	2.48
Body#4*	2.50	2.35	0.25	1.00	30	4.12	4190	575	Tunnel 2	Pr. Ph.	9	2.36
	2.50	2.35	0.25	1.00	30	2.88	2924	574	Tunnel 2	Pr. Ph.	10	3.09
	2.50	2.35	0.25	1.00	30	1.79	2576	560	Tunnel 2	Pr. Ph.	11	4.25
	2.50	2.10	0.50	1.00	30	4.84	6130	560	Tunnel 2	Pr. Ph.	12	2.68
Body#5*	2.50	2.10	0.50	1.00	30	4.12	4200	573	Tunnel 2	Pr. Ph.	13	2.37
	2.50	2.10	0.50	1.00	30	2.88	2780	578	Tunnel 2	Pr. Ph.	14	2.95
	2.50	2.10	0.50	1.00	30	1.79	2535	572	Tunnel 2	Pr. Ph.	15	4.54
	2.50	1.61	1.0	1.00	30	4.84	5570	558	Tunnel 2	Pr. Ph.	16	2.45
	2.50	1.61	1.0	1.00	30	4.12	4170	569	Tunnel 2	Pr. Ph.	17	2.39
	2.50	1.61	1.0	1.00	30	2.88	2785	574	Tunnel 2	Pr. Ph.	18	2.94
	2.50	1.61	1.0	1.00	30	1.79	2550	566	Tunnel 2	Pr. Ph.	19	4.65

TABLE I (Cont'd)

Config- uration	h inches	L inches	r inches	a inches	$\theta^\circ$	M <sub>00</sub>	P <sub>01</sub> lbs/ft <sup>2</sup> abs.	T <sub>01</sub> H	Facility	Data Taken	Fig. Nos.	Re $\phi$ /ft x 10 <sup>-6</sup>
Body#6	1.0	0.94	0.10	0.40	30	5.1	12,840	762	Tunnel 4	Pressure	20	3.03
	1.0	0.94	0.10	0.40	30	6.4	14,860	933	Tunnel 4	Pressure	21	1.55
	1.0	0.94	0.10	0.40	30	7.2	21,340	1122	Tunnel 4	Pressure	22	1.23
	1.0	0.94	0.10	0.40	30	8.1	37,970	1288	Tunnel 4	Pressure	23	1.29
Body#7	+1.0	0.94	0.10	0.40	30	3.85	699	2085	Pres.Range	Photos.	42	Round 1989
	1.0	0.94	0.10	0.40	30	3.19	847	1615	Pres.Range	Photos.	43	Round 1985
	1.0	0.94	0.10	0.40	30	2.92	6350	1440	Pres.Range	Photos.	44	Round 1986
	1.0	0.94	0.10	0.40	30	2.78	1693	1354	Pres.Range	Photos.	45	Round 1984
	1.0	0.94	0.10	0.40	30	2.73	10584	1325	Pres.Range	Photos.	46	Round 1990

\*hyperbolic body

\*\*roughness in stagnation region

+shadowgraphs given are for range station 1

Pr. - pressure

ph. - photographs (schlieren and shadowgraph)

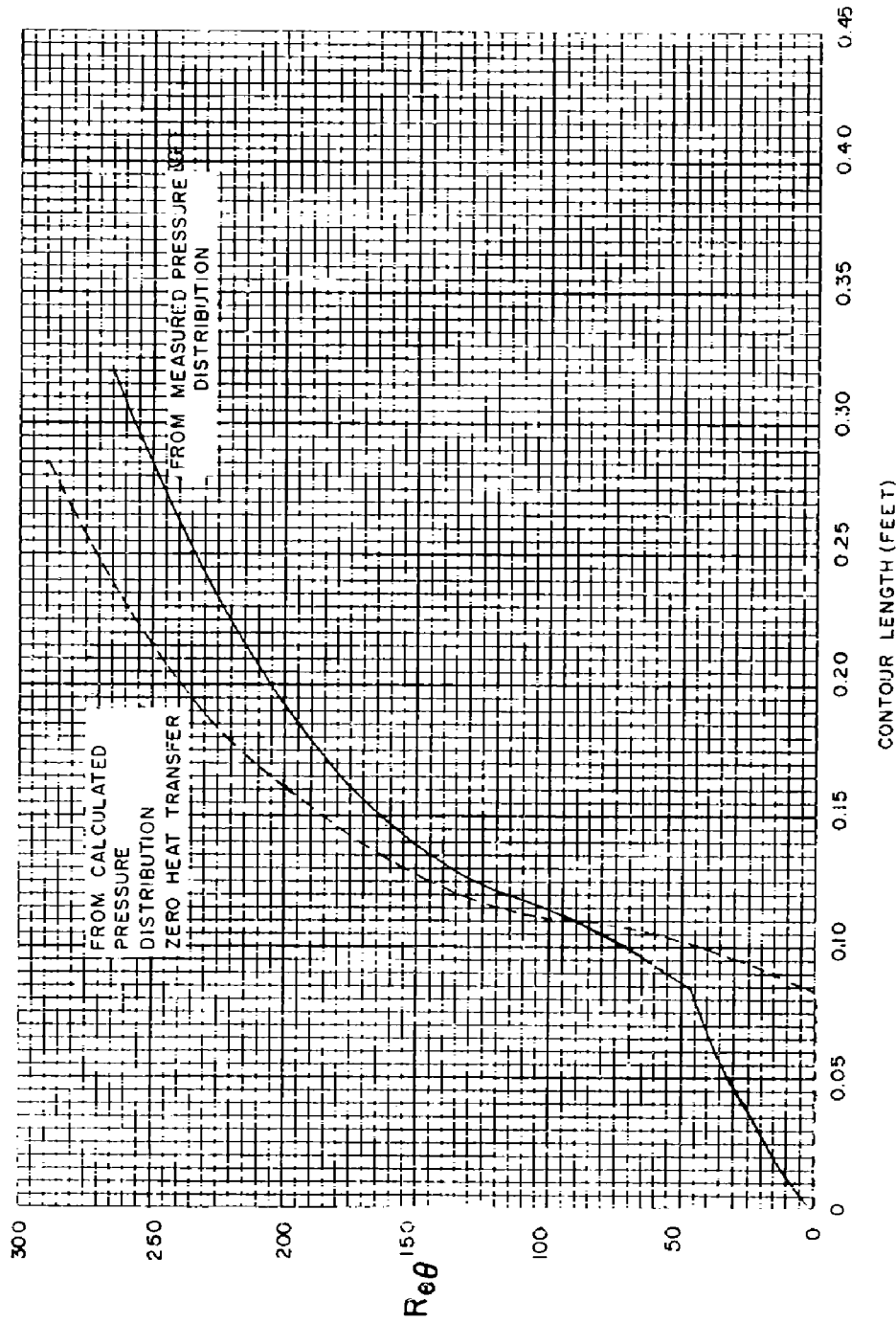


FIG.1 THE VARIATION OF  $Re_\theta$  ALONG THE CONTOUR OF BODY #1 (  $M = 4.84$  ) AS CALCULATED BY USING BOTH THE PRESSURE DISTRIBUTION CALCULATED FROM THE MODIFIED NEWTONIAN CONCEPT AND THAT DETERMINED EXPERIMENTALLY.

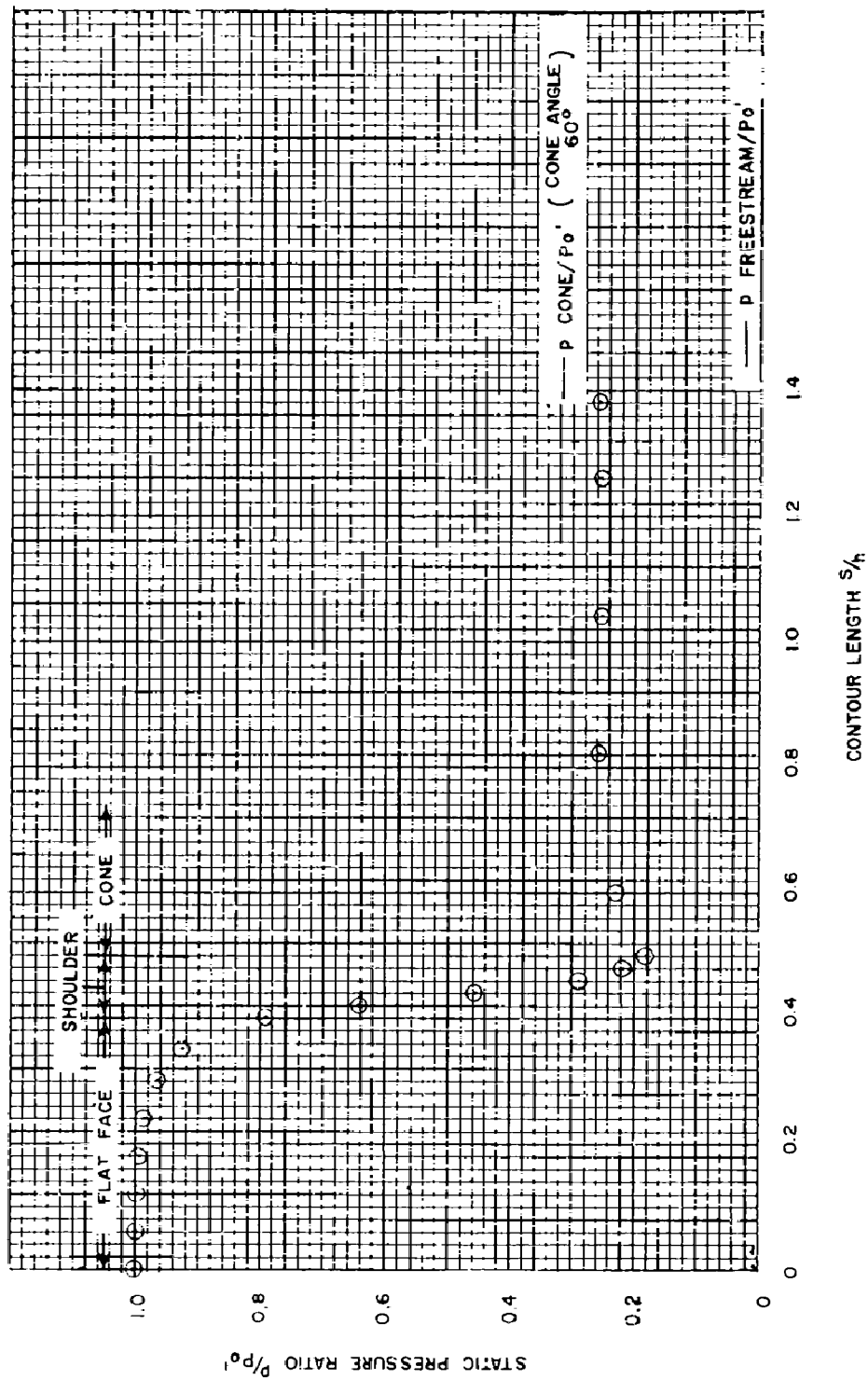


FIG.2 THE STATIC PRESSURE DISTRIBUTION ON BODY #1 AT  $M=4.84$   
 $\epsilon=0^\circ$

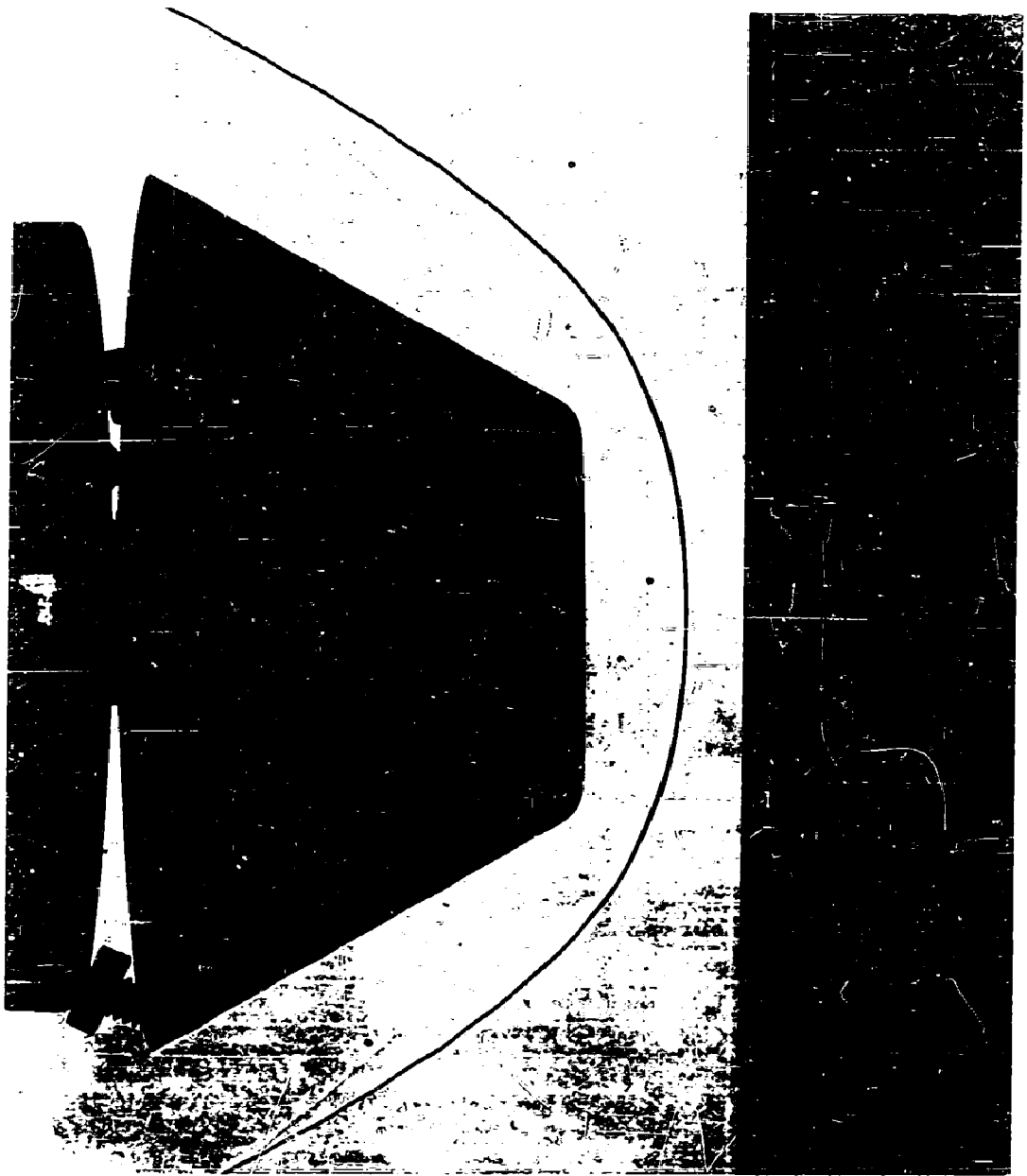


FIG. 2a SHADOWGRAPH OF BODY #1 AT  $M = 4.84$ ,  $\epsilon = 0^\circ$

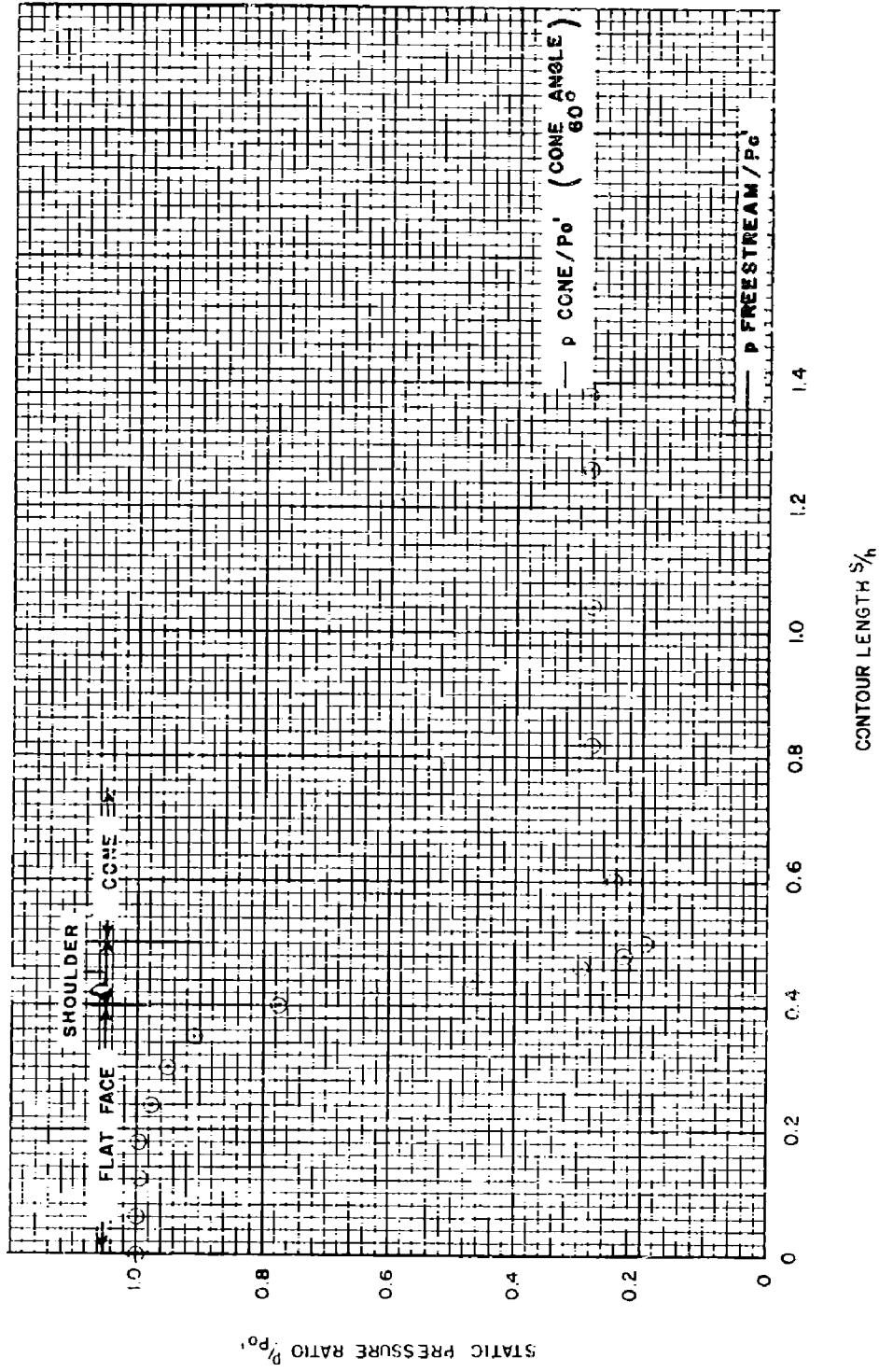


FIG 3 THE STATIC PRESSURE DISTRIBUTION ON BODY #1 AT  $M=4.12$   
 $\epsilon=0^\circ$

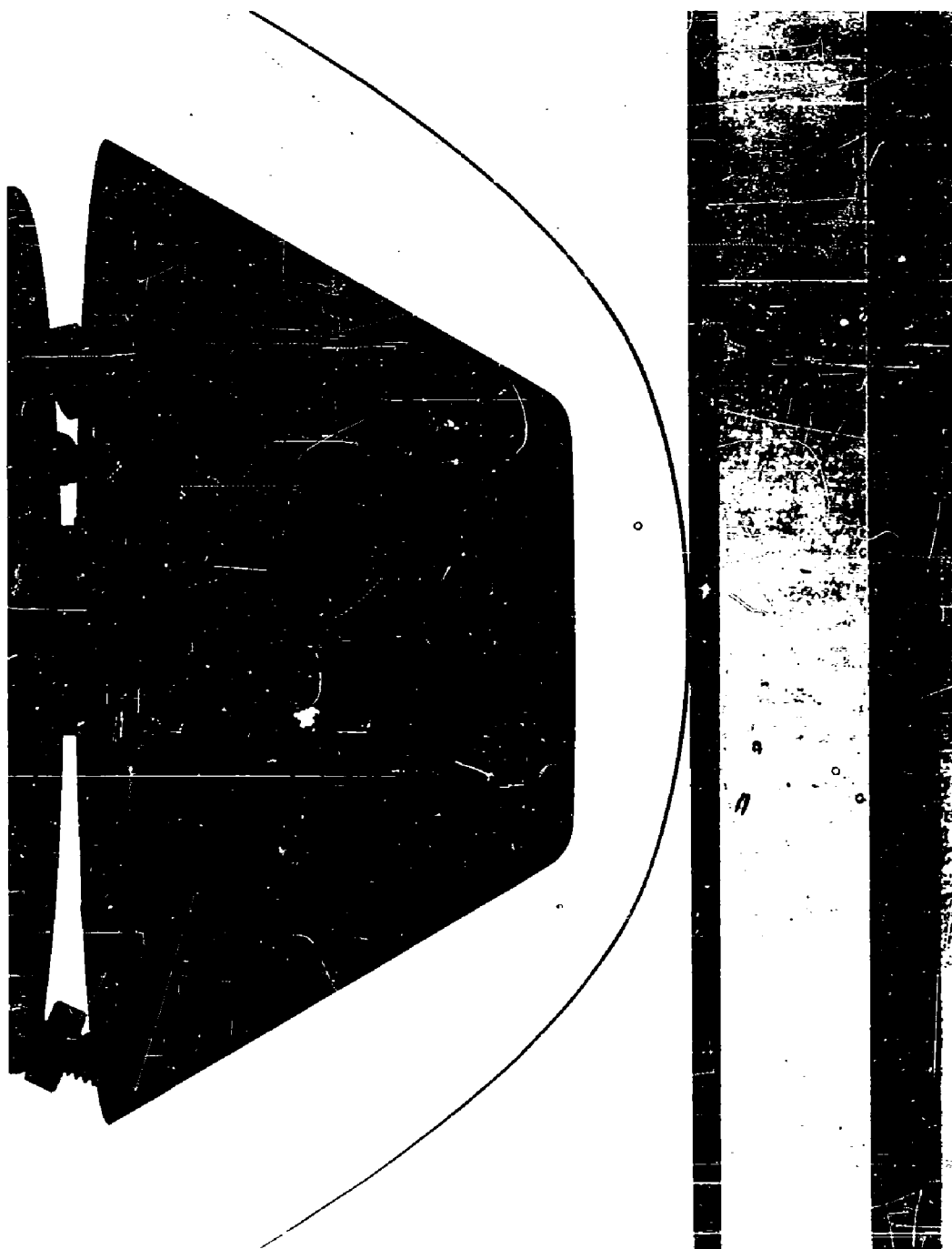


FIG. 3a SHADOWGRAPH OF BODY #1 AT  $M = 4.12$ ,  $\epsilon = 0^\circ$

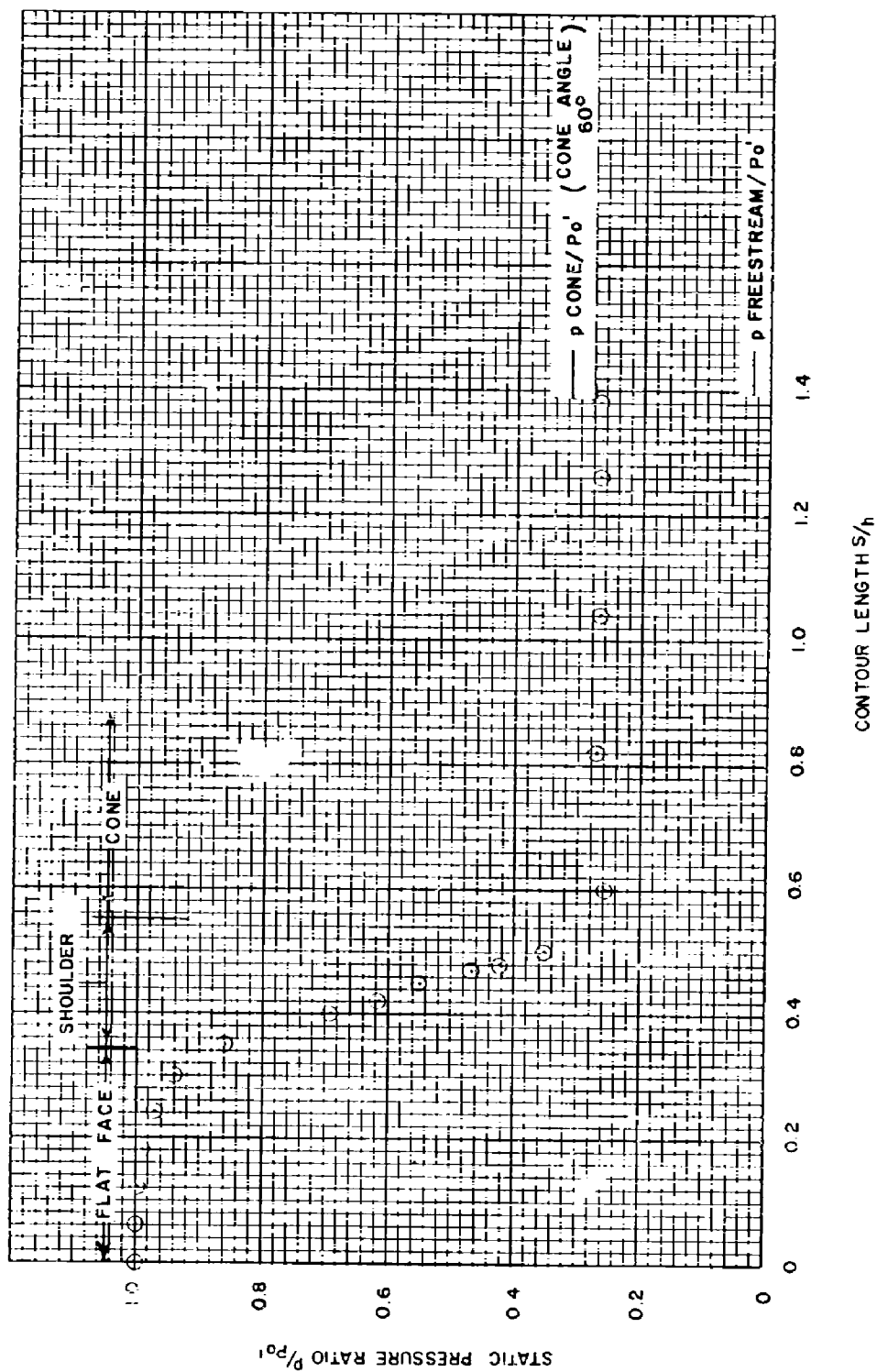


FIG.4 THE STATIC PRESSURE DISTRIBUTION ON BODY #2 AT  $M=4.84$   
 $\epsilon=0^\circ$

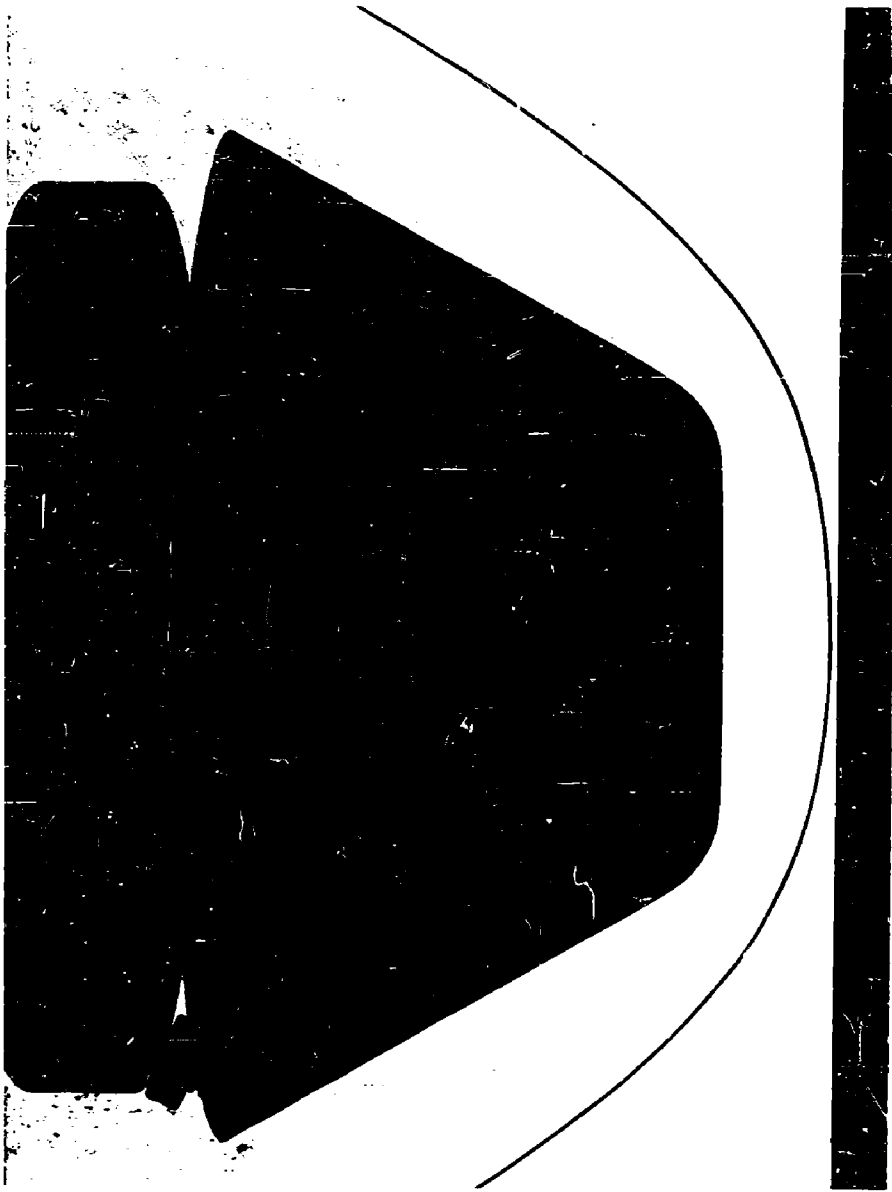


FIG. 4a SHADOWGRAPH OF BODY # 2 AT  $M=4.84$ ,  $\epsilon = 0^\circ$

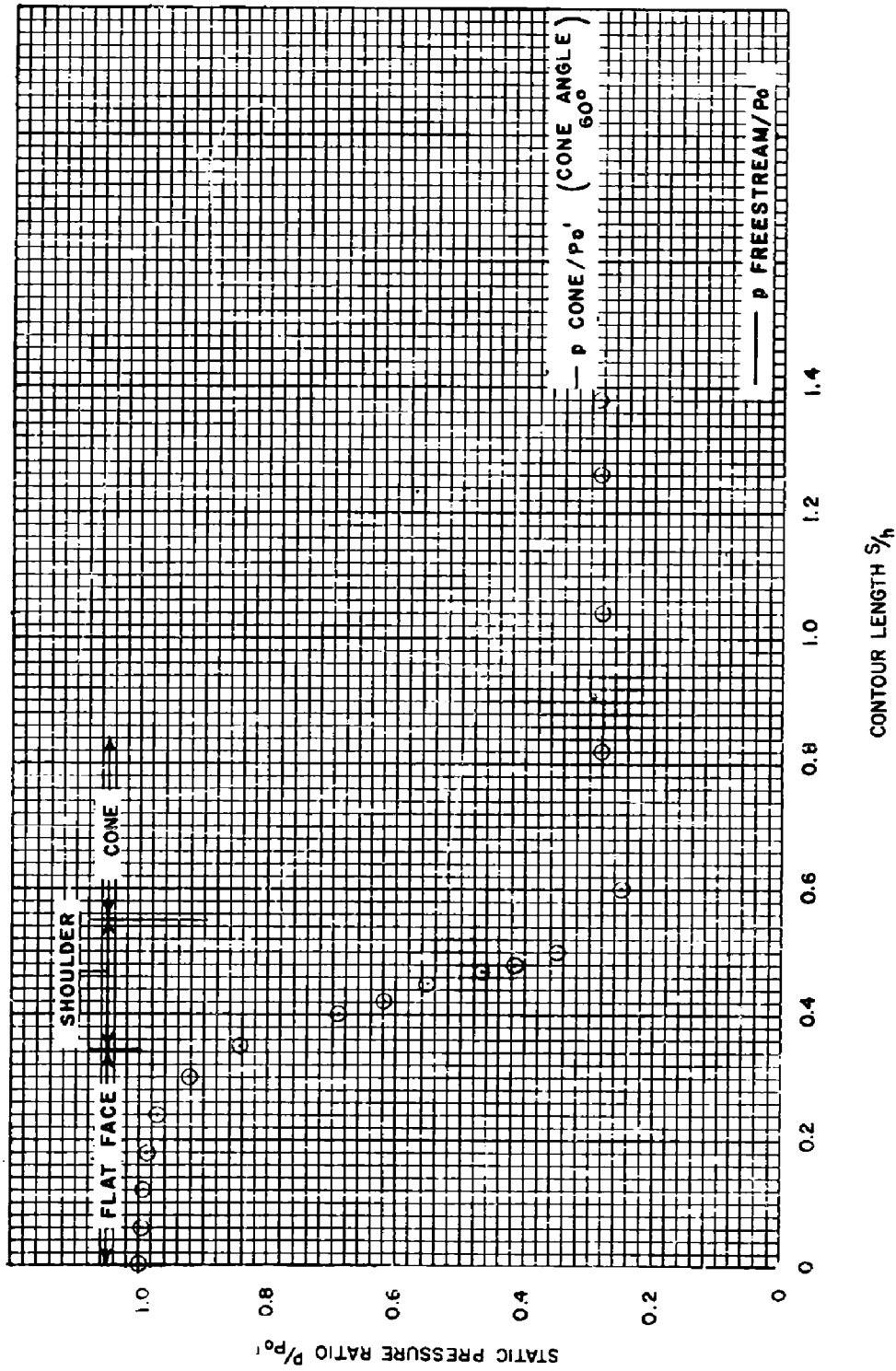


FIG. 5 THE STATIC PRESSURE DISTRIBUTION ON BODY #2 AT  $M=4.12$   
 $\epsilon = 0^\circ$



FIG. 50 SHADOWGRAPH OF BODY #2 AT  $M = 4.12$ ,  $\epsilon = 0^\circ$

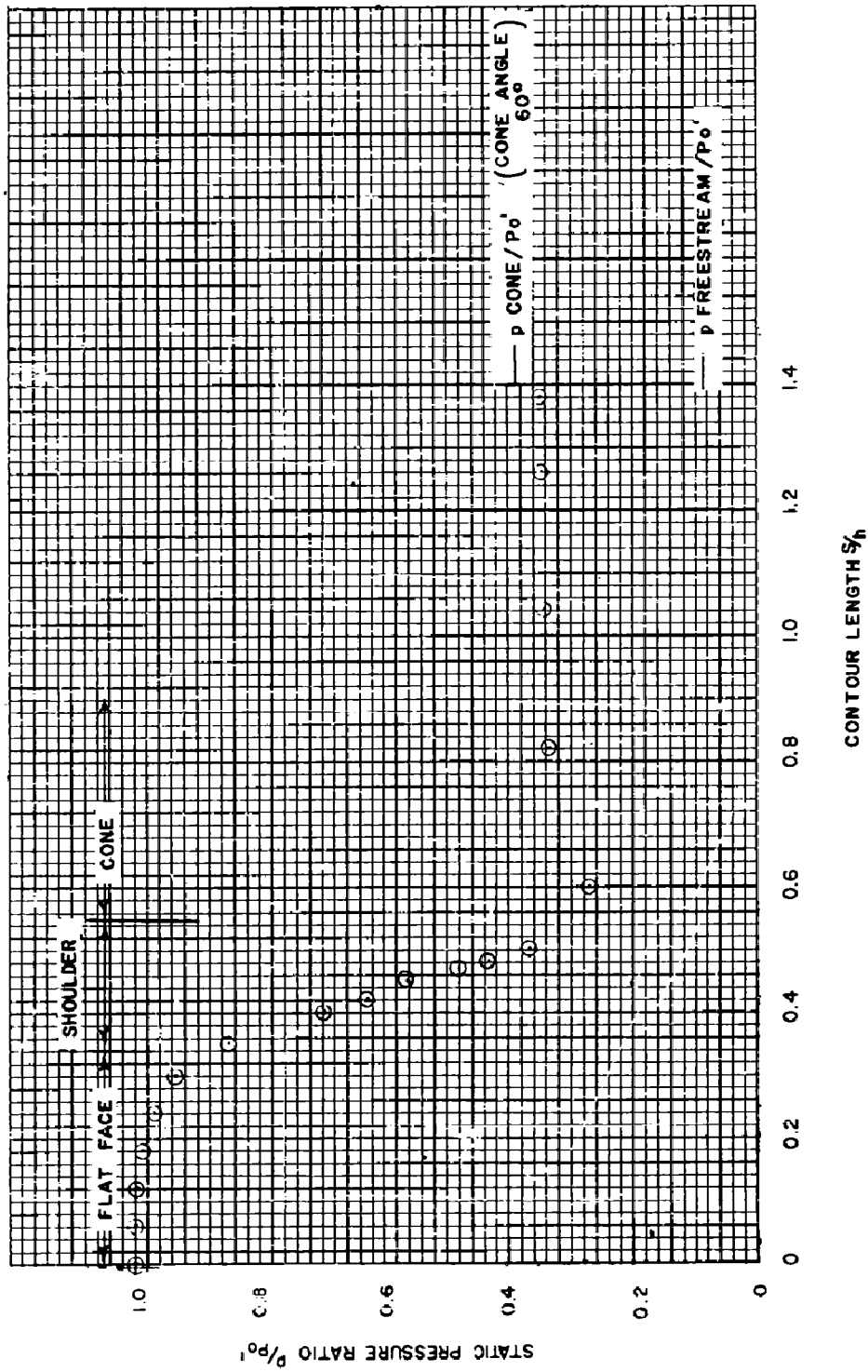


FIG. 6 THE STATIC PRESSURE DISTRIBUTION ON BODY #2 AT  $M=2.88$   
 $\epsilon=0^\circ$



FIG. 6a SHADOWGRAPH OF BODY #2 AT  $M = 2.88$ ,  $\epsilon = 0^\circ$

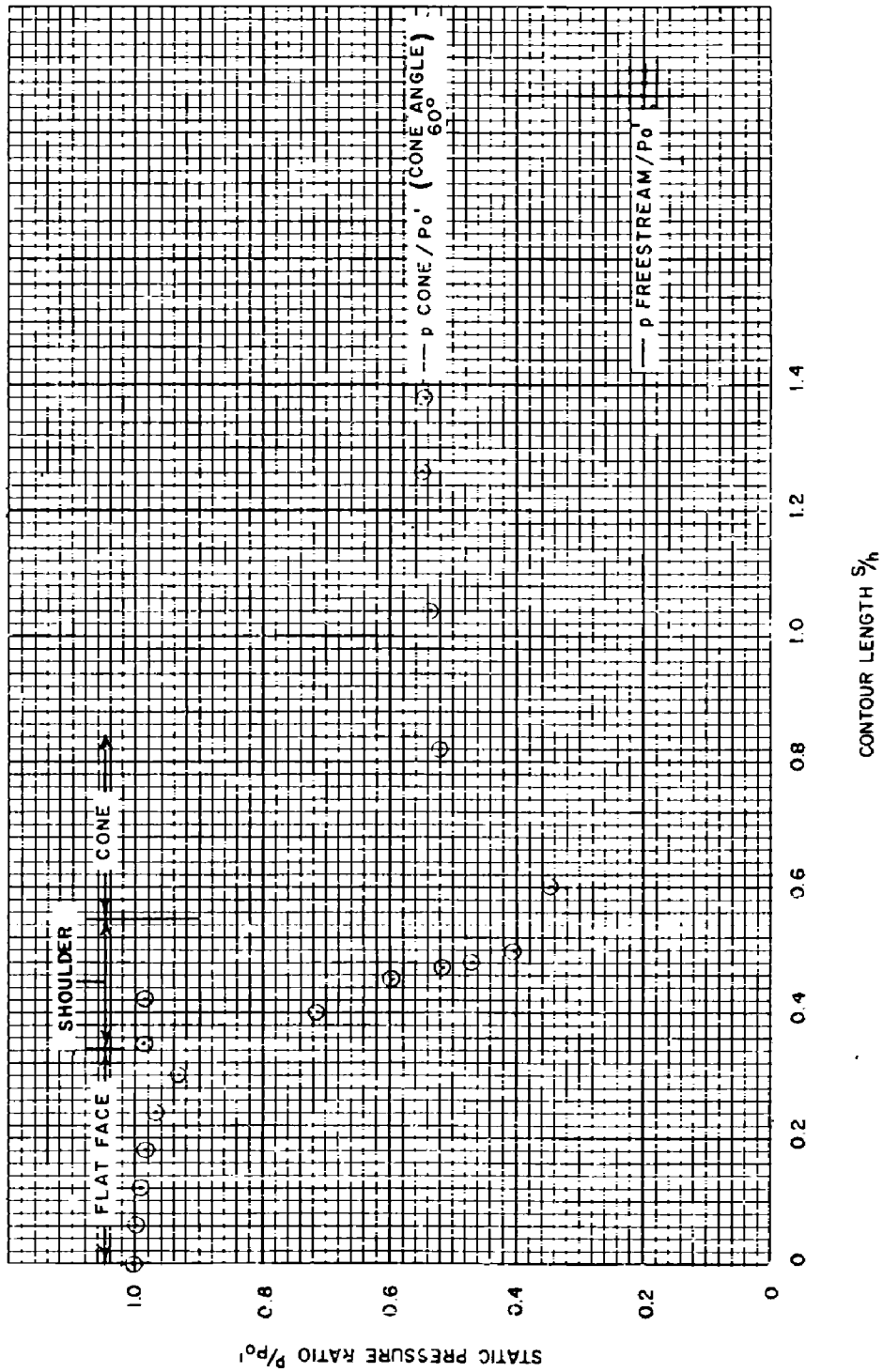


FIG. 7 THE STATIC PRESSURE DISTRIBUTION ON BODY # 2 AT  $M=1.79$   
 $\epsilon=0^\circ$

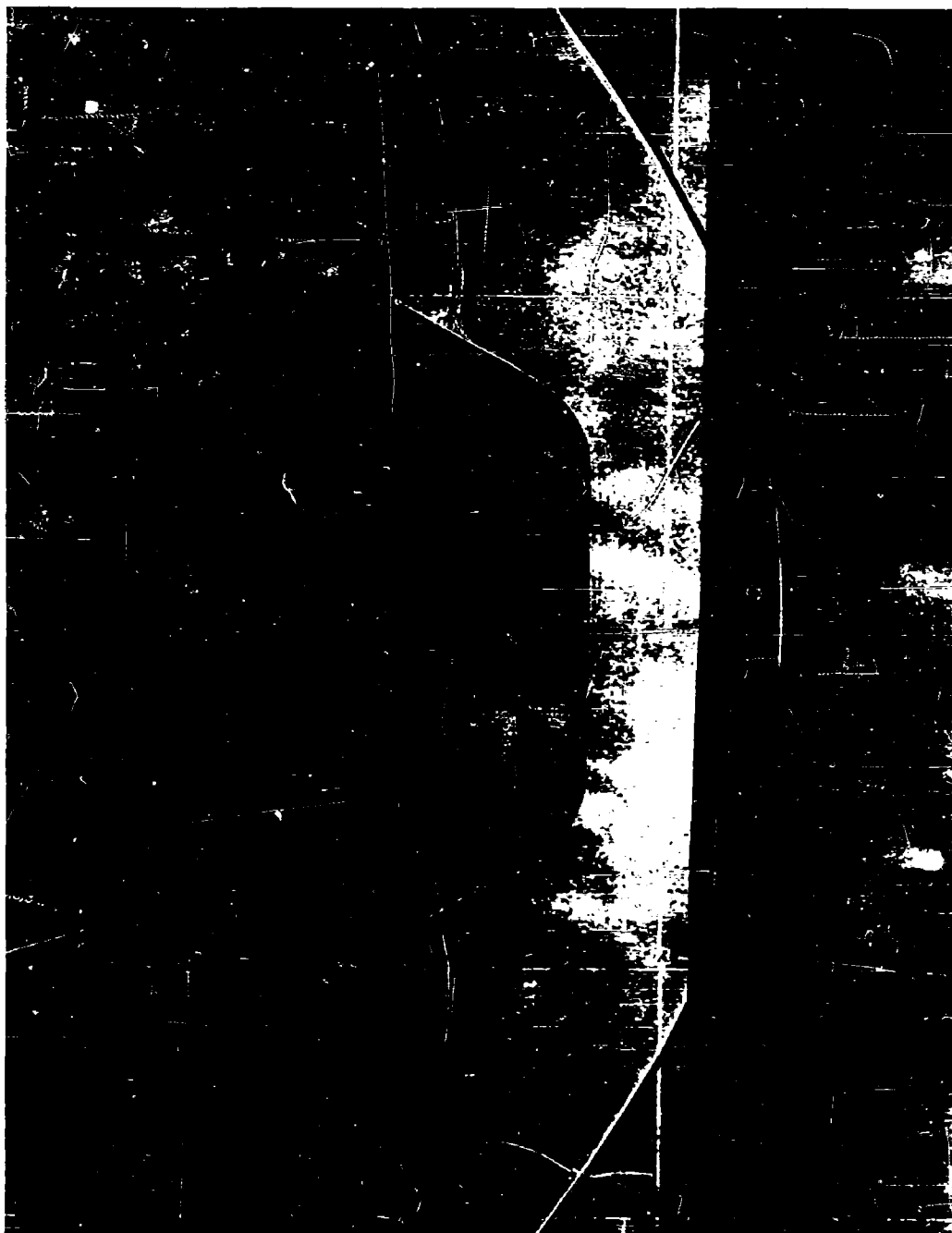


FIG. 7a SHADOWGRAPH OF BODY #2 AT  $M=1.79$ ,  $\epsilon = 0^\circ$

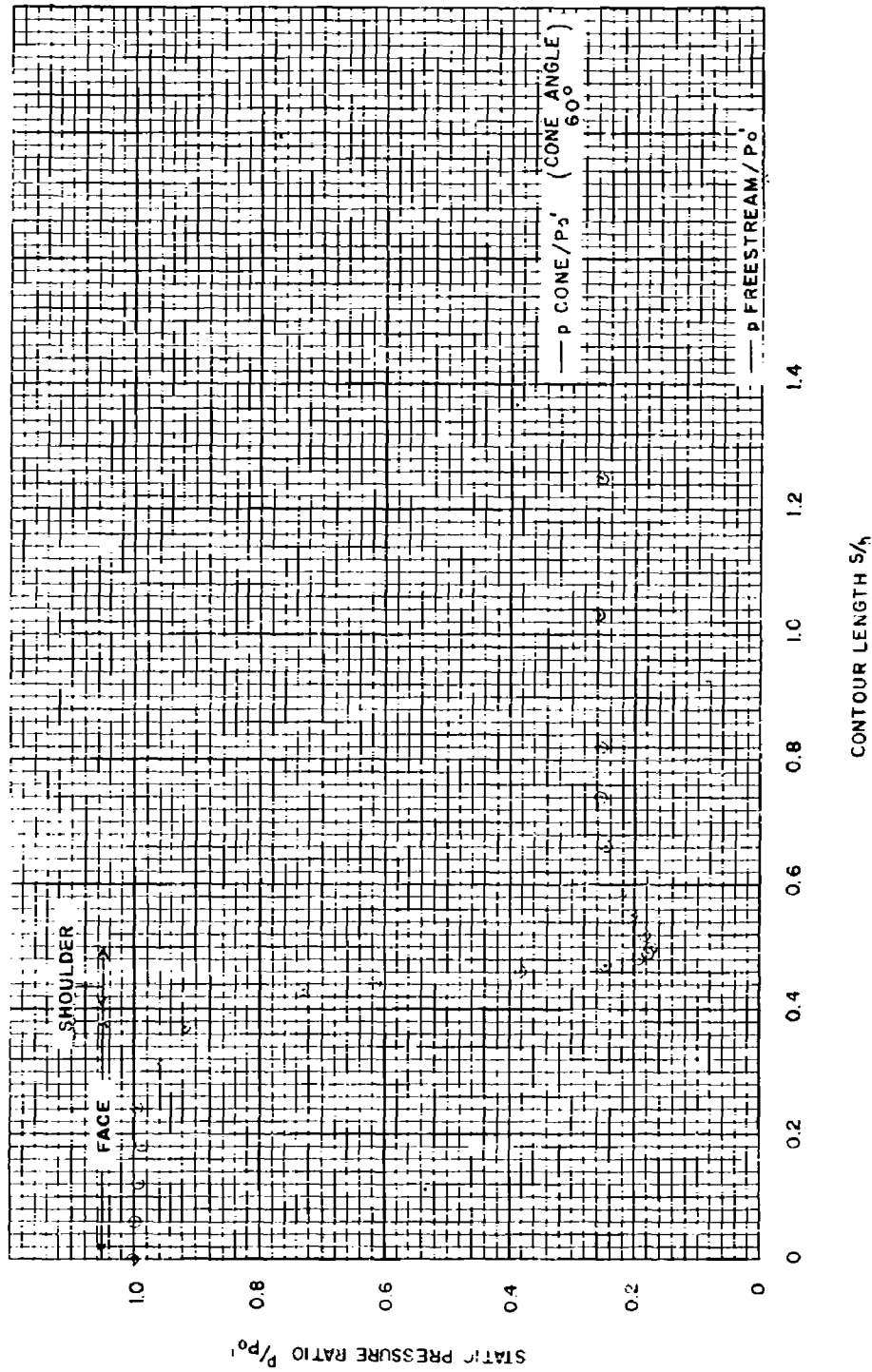


FIG. 8 THE STATIC PRESSURE DISTRIBUTION ON BODY #3 AT  $M=4.84$   
 $\epsilon=0^\circ$

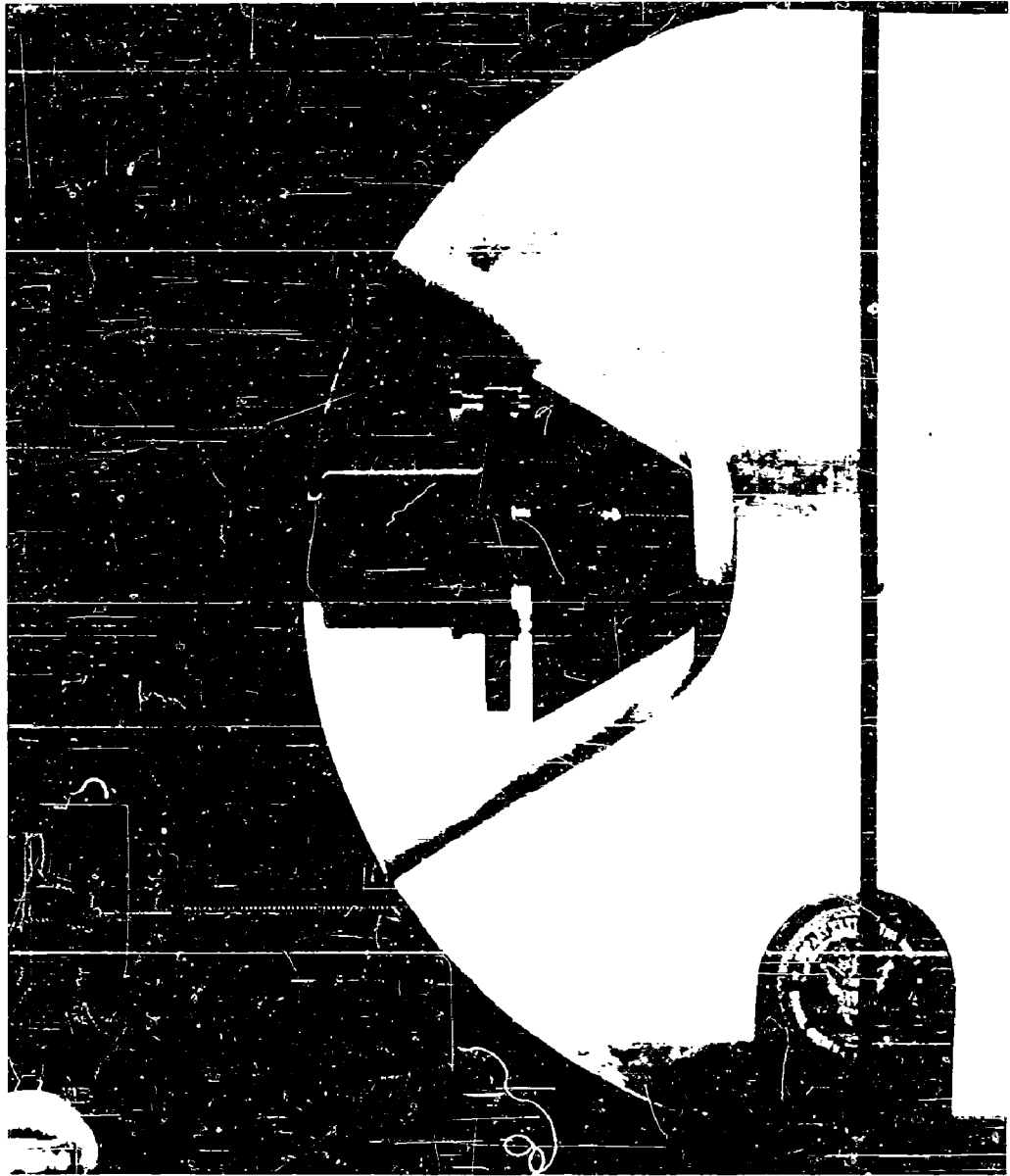


FIG. 8a SCHLIEREN PHOTOGRAPH OF BODY #3 AT  $M = 4.84$ ,  $\epsilon = 0^\circ$

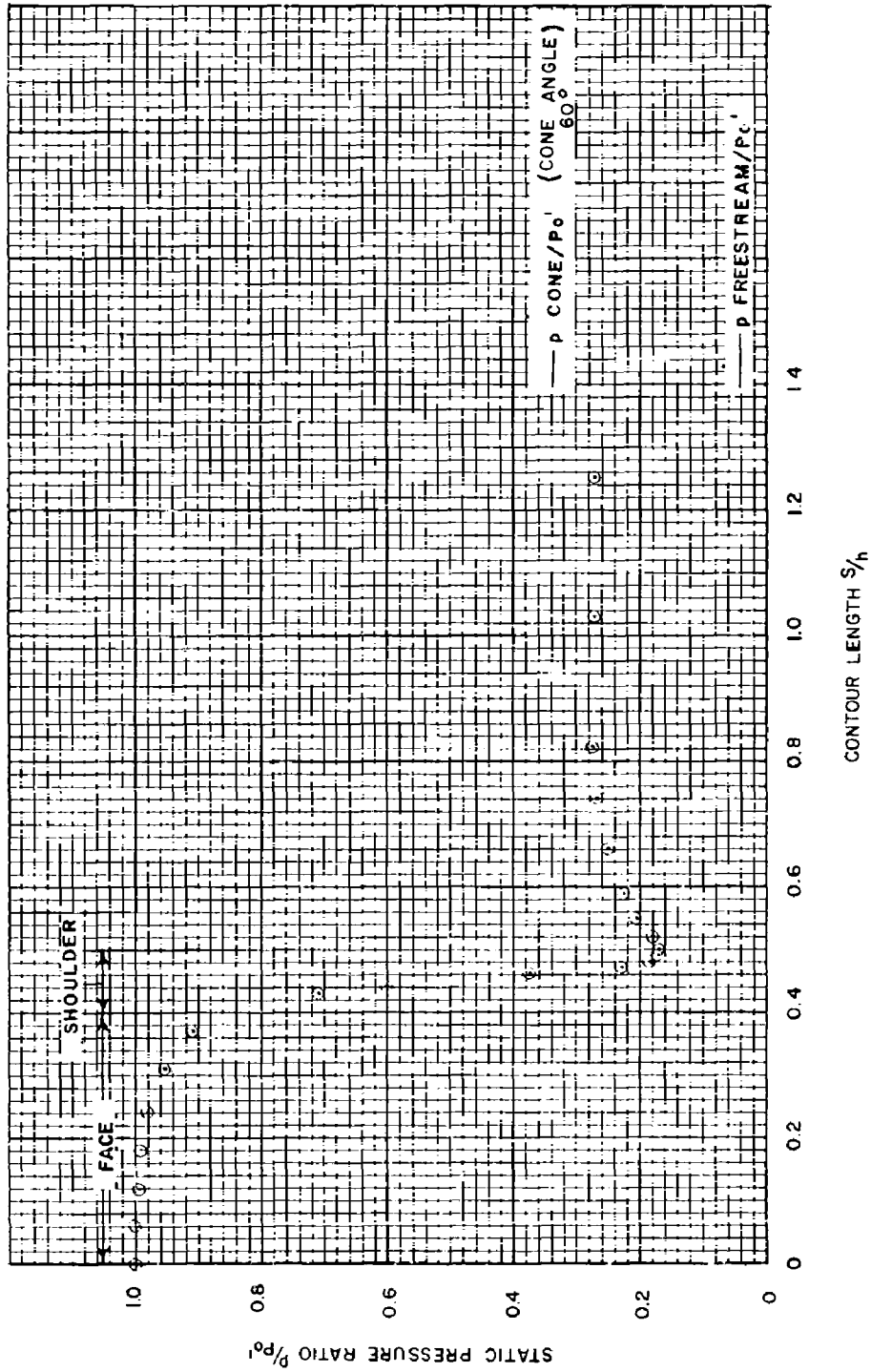


FIG. 9 THE STATIC PRESSURE DISTRIBUTION ON BODY #3 AT  $M=4.12$   
 $\epsilon=0^\circ$



FIG. 9a SHADOWGRAPH OF BODY #3 AT  $M = 4.12$ ,  $\epsilon = 0^\circ$

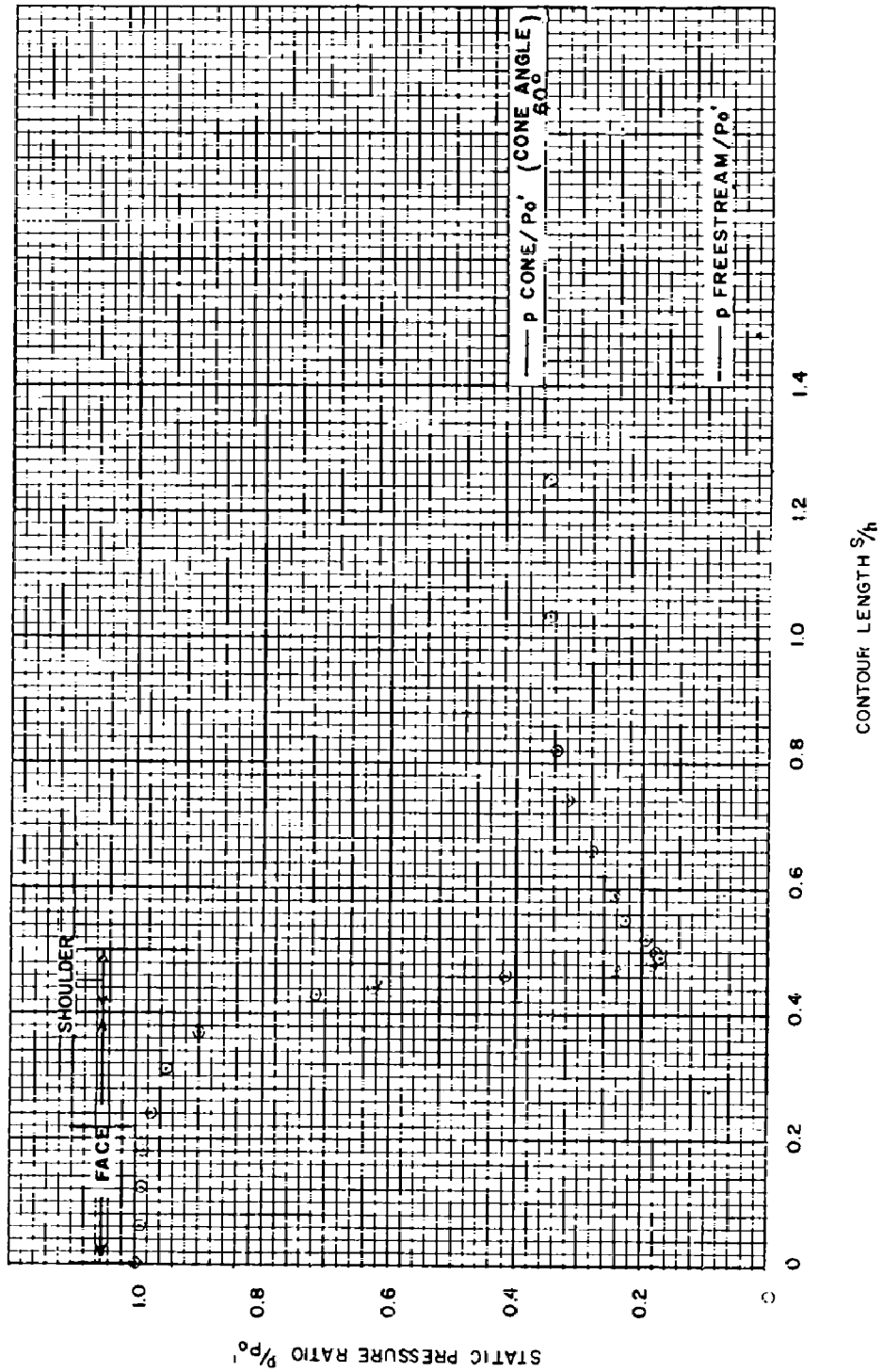


FIG.10 THE STATIC PRESSURE DISTRIBUTION ON BODY # 3 AT  $M=2.88$   
 $\epsilon=0^\circ$

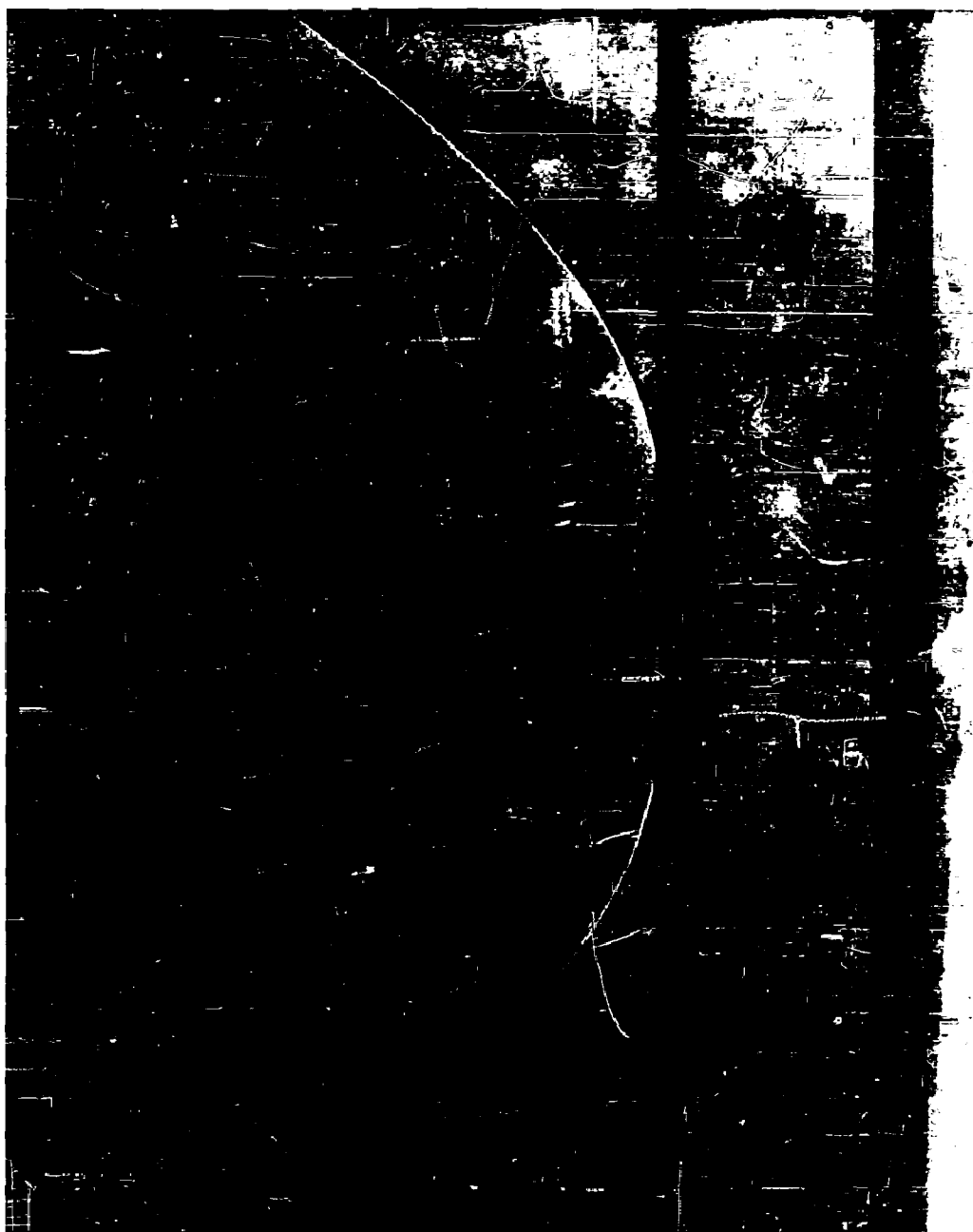


FIG. 10a SHADOWGRAPH OF BODY #3 AT  $M = 2.88$ ,  $\epsilon = 0^\circ$

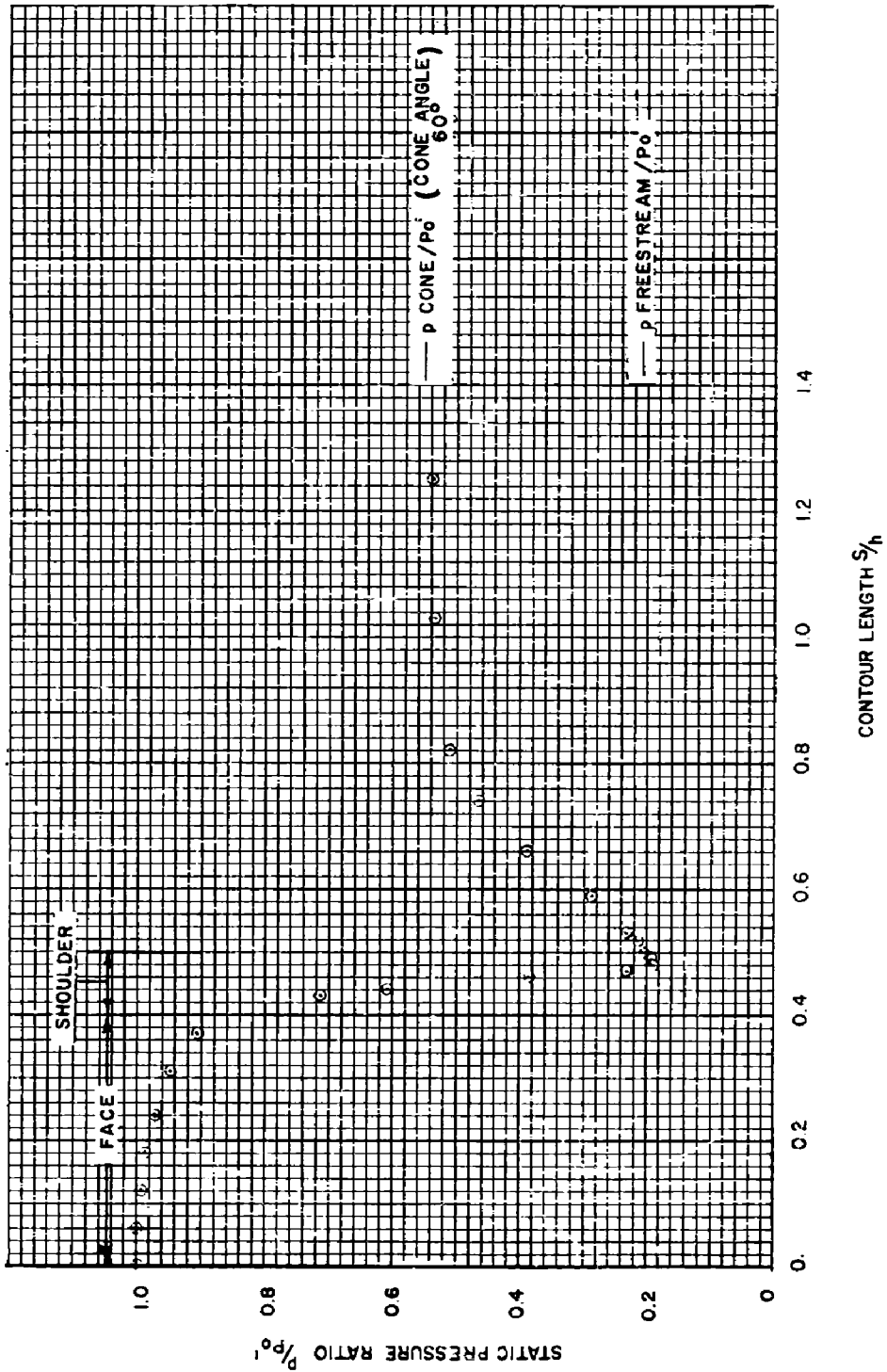


FIG. 11 THE STATIC PRESSURE DISTRIBUTION ON BODY # 3 AT  $M=1.79$   
 $\epsilon=0^\circ$

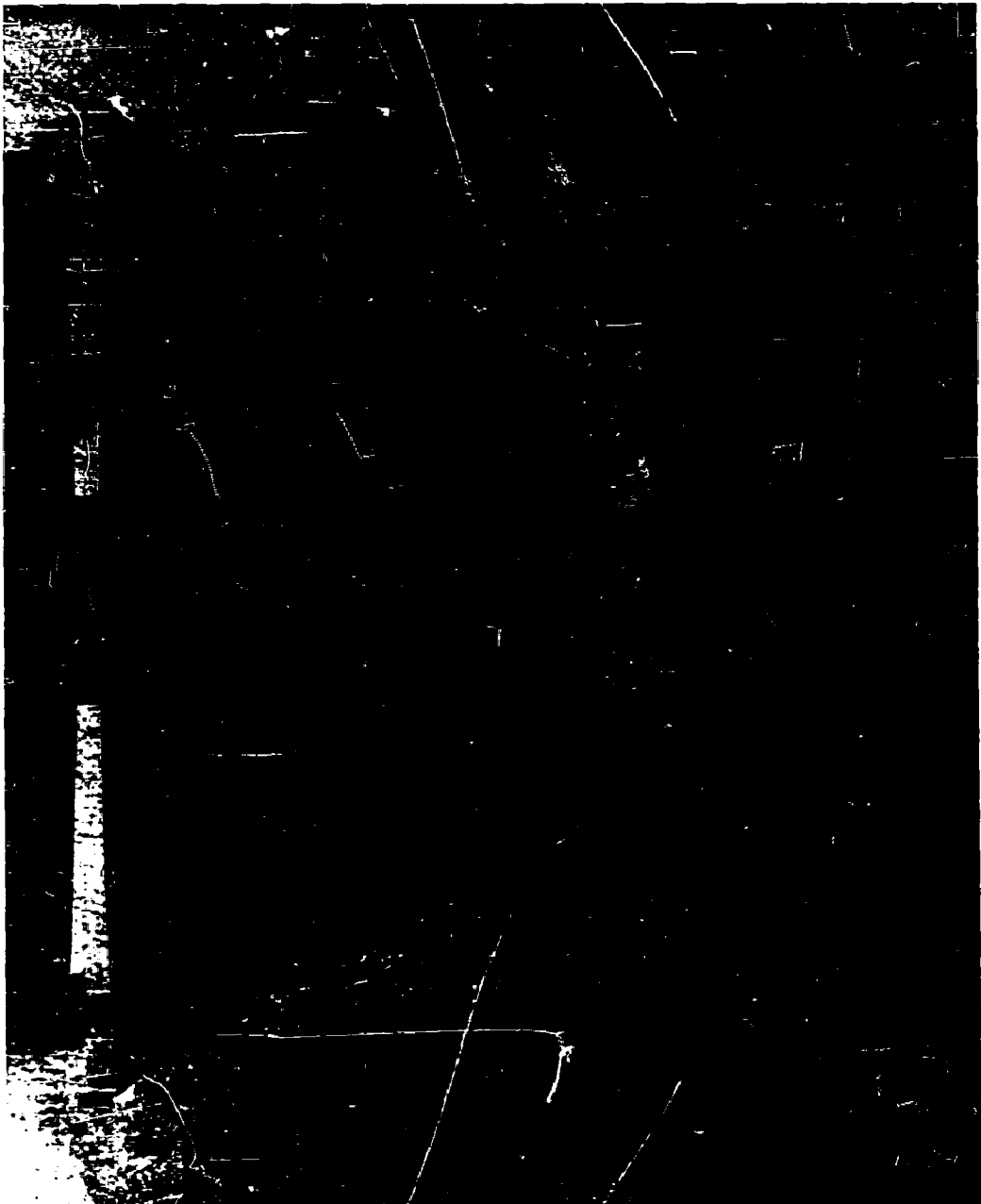


FIG. IIc SHADOWGRAPH OF BODY #3 AT  $M = 1.79$ ,  $\alpha = 3^\circ$

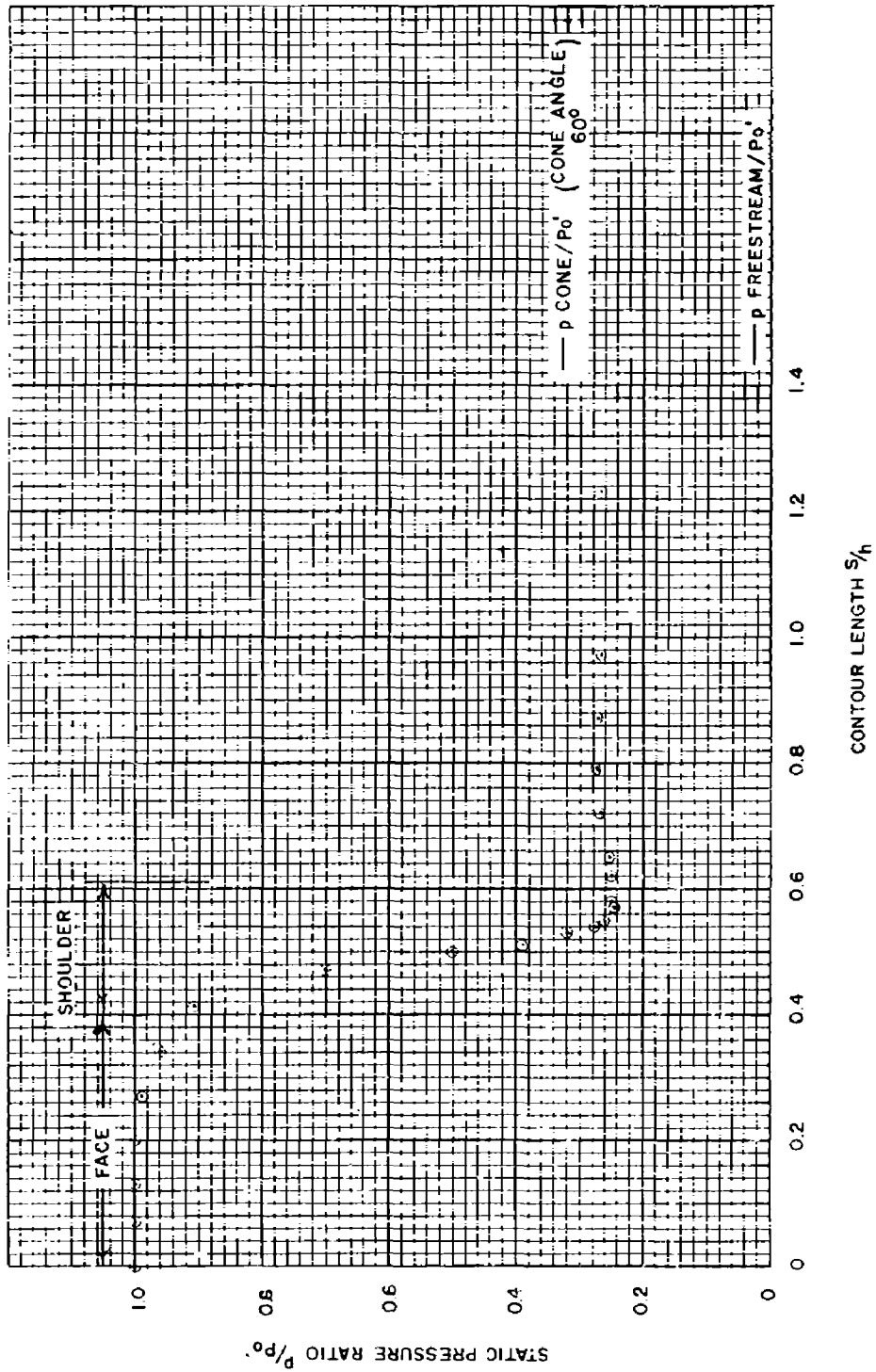


FIG.12 THE STATIC PRESSURE DISTRIBUTION ON BODY #4 AT  $M=4.84$   
 $\epsilon=0^\circ$

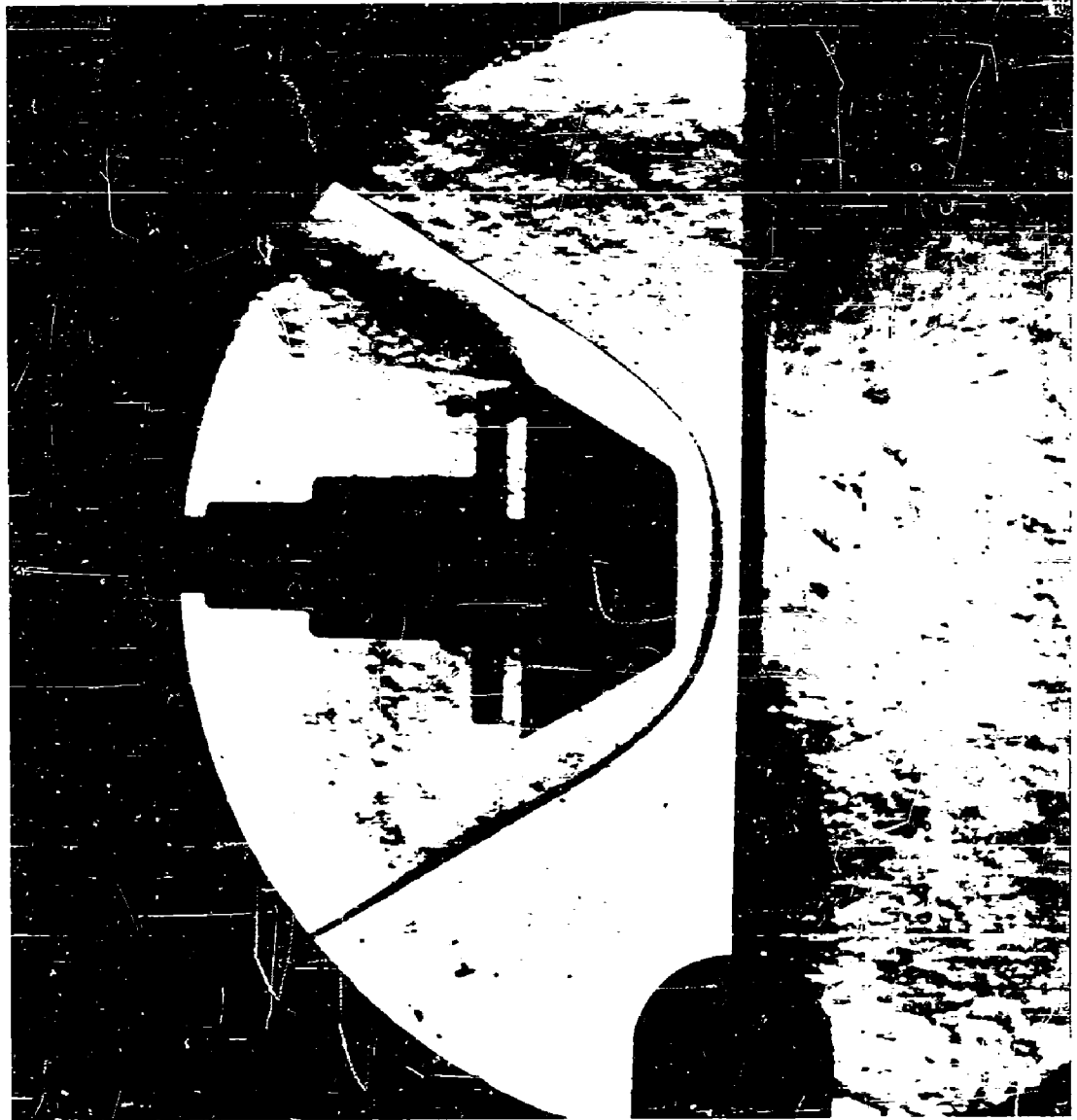


FIG. 12a SCHLIEREN PHOTOGRAPH OF BODY #4 AT  $M = 4.84$ ,  $\epsilon = 0^\circ$

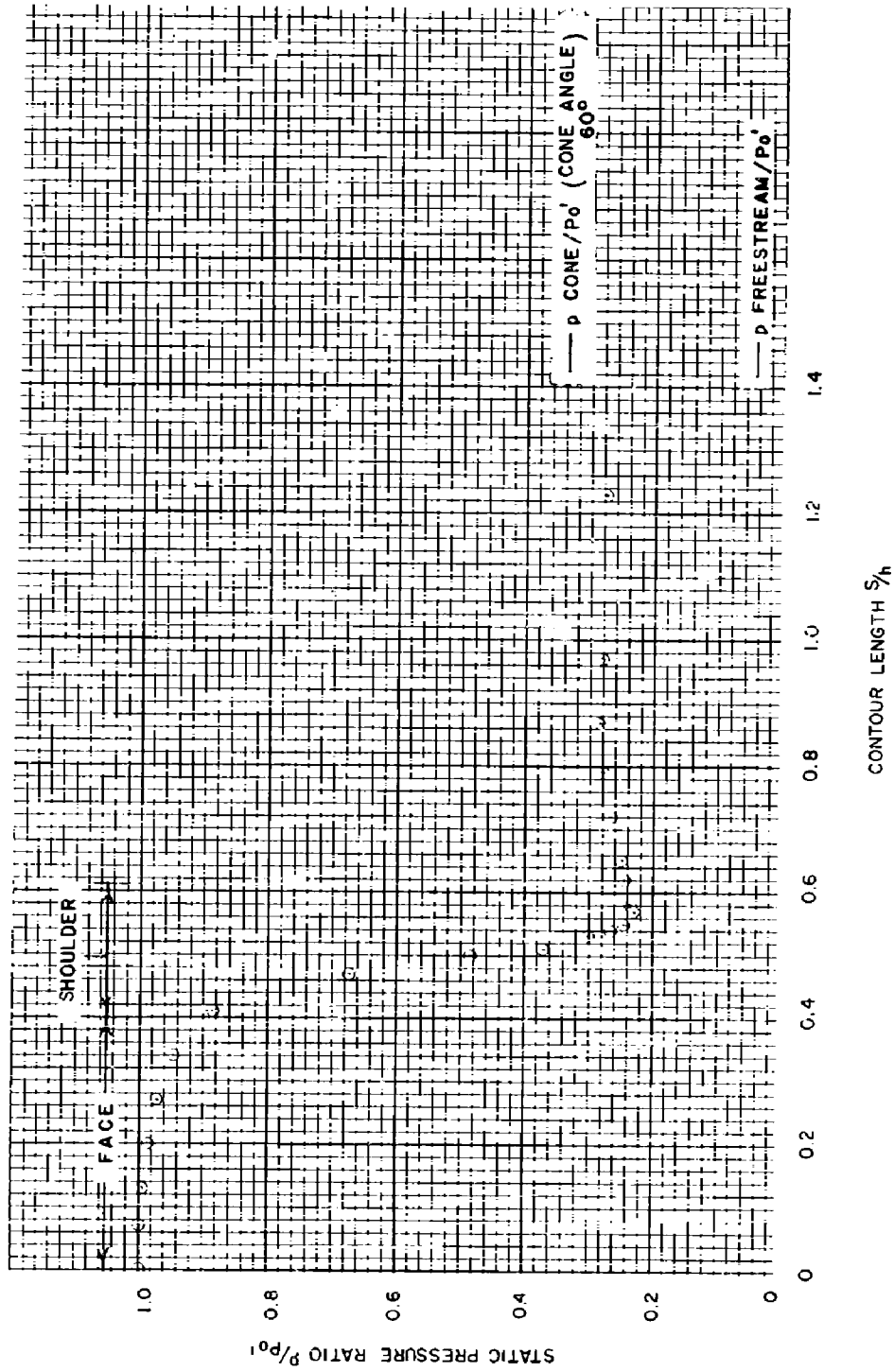


FIG. 13 THE STATIC PRESSURE DISTRIBUTION ON BODY # 4 AT  $M=4.2$   
 $\epsilon=0^\circ$



FIG. 14 THE STATIC PRESSURE DISTRIBUTION ON BODY #4 AT  $M=2.88$   
 $\epsilon=0^\circ$

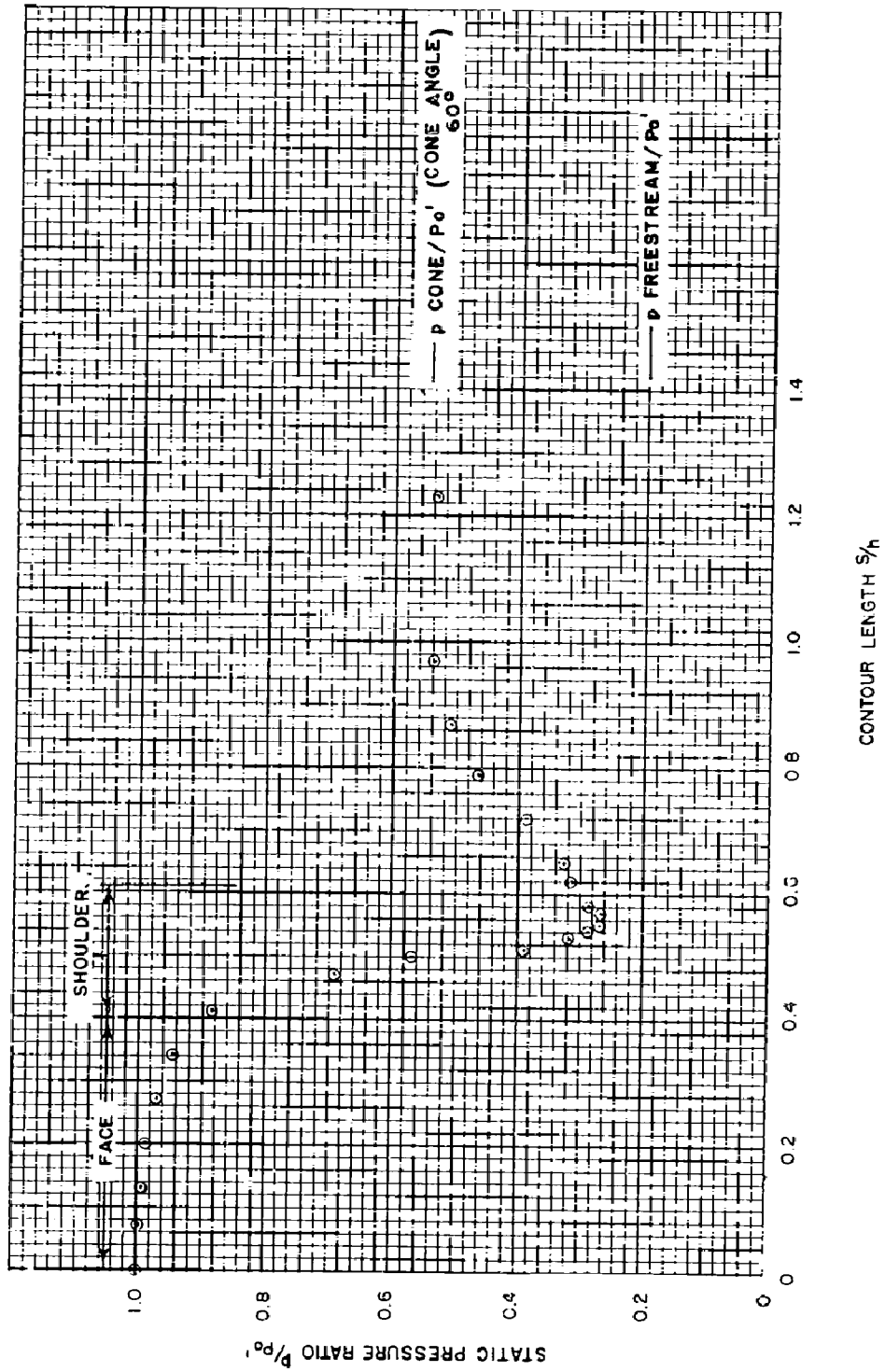


FIG. 15 THE STATIC PRESSURE DISTRIBUTION ON BODY #4 AT  $M=1.79$   
 $\epsilon=0^\circ$

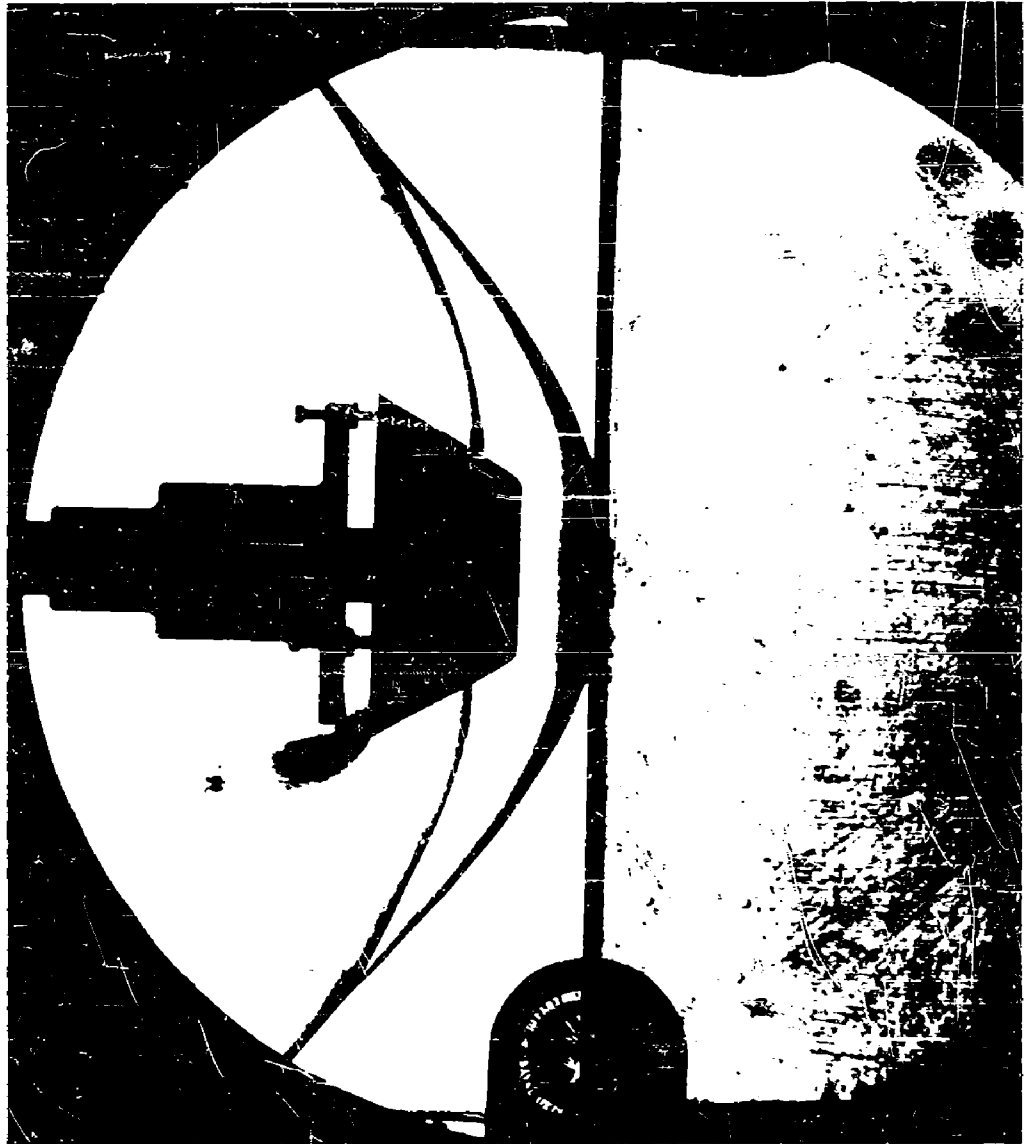


FIG. 15a SCHLIEREN PHOTOGRAPH OF BODY #4 AT  $M=1.79$ ,  $\epsilon = 0^\circ$

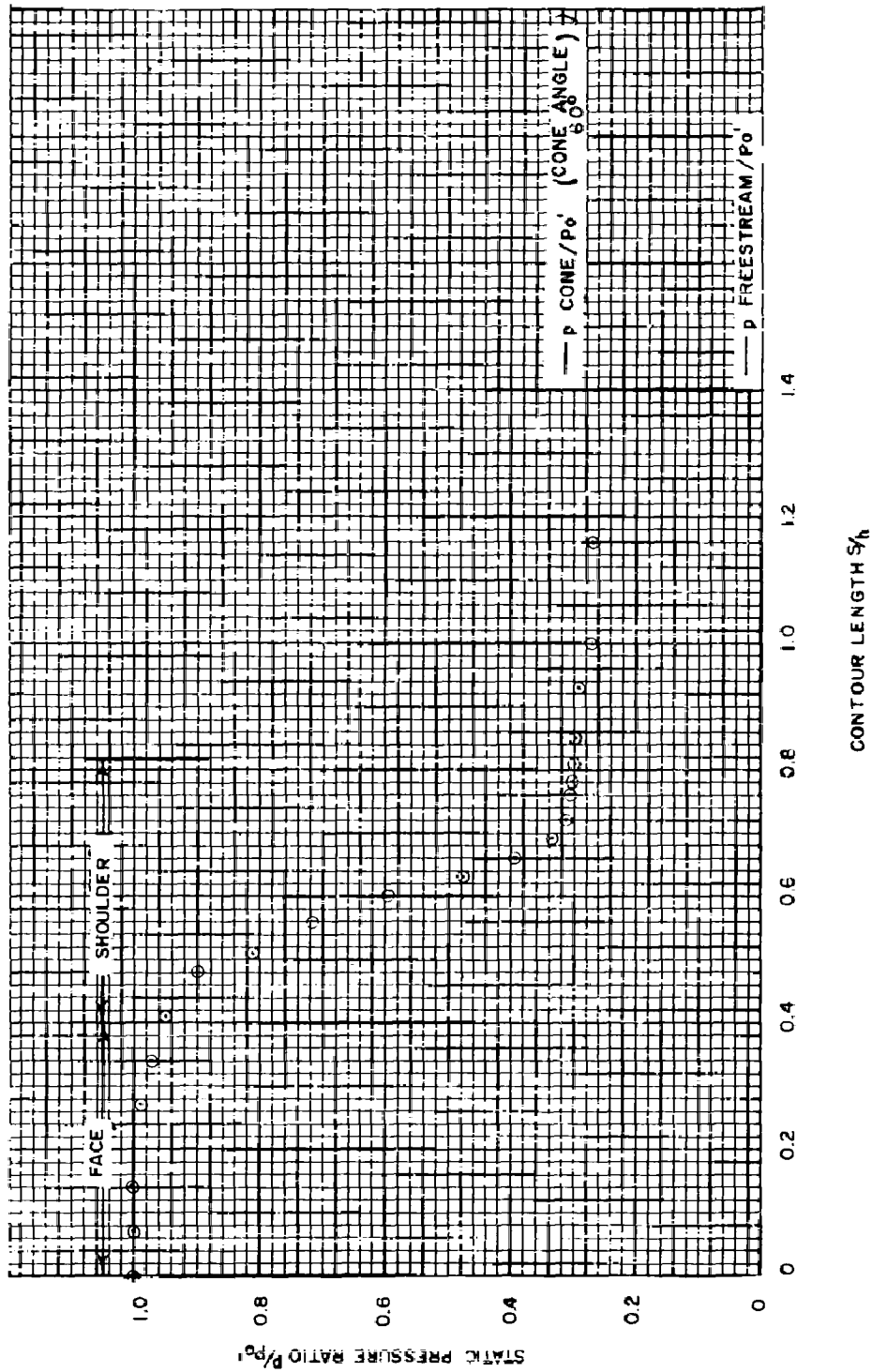


FIG. 16 THE STATIC PRESSURE DISTRIBUTION ON BODY # 5 AT  $M=4.84$   
 $\epsilon=0^\circ$

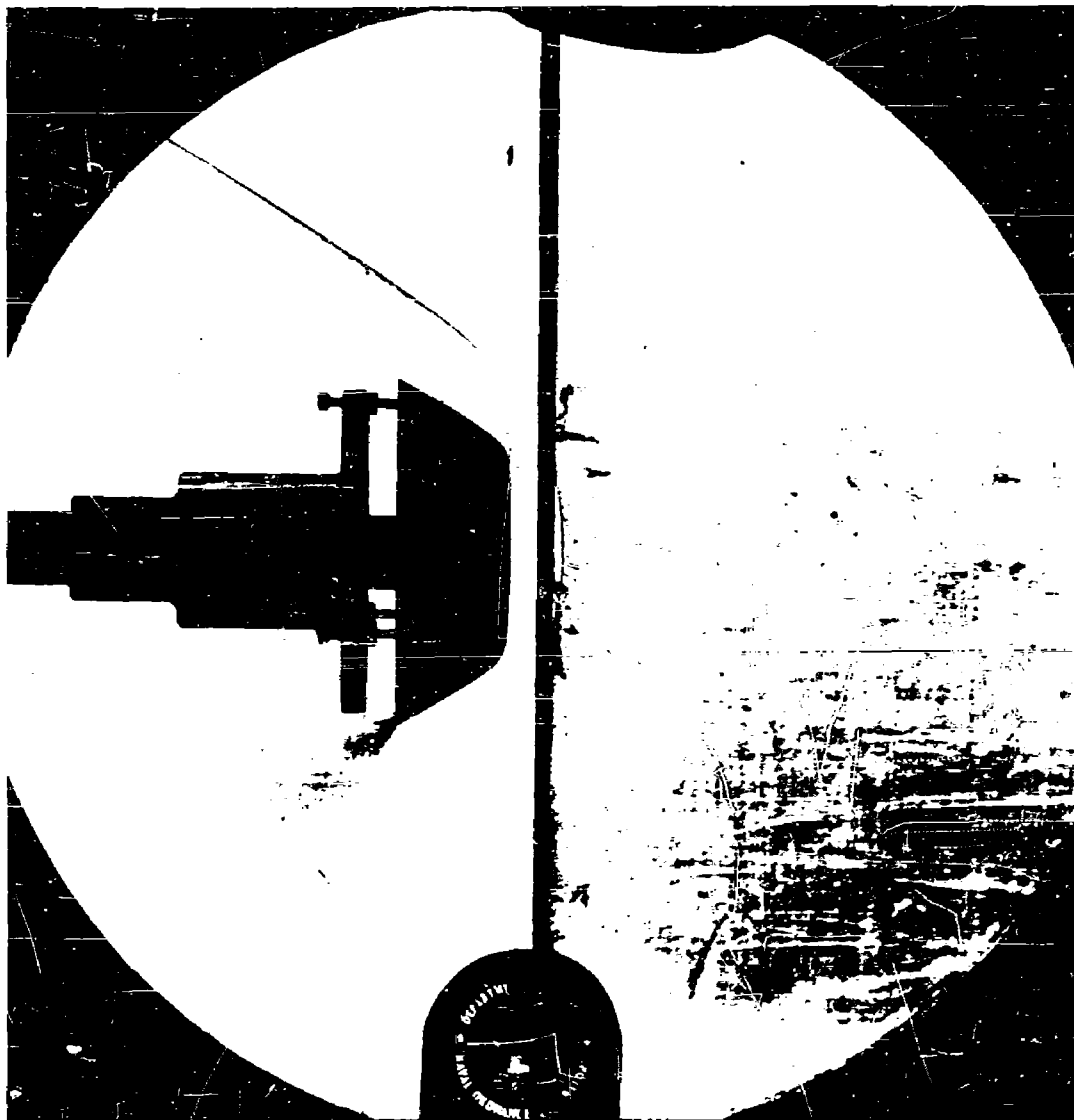


FIG. 16a SCHLIEREN PHOTOGRAPH OF BODY #5 AT  $M = 4.84$ ,  $\epsilon = 0^\circ$

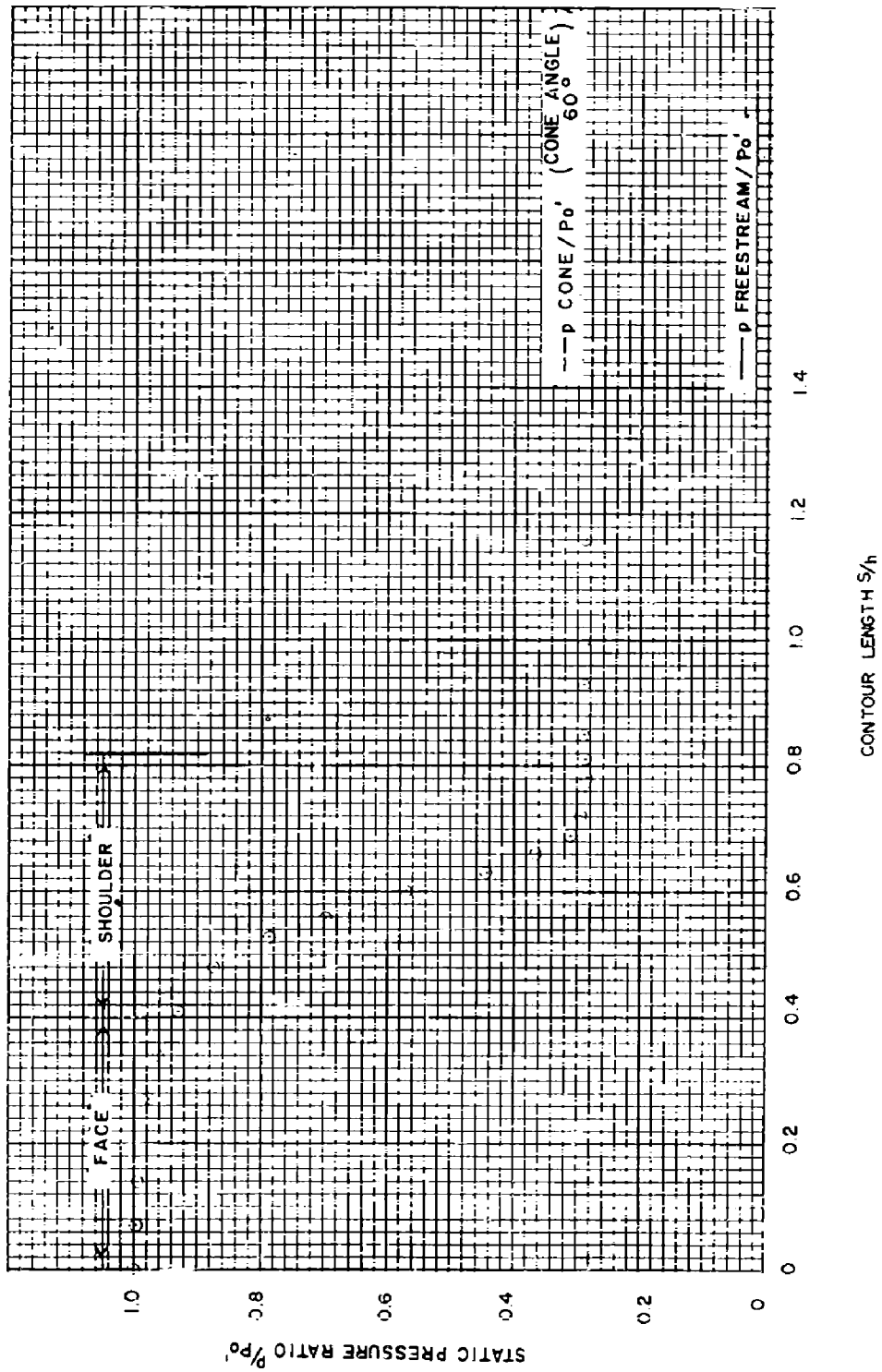


FIG. 17 THE STATIC PRESSURE DISTRIBUTION ON BODY # 5 AT  $M=4.12$   
 $\epsilon=0^\circ$

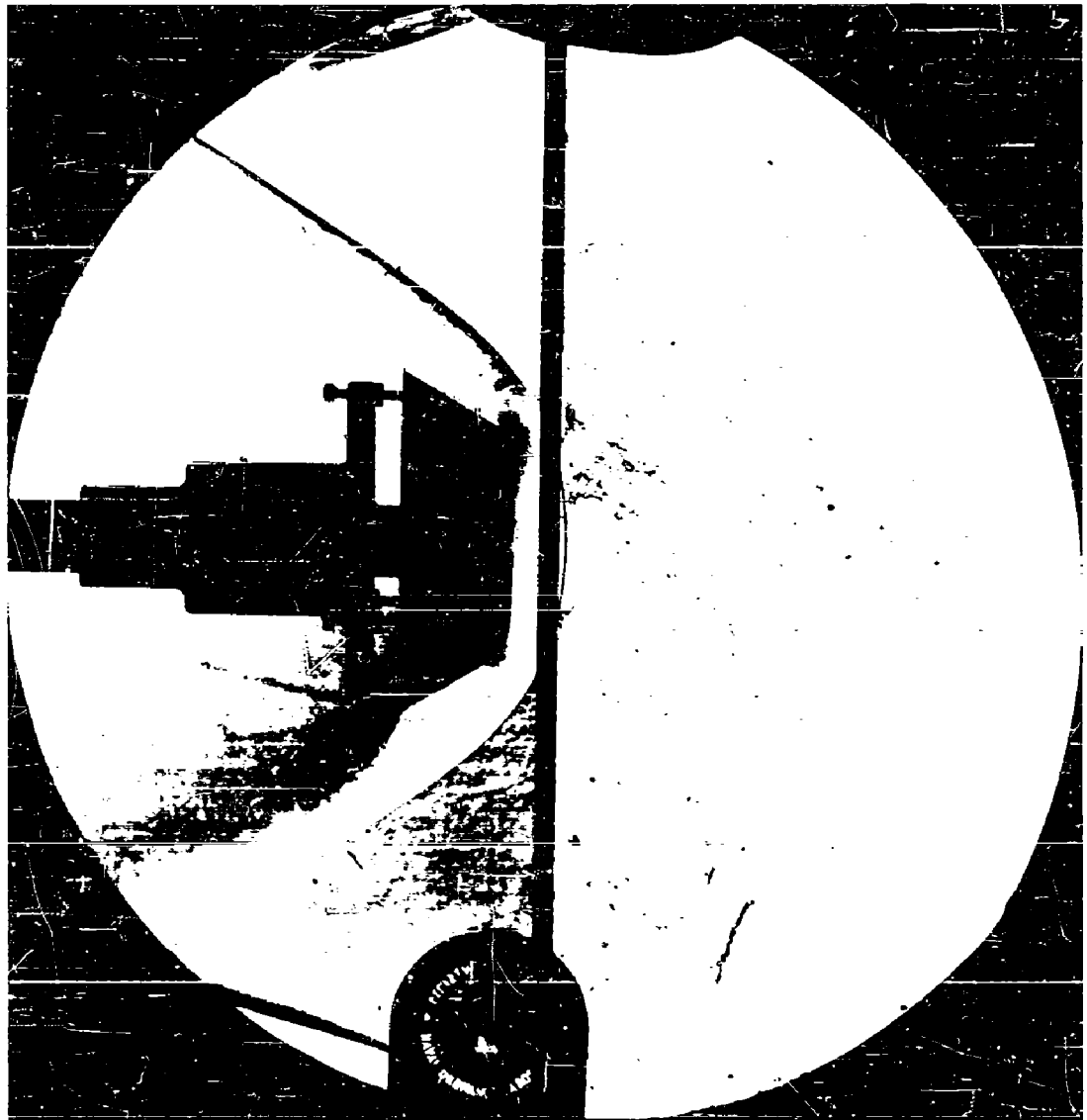


FIG. 17a SCHLIEREN PHOTOGRAPH OF BODY #5 AT  $M = 4.12$ ,  $\epsilon = 0^\circ$

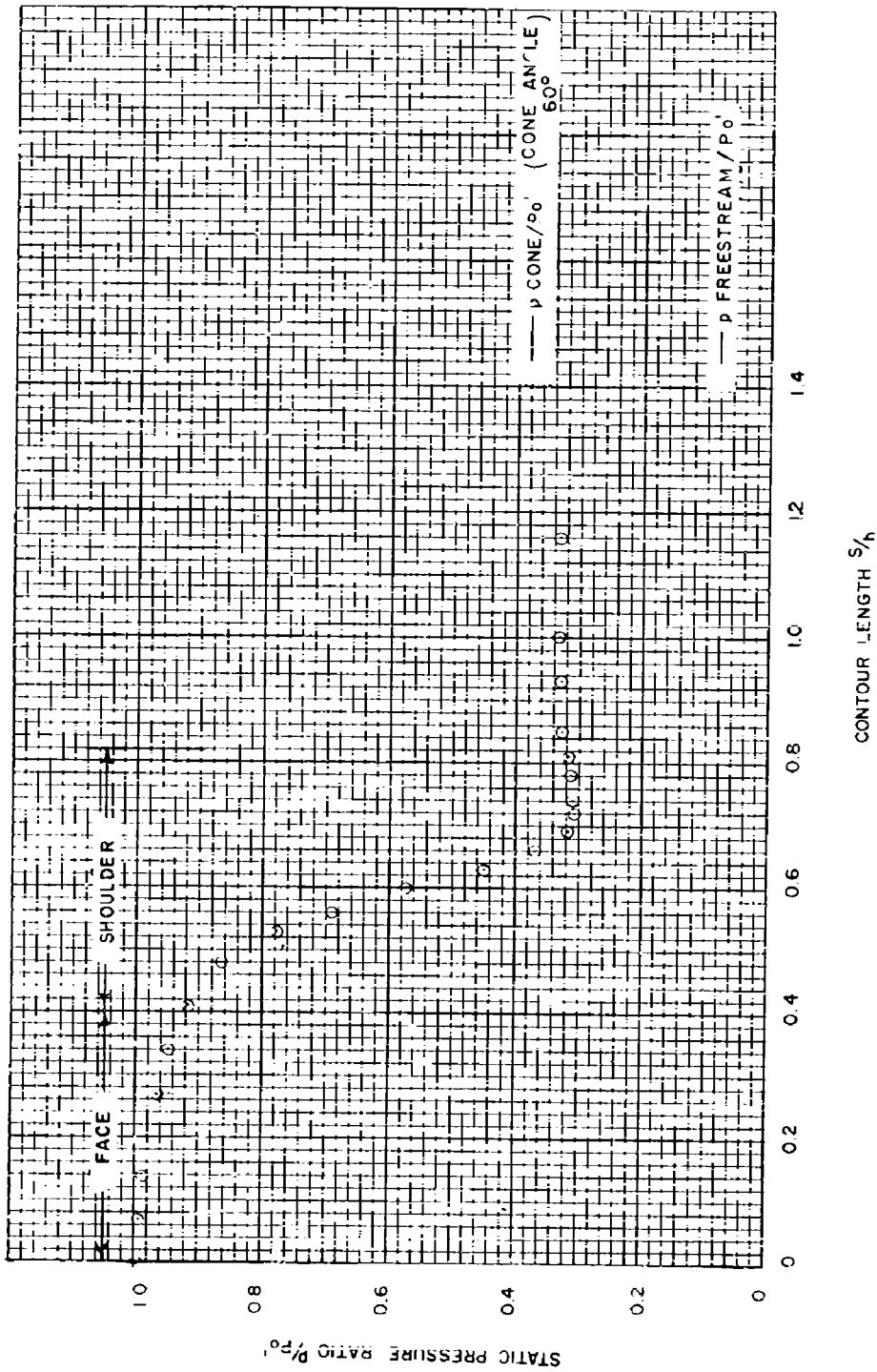


FIG.18 THE STATIC PRESSURE DISTRIBUTION ON BODY #5 AT  $M=2.88$   
 $\epsilon=0^\circ$

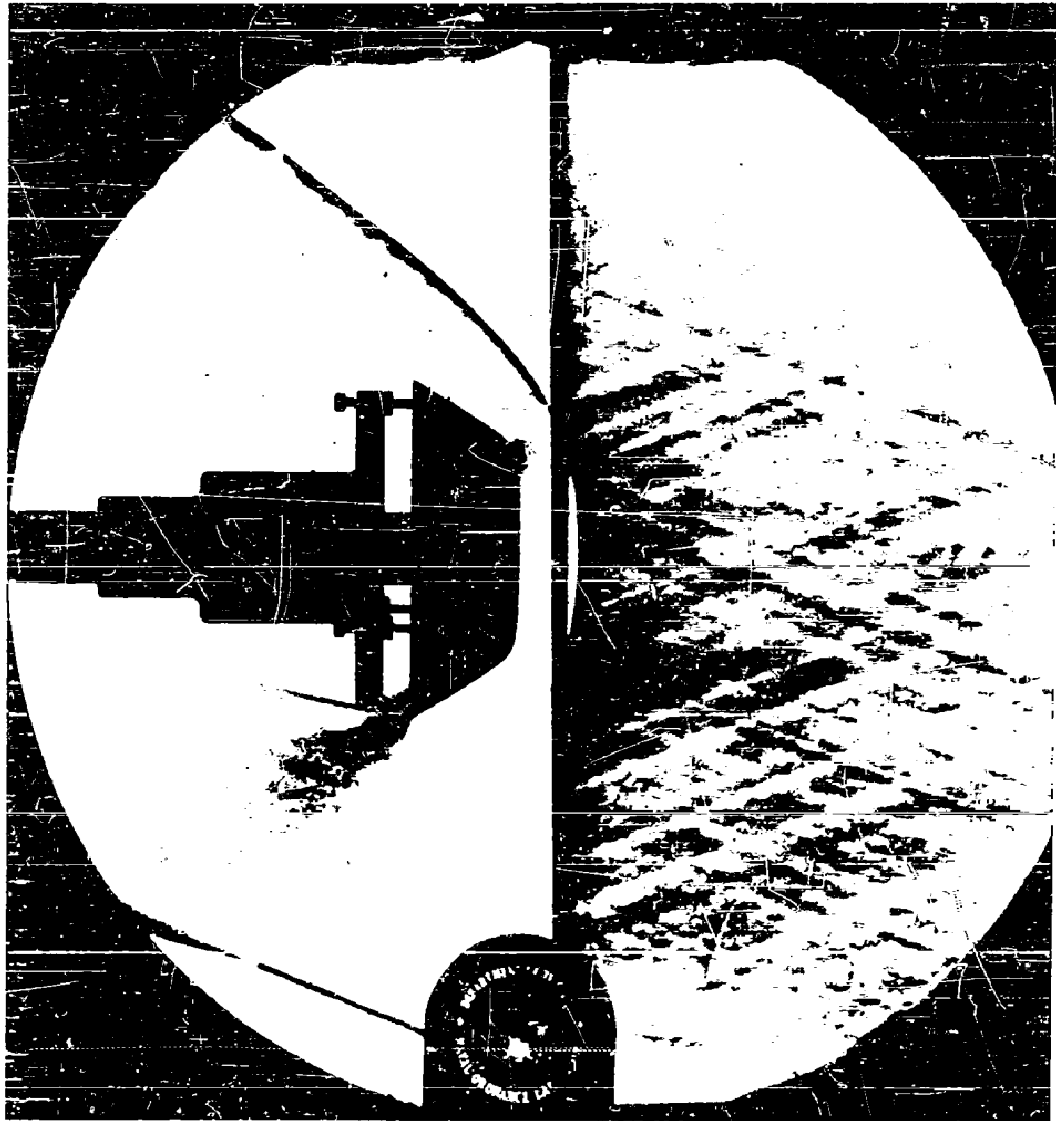


FIG. 18a SCHLIEREN PHOTOGRAPH OF BODY #5 AT  $M = 2.88$ ,  $\epsilon = 0^\circ$

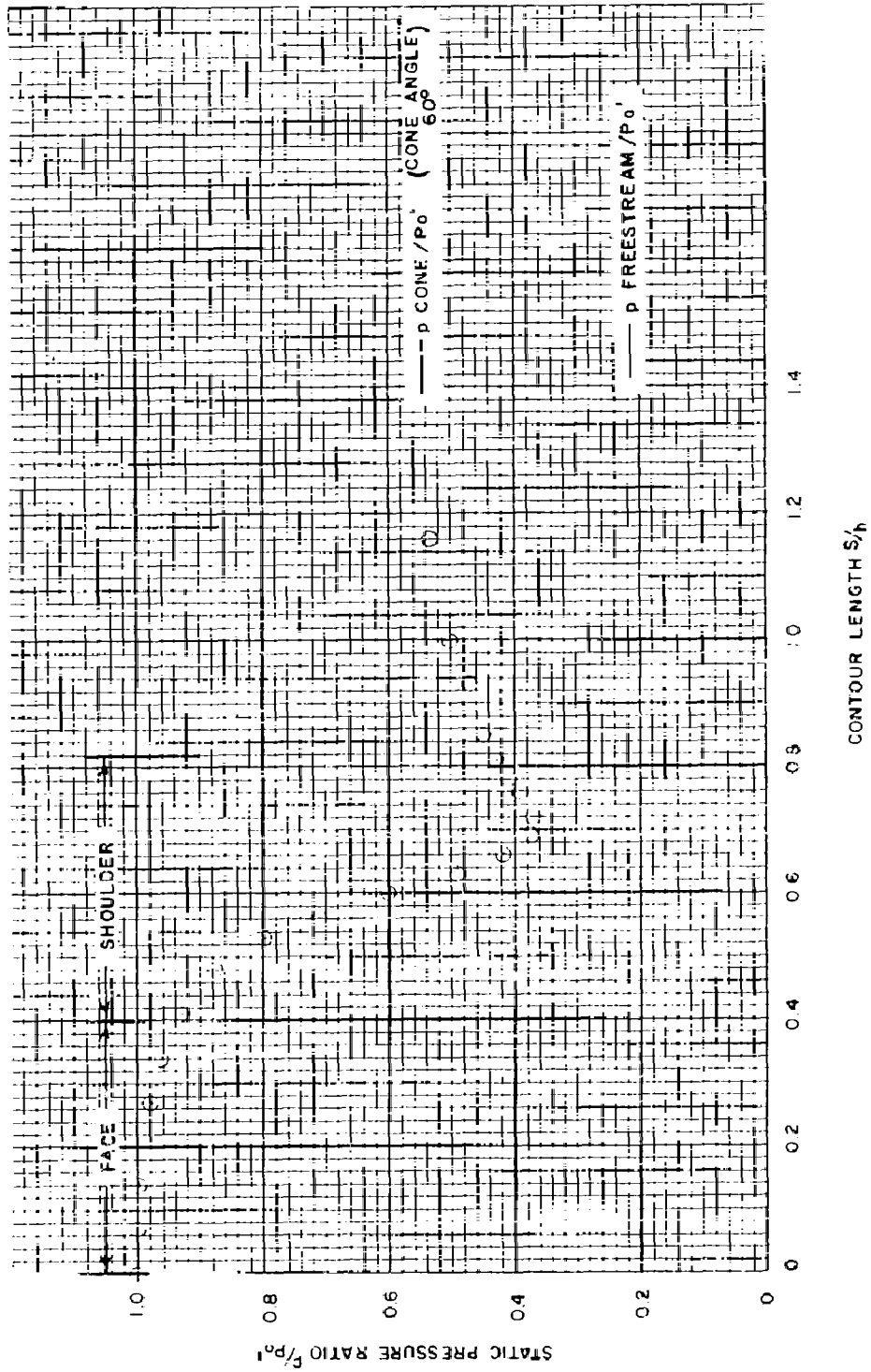


FIG. 19 THE STATIC PRESSURE DISTRIBUTION ON BODY # 5 AT  $M=1.79$   
 $\epsilon=0^\circ$

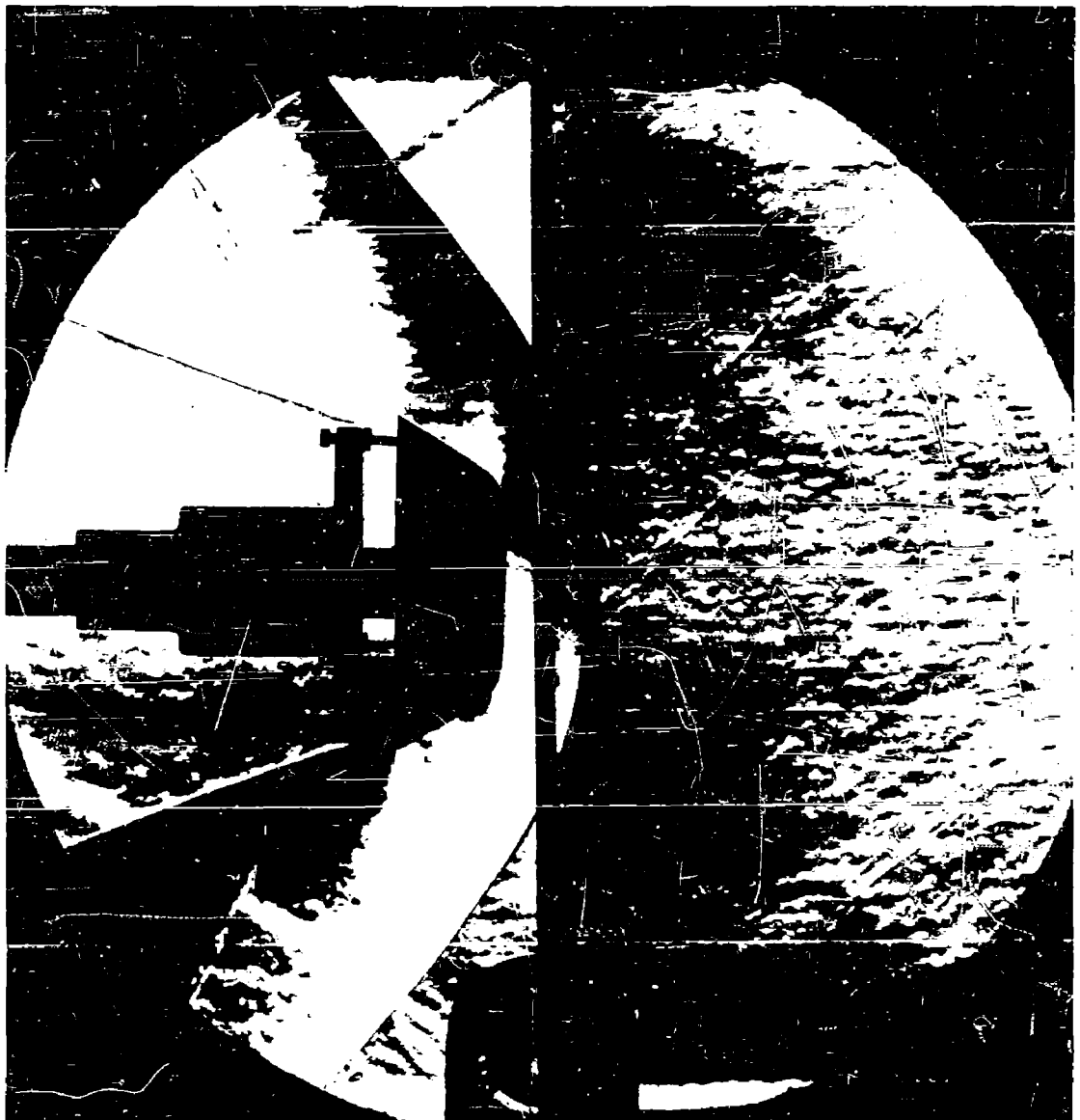


FIG. 19a SCHLIEREN PHOTOGRAPH OF BODY #5 AT  $M = 1.79$ ,  $\epsilon = 0^\circ$

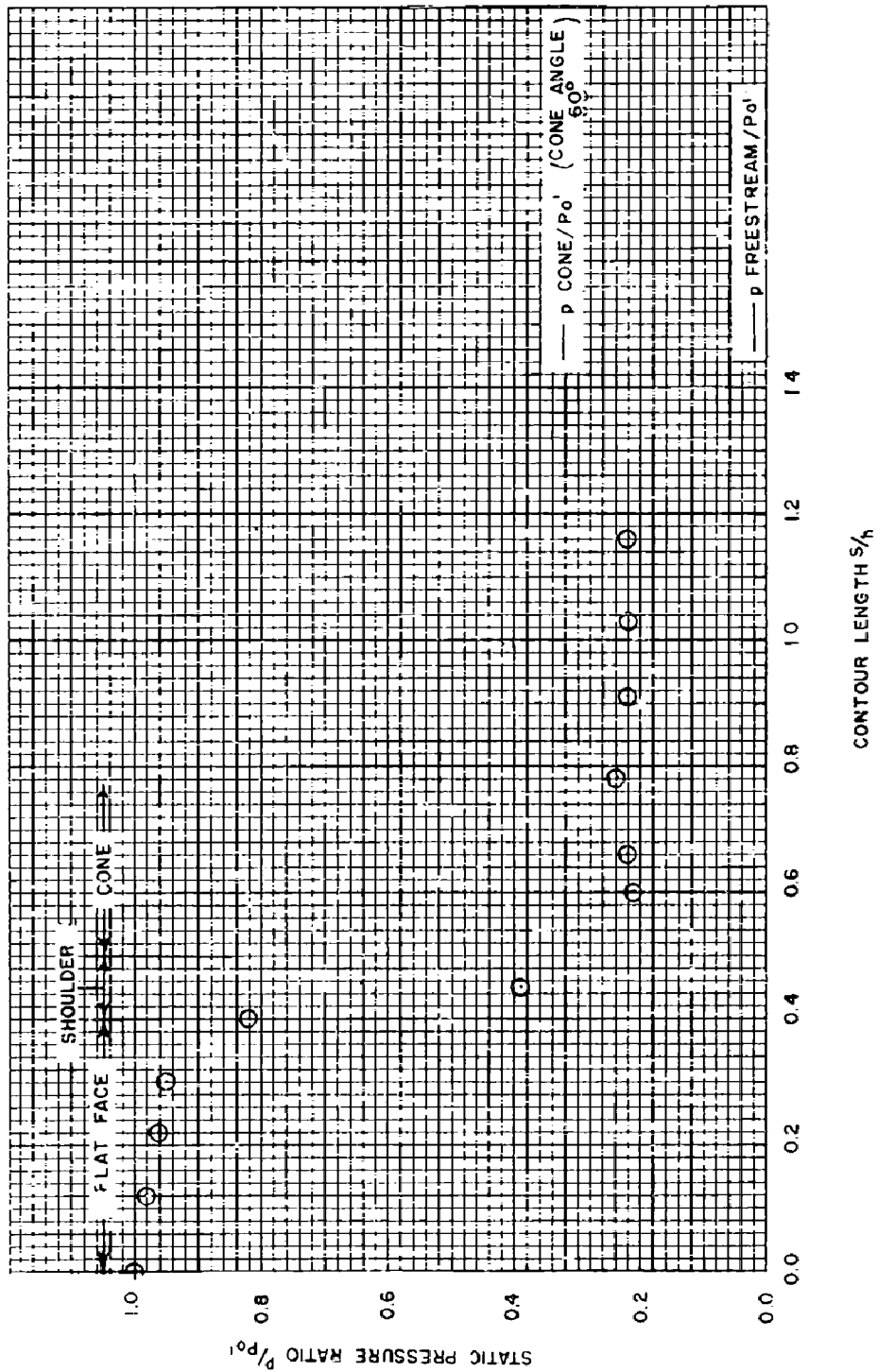


FIG.20 THE STATIC PRESSURE DISTRIBUTION ON BODY #6 AT  $M=5.1$   
 $\epsilon=0^\circ$

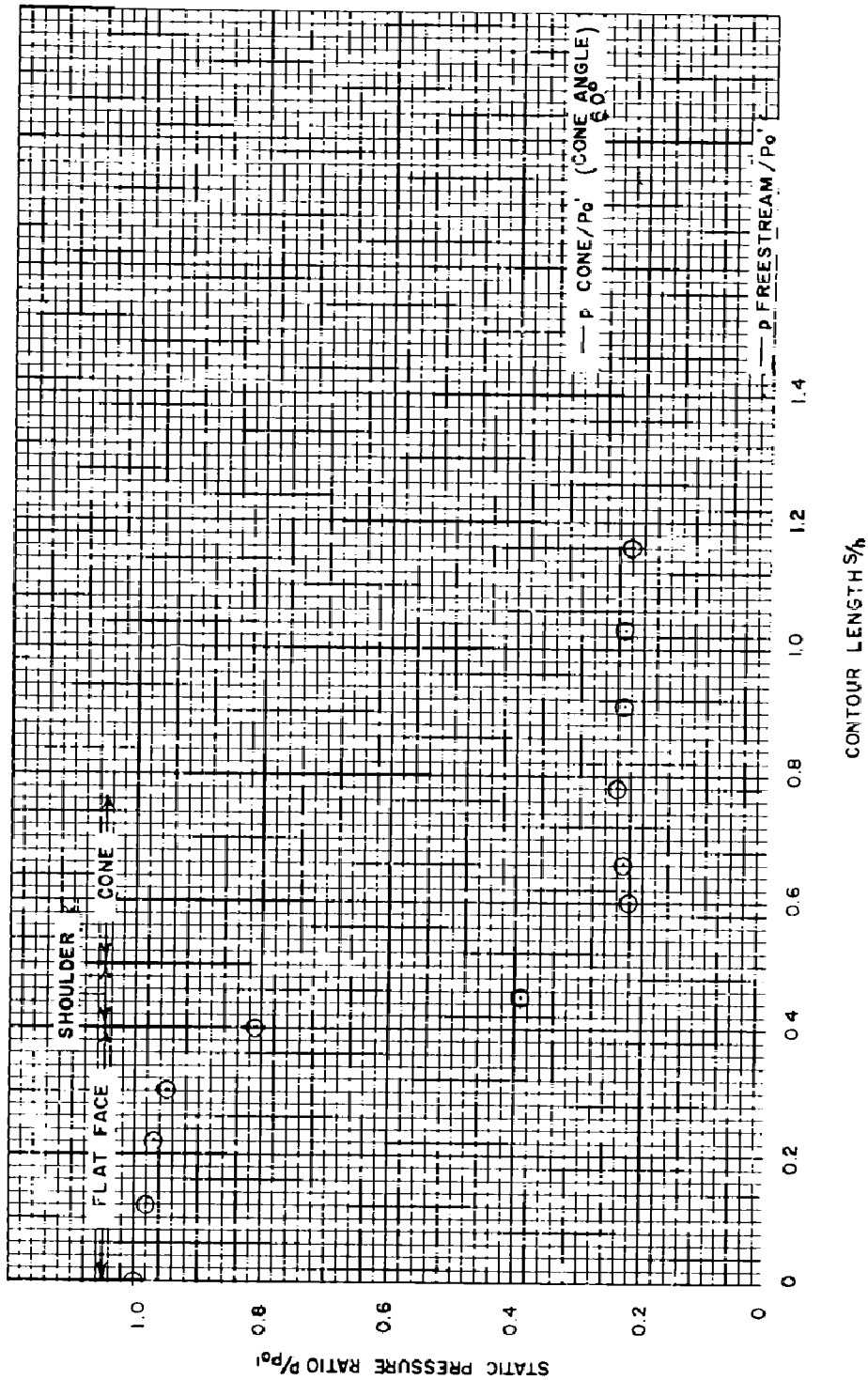


FIG. 21 THE STATIC PRESSURE DISTRIBUTION ON BODY # 6 AT  $M=6.4$   
 $\epsilon = 0^\circ$

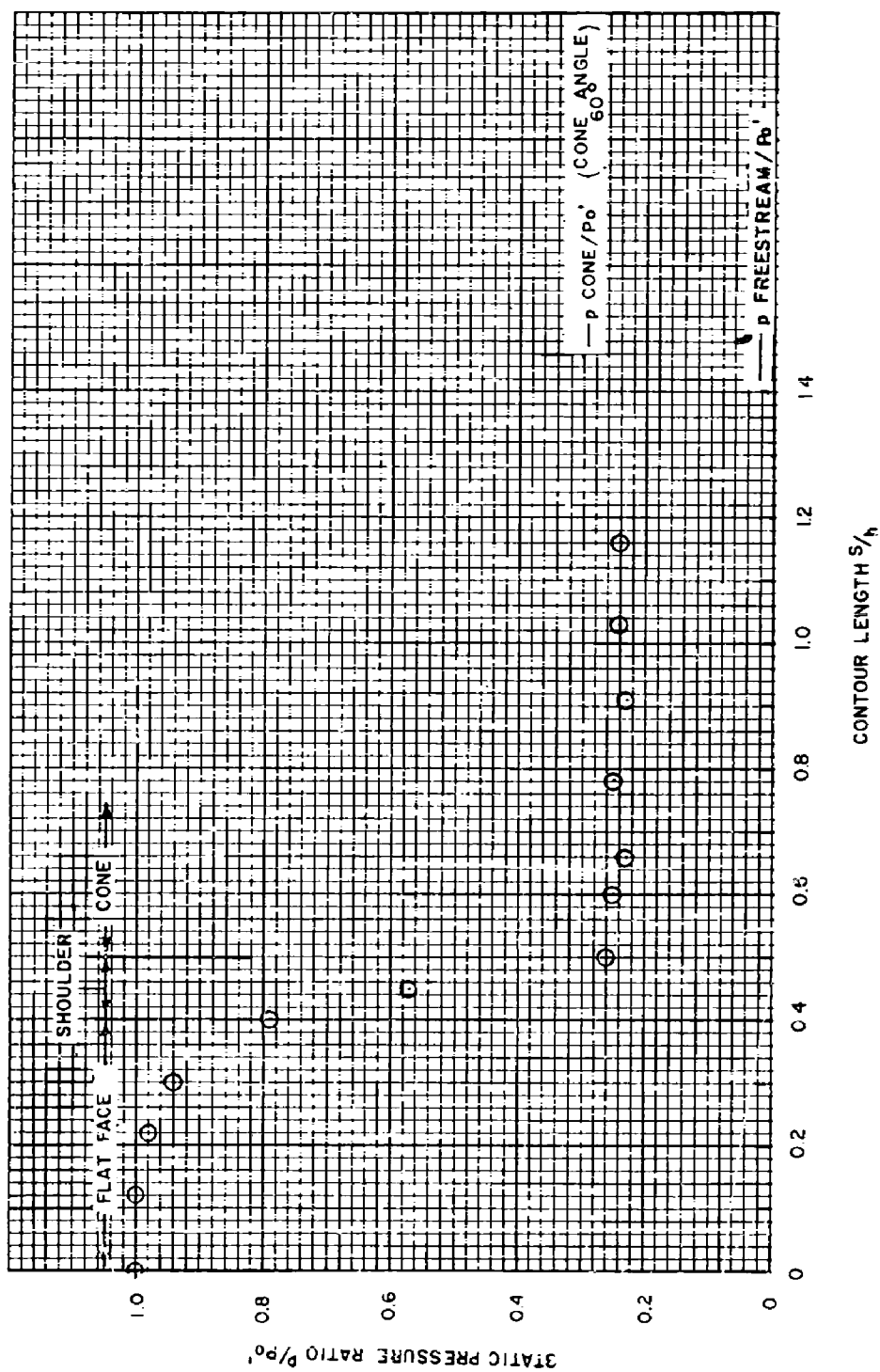


FIG. 22 THE STATIC PRESSURE DISTRIBUTION ON BODY # 6 AT  $M=7.2$   
 $\epsilon=0^\circ$

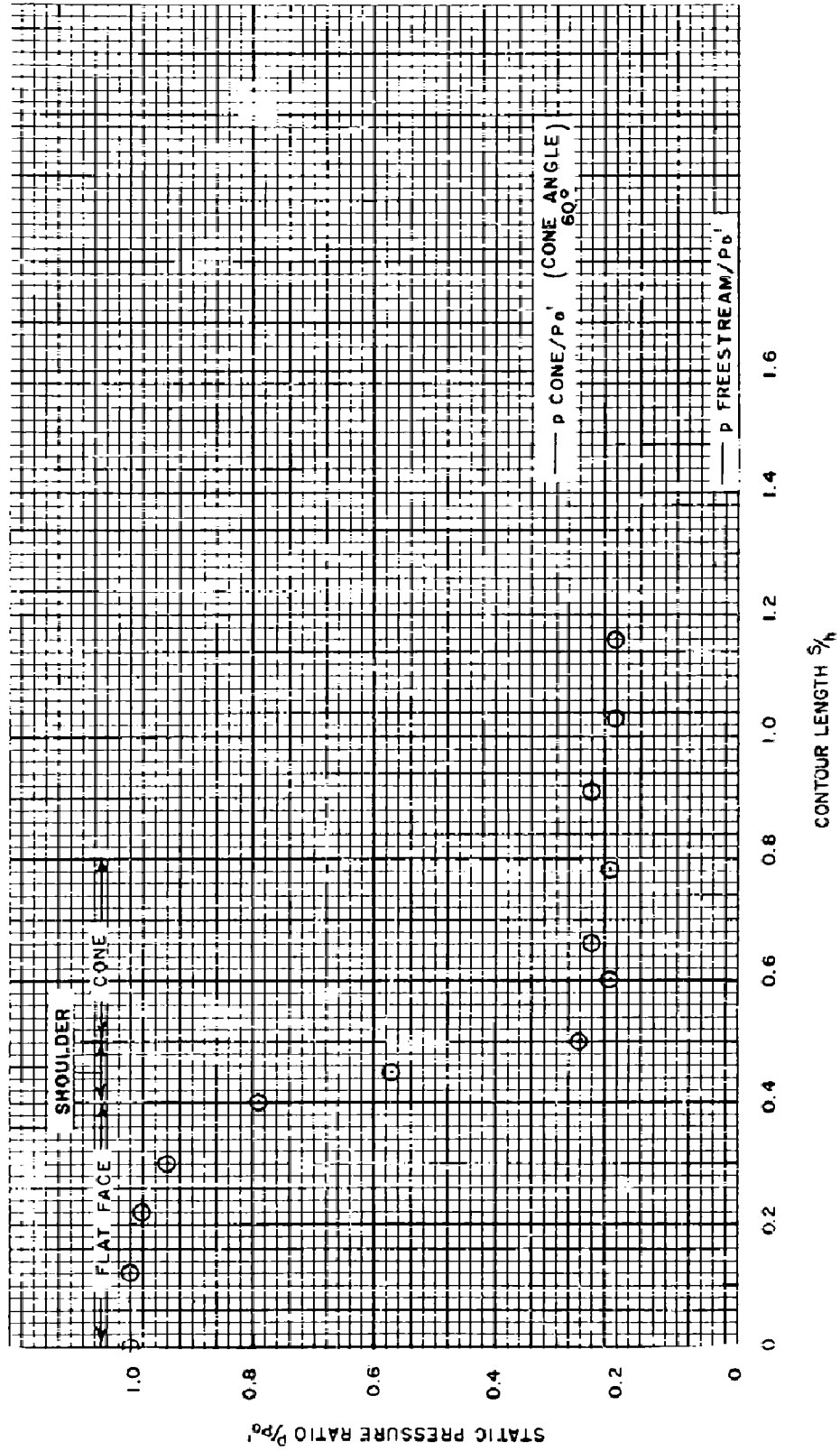


FIG. 23 THE STATIC PRESSURE DISTRIBUTION ON BODY #6 AT  $M = 8.1$   
 $\epsilon = 0^\circ$

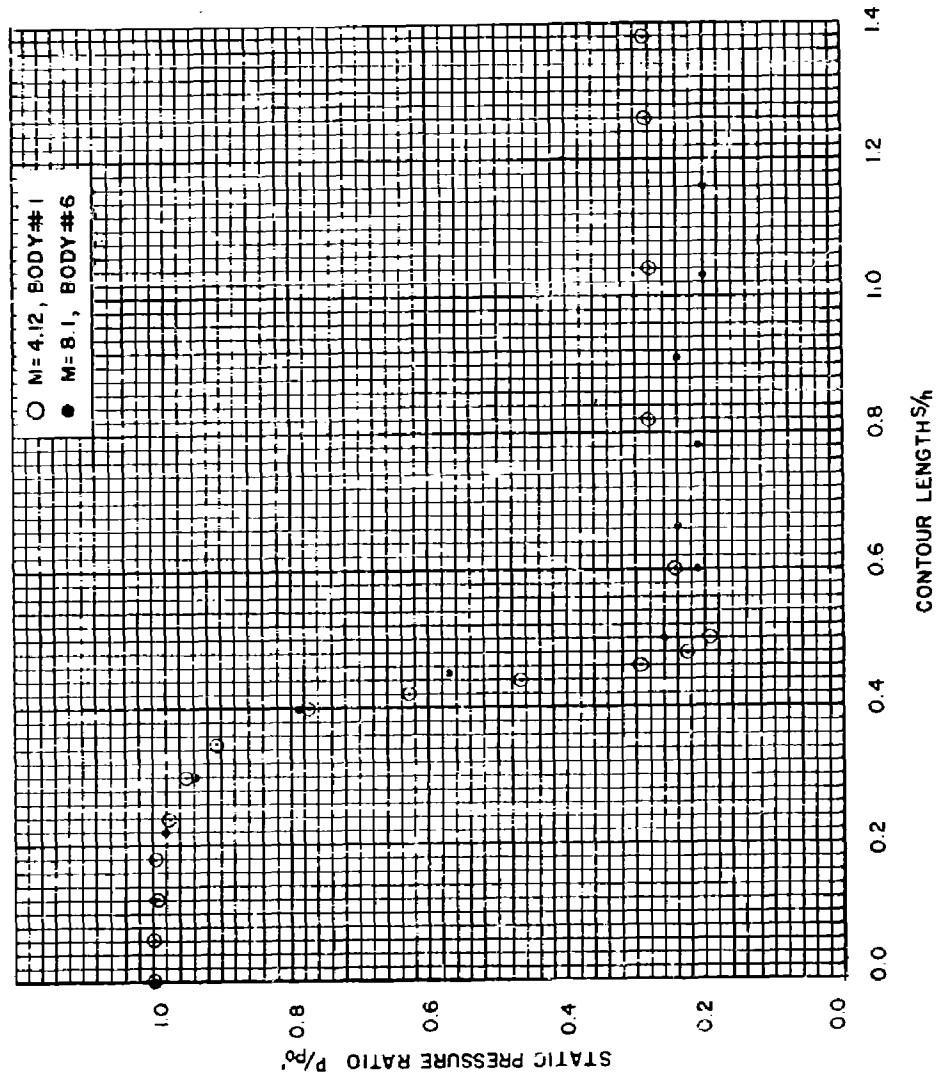


FIG. 24 THE EFFECT OF MACH NUMBER ON THE PRESSURE DISTRIBUTION ON GEOMETRICALLY SIMILAR BODIES  
(BODY #1 & BODY #6),  $\epsilon = 0^\circ$

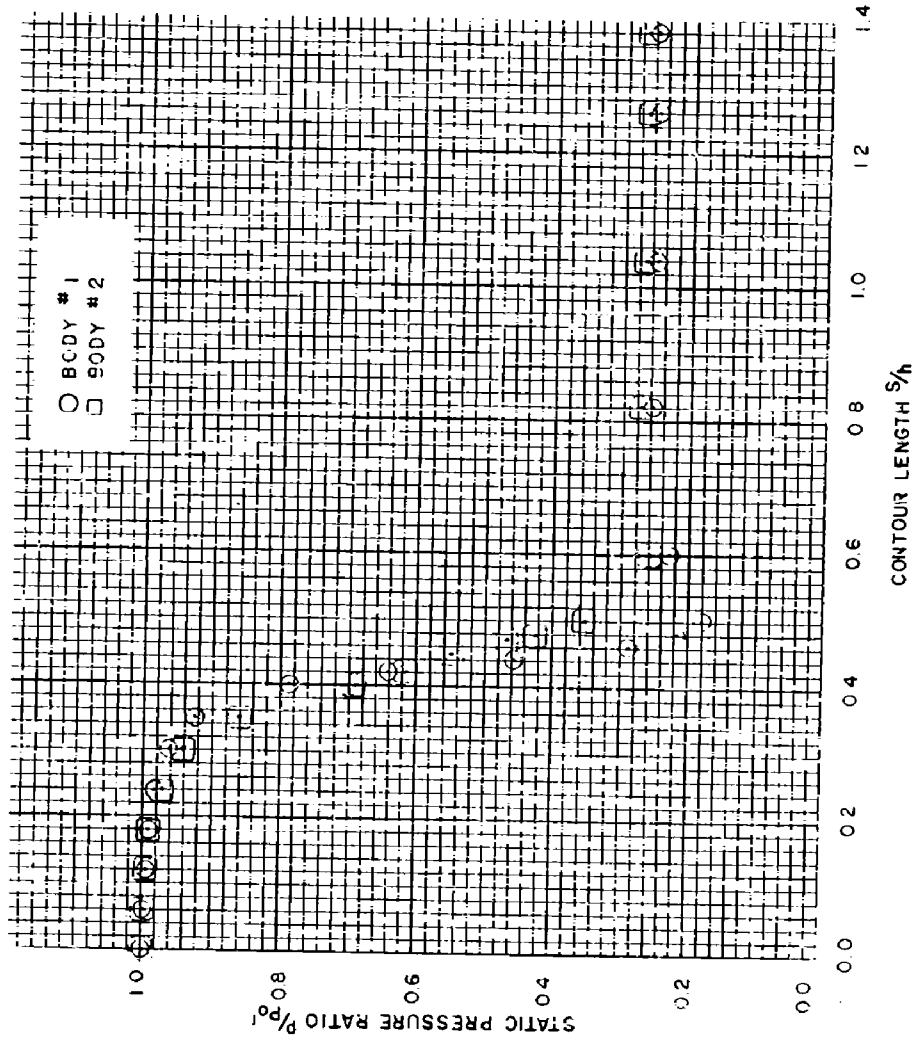


FIG. 25 THE EFFECT OF CORNER RADIUS ON PRESSURE DISTRIBUTION AT  $M=4.84$ , (BODY #1 AND BODY #2),  $\epsilon=0^\circ$

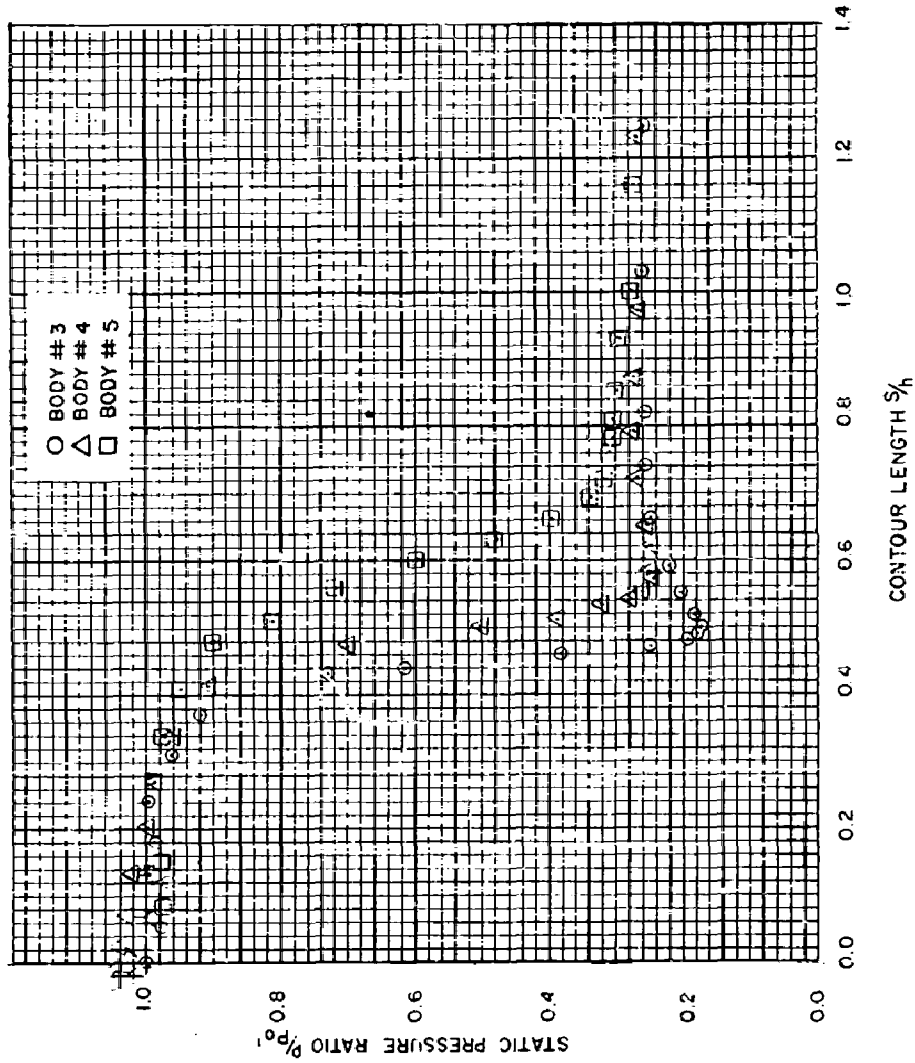


FIG. 26 THE EFFECT OF CORNER RADIUS ON PRESSURE DISTRIBUTION AT  $M=4.84$ , (BODIES #3, #4, AND #5),  $\epsilon=0^\circ$

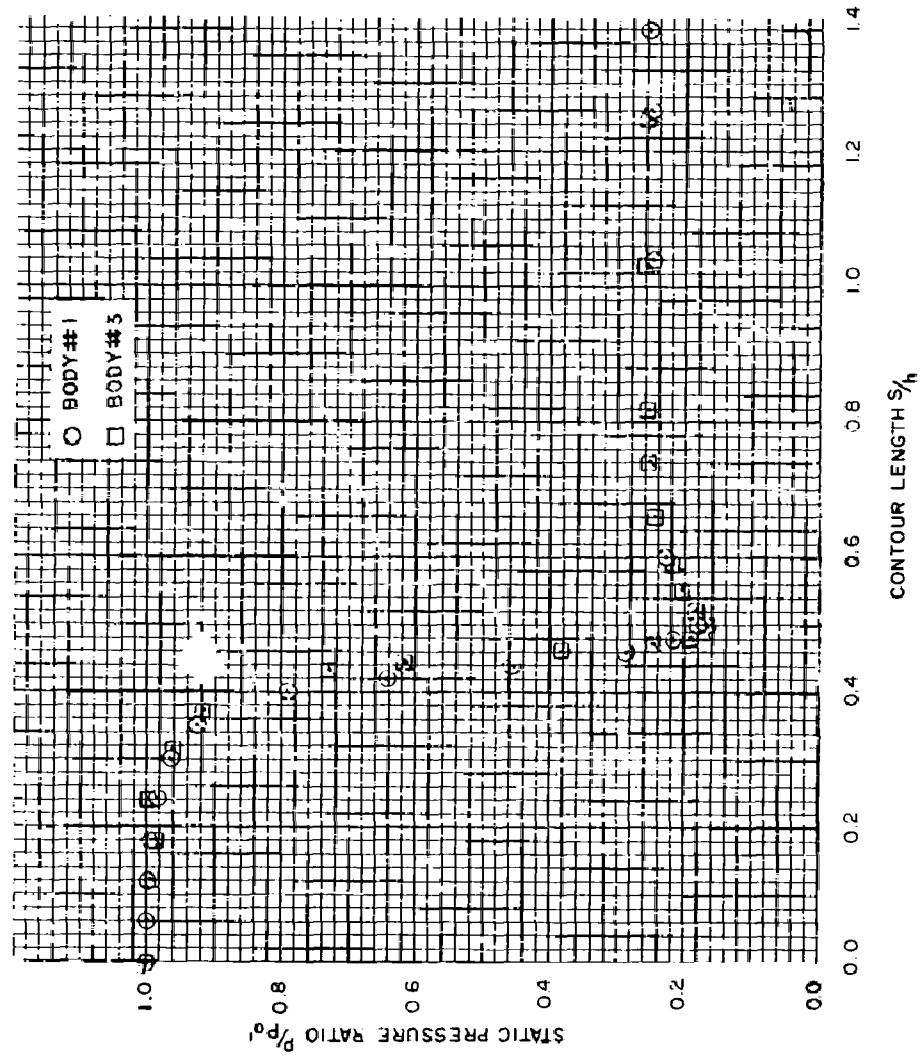


FIG. 27 THE EFFECT OF MODEL CURVATURE CONTINUITY  
ON PRESSURE DISTRIBUTION,  $M = 4.84$ , (BODY #1 AND BODY #3),  $\epsilon = 0^\circ$

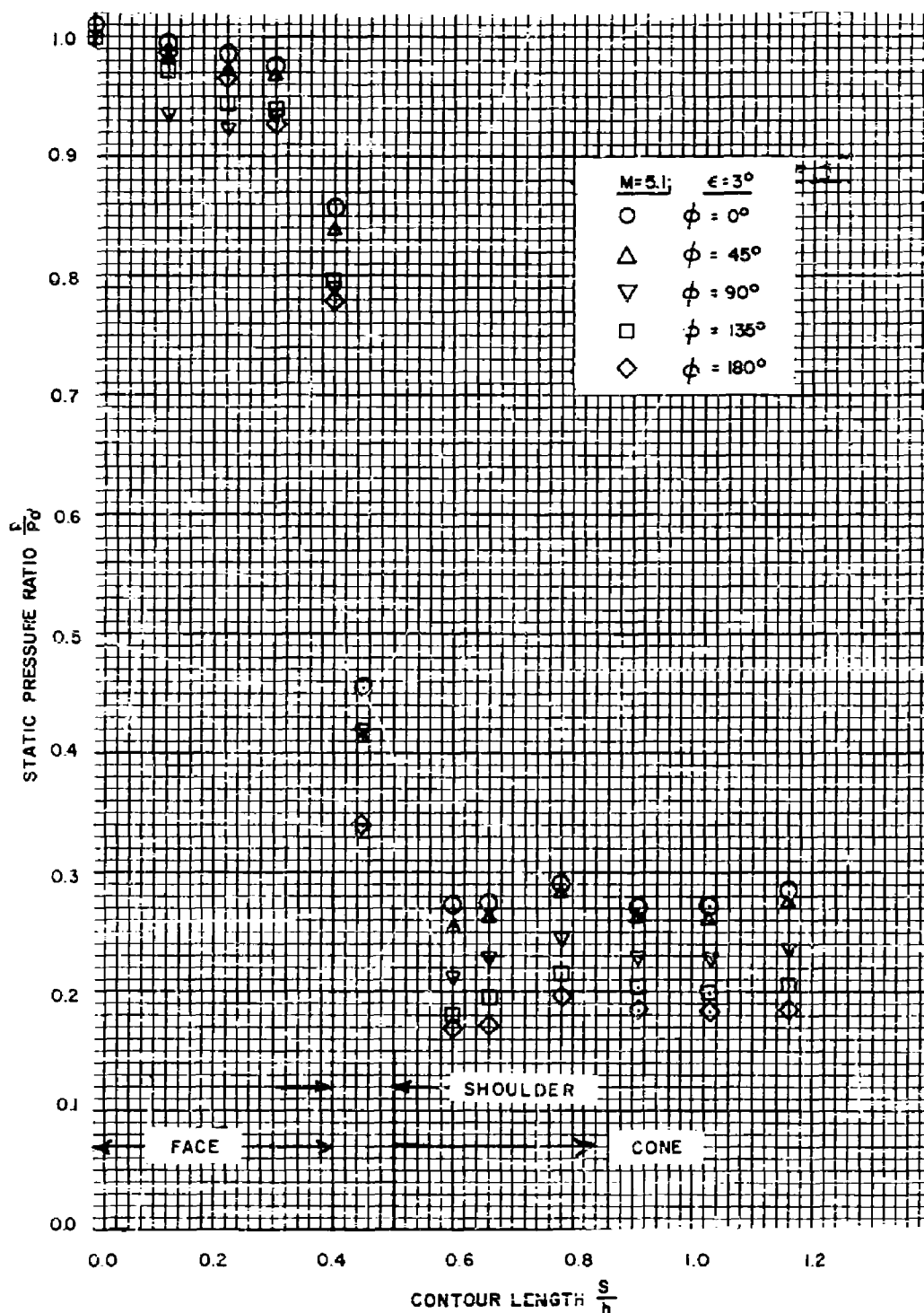


FIG.28 THE STATIC PRESSURE DISTRIBUTION ON BODY  
#6 AT  $M=5.1, \epsilon=3^\circ$

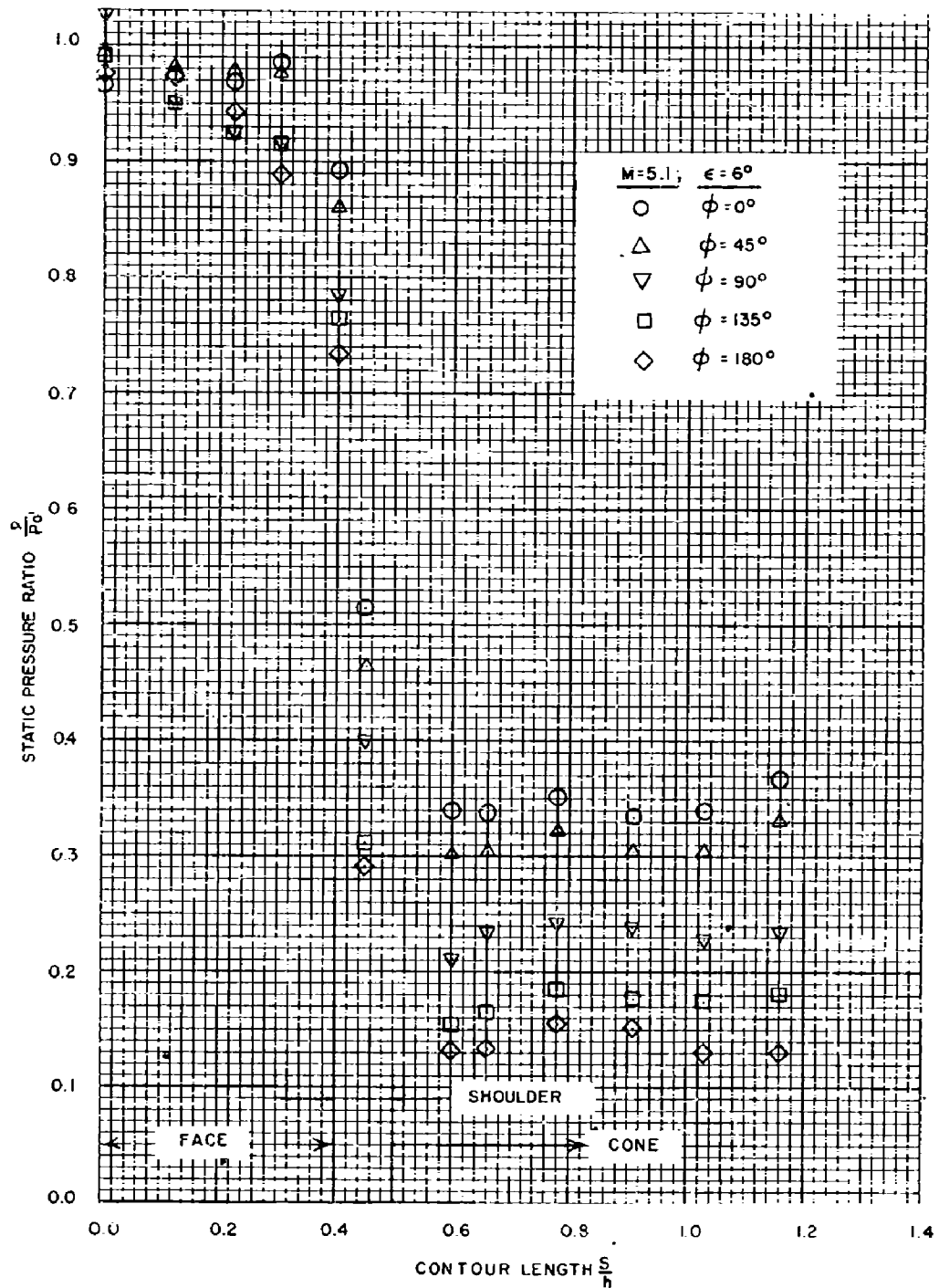


FIG. 29 THE STATIC PRESSURE DISTRIBUTION ON BODY #6 AT  $M=5.1, \epsilon=6^\circ$

NAVORD REPORT 5659

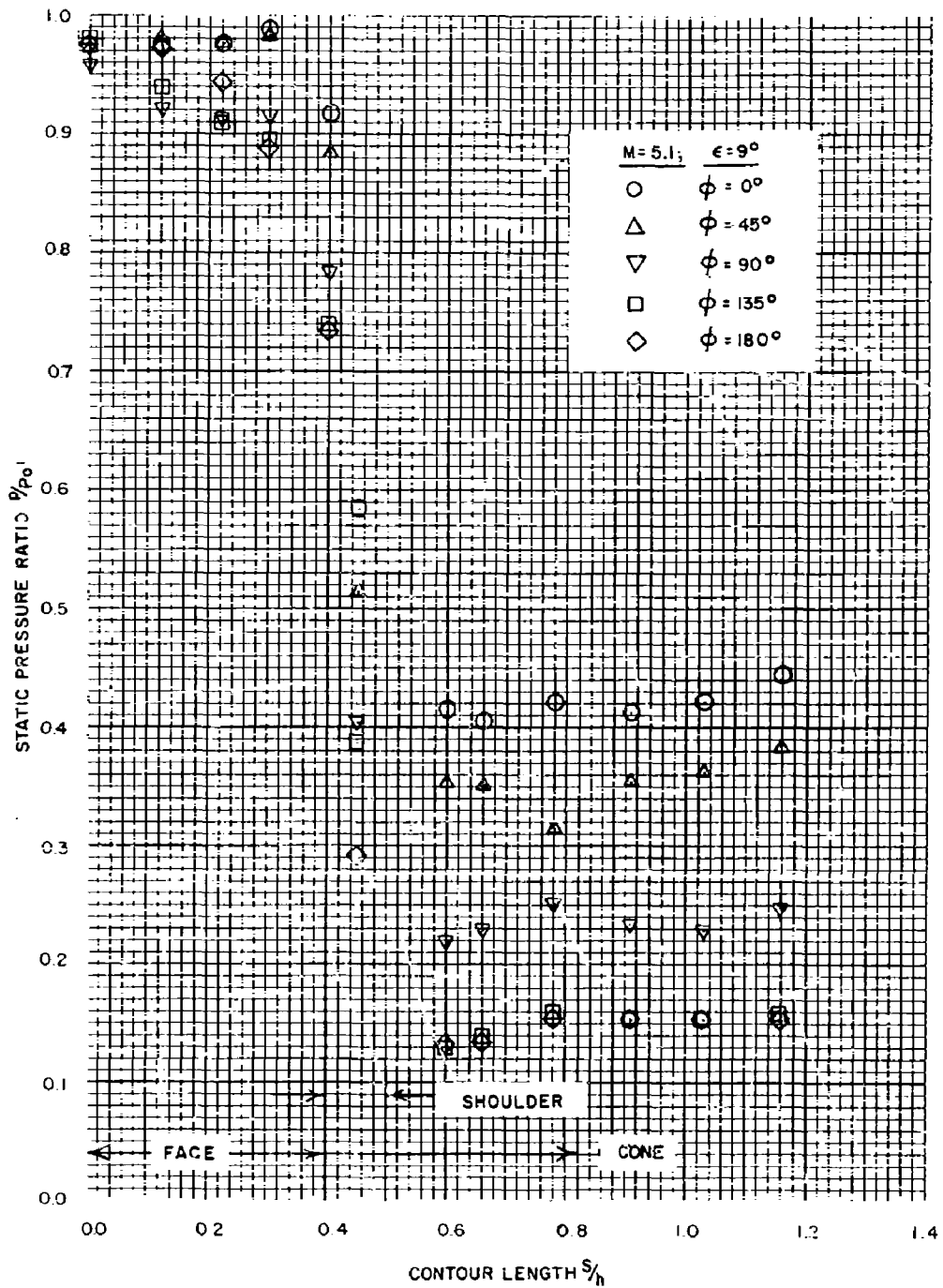


FIG.30 THE STATIC PRESSURE DISTRIBUTION ON BODY  
# 6 AT  $M=5.1, \epsilon=9^\circ$

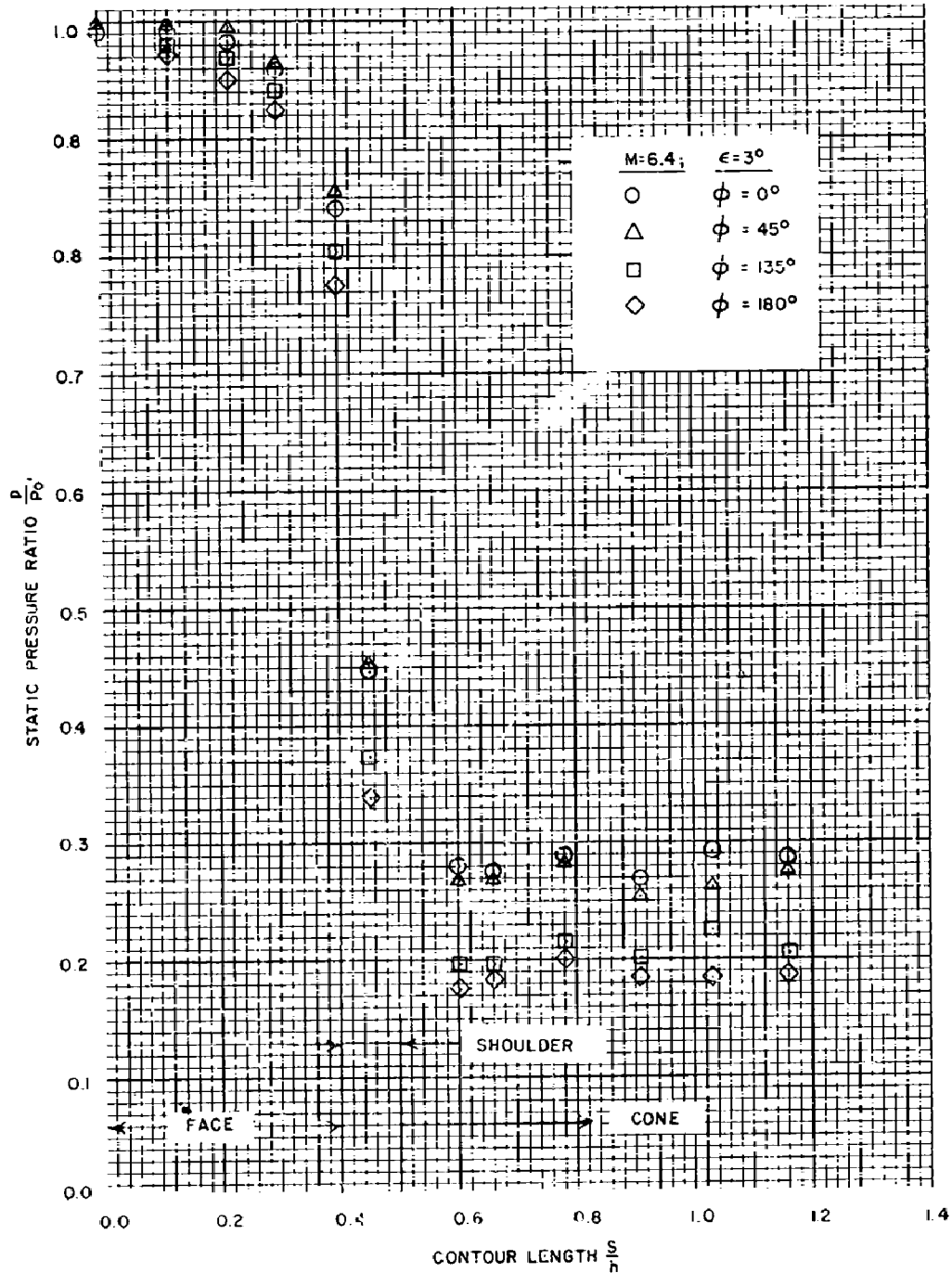


FIG. 31 THE STATIC PRESSURE DISTRIBUTION ON BODY #6 AT  $M=6.4, \epsilon=3^\circ$

# NAVORD REPORT 5659

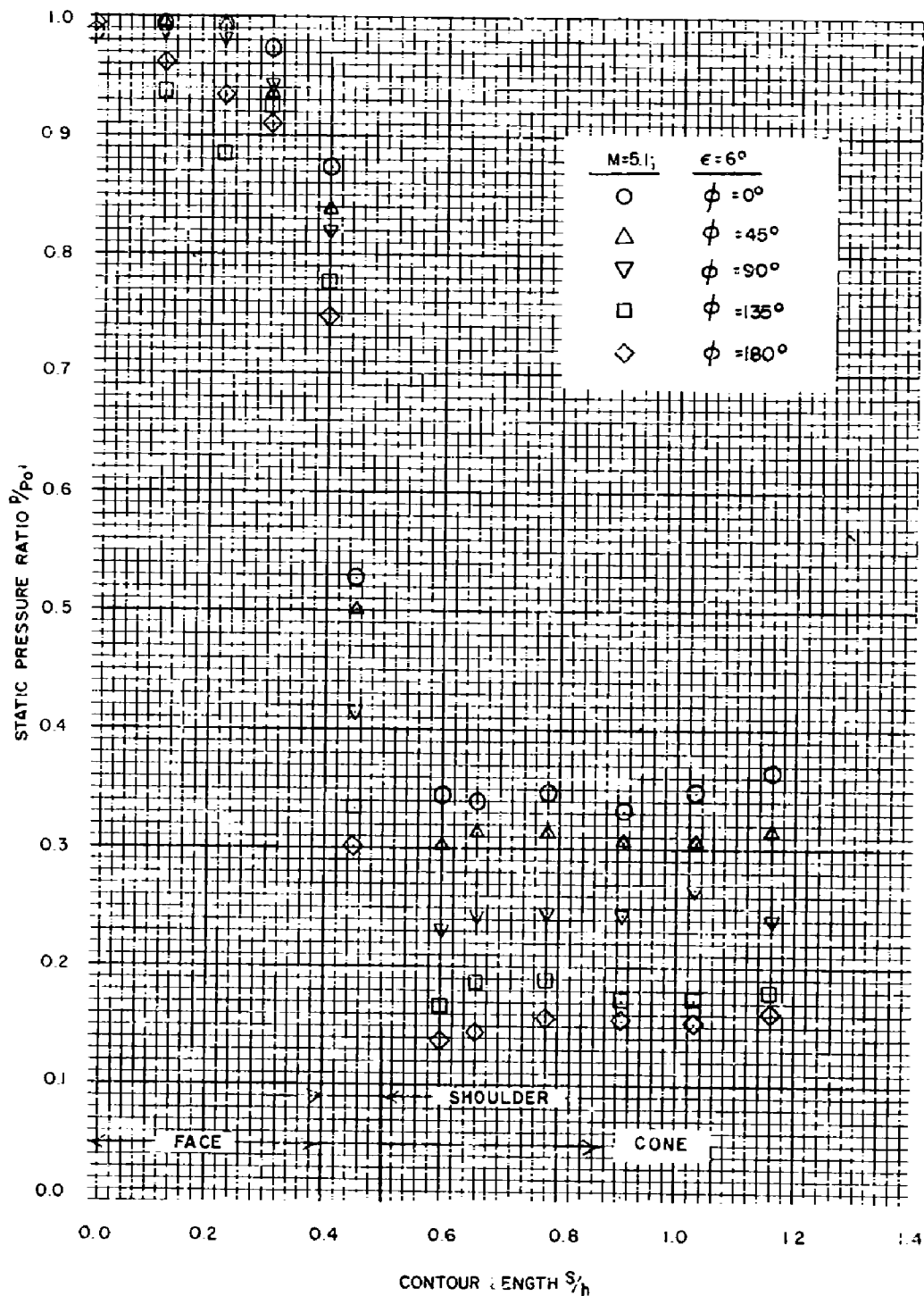


FIG.32 THE STATIC PRESSURE DISTRIBUTION ON BODY  
# 6 AT  $M=6.4, \epsilon=6^\circ$

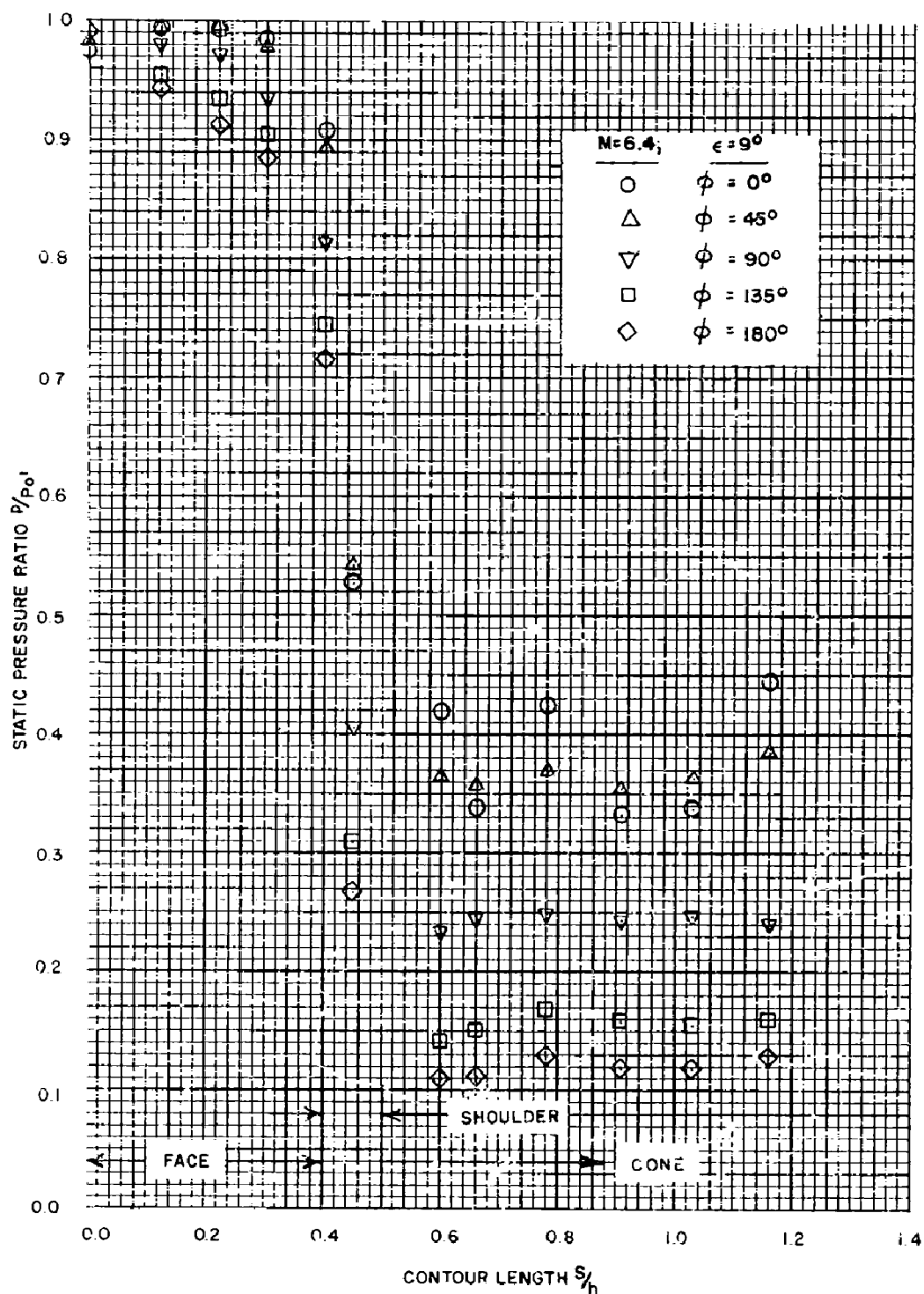


FIG. 33 THE STATIC PRESSURE DISTRIBUTION ON BODY #6 AT  $M=6.4, \epsilon=9^\circ$

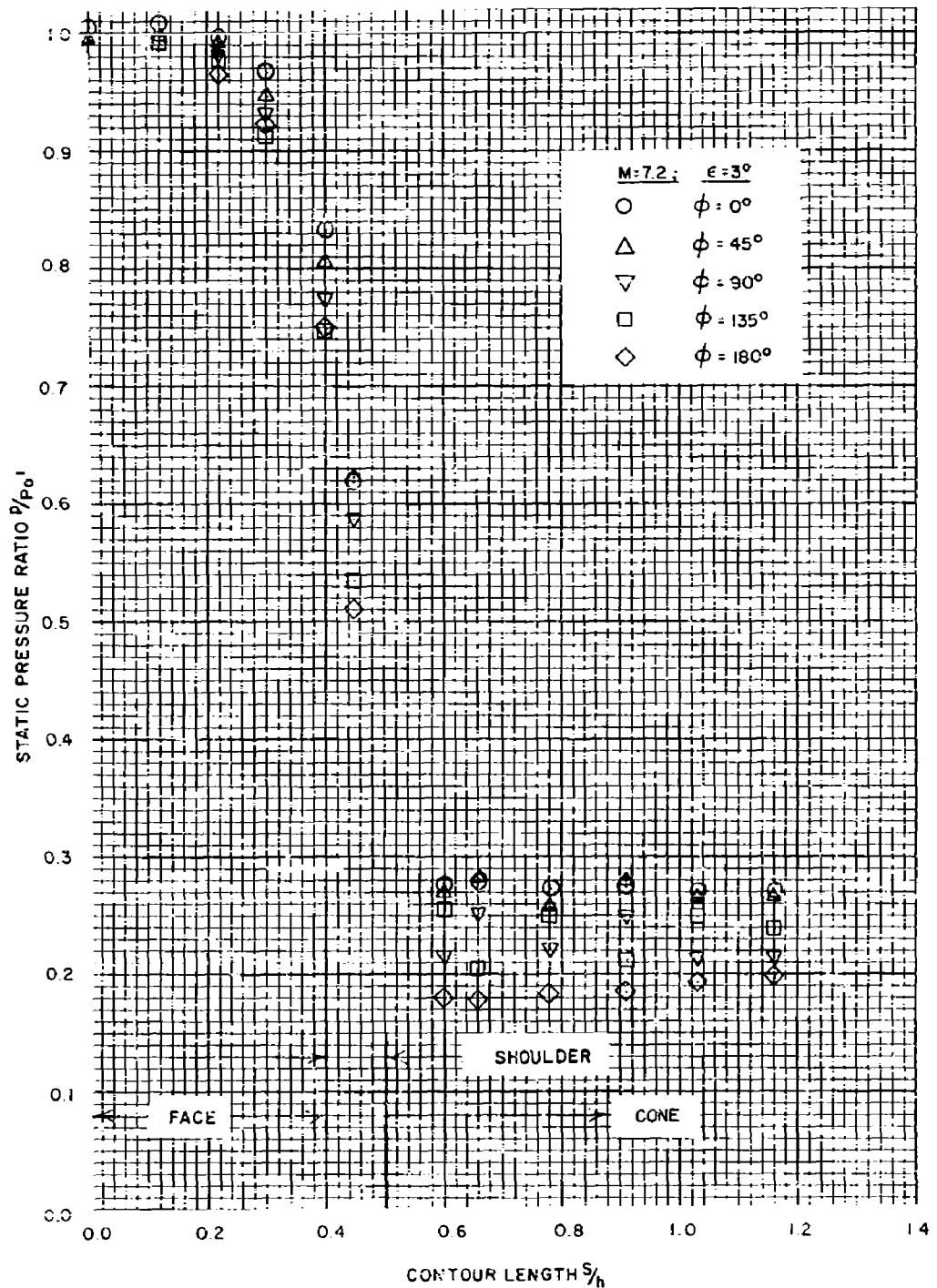


FIG.34 THE STATIC PRESSURE DISTRIBUTION ON BODY # 6 AT  $M=7.2, \epsilon=3^\circ$

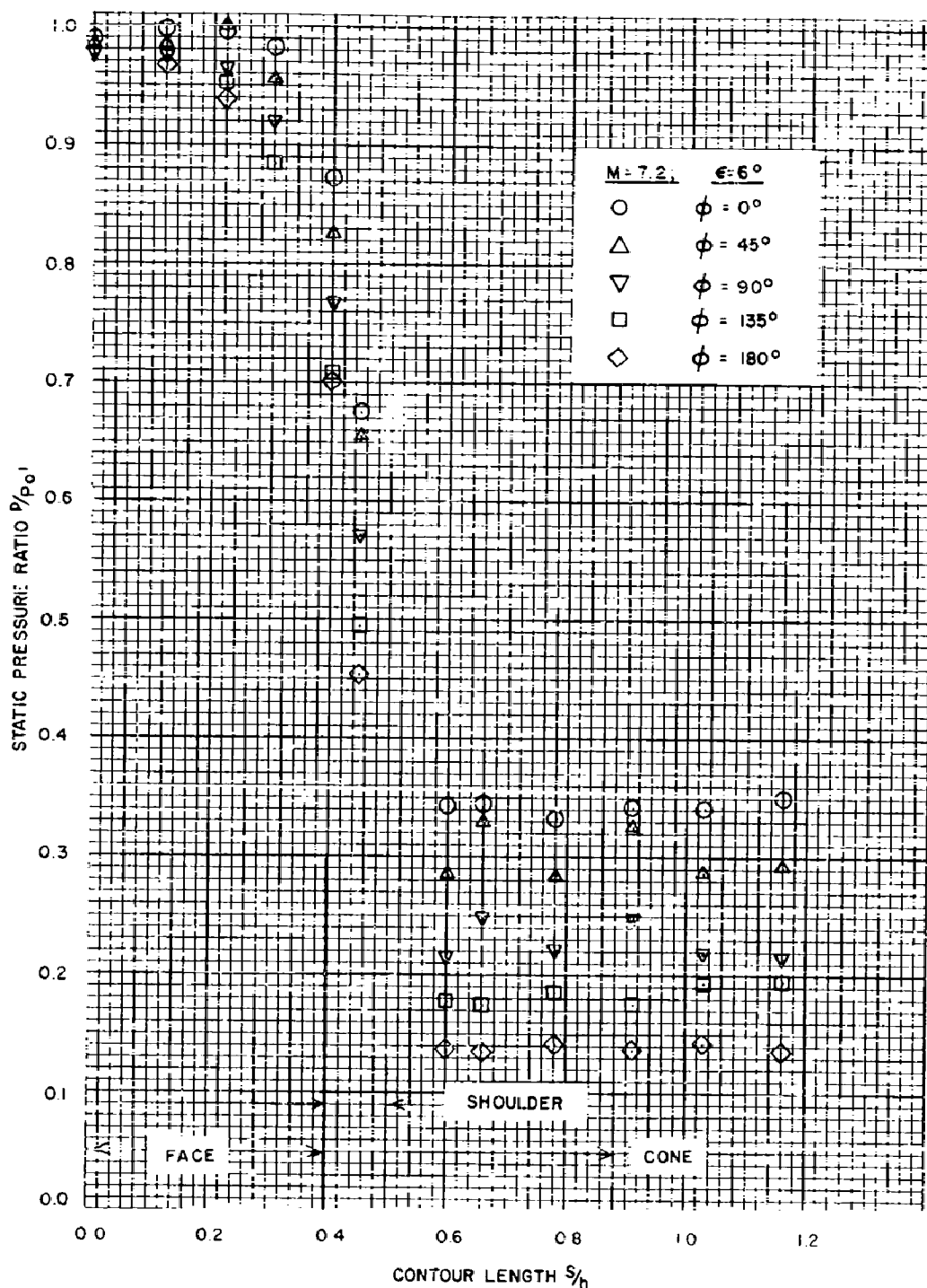


FIG. 35 THE STATIC PRESSURE DISTRIBUTION ON BODY #6 AT  $M=7.2$ ,  $\epsilon=6^\circ$

NAVORD REPORT 5659

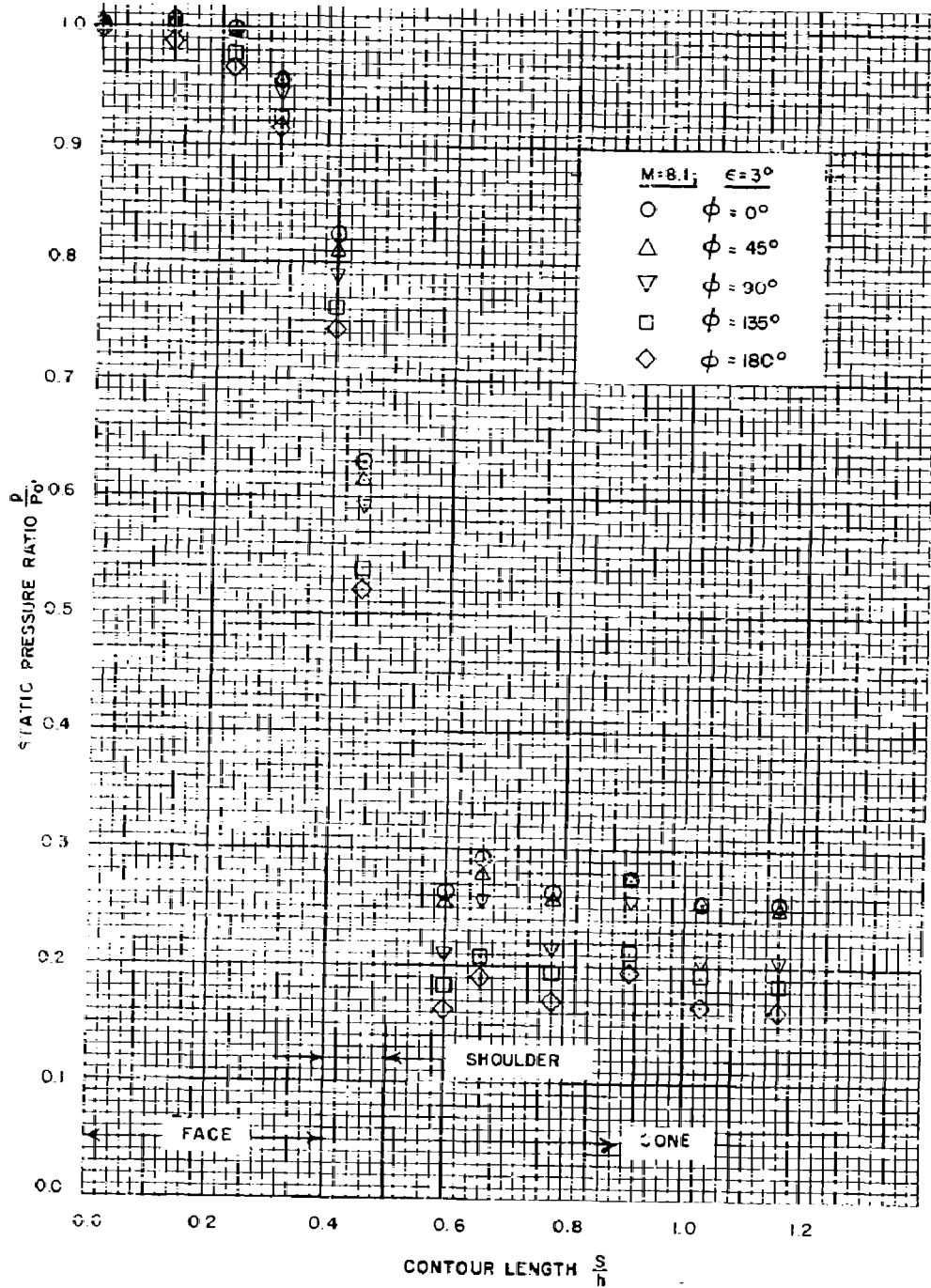


FIG. 36 THE STATIC PRESSURE DISTRIBUTION ON BODY #6 AT  $M=8.1, \epsilon=3^\circ$

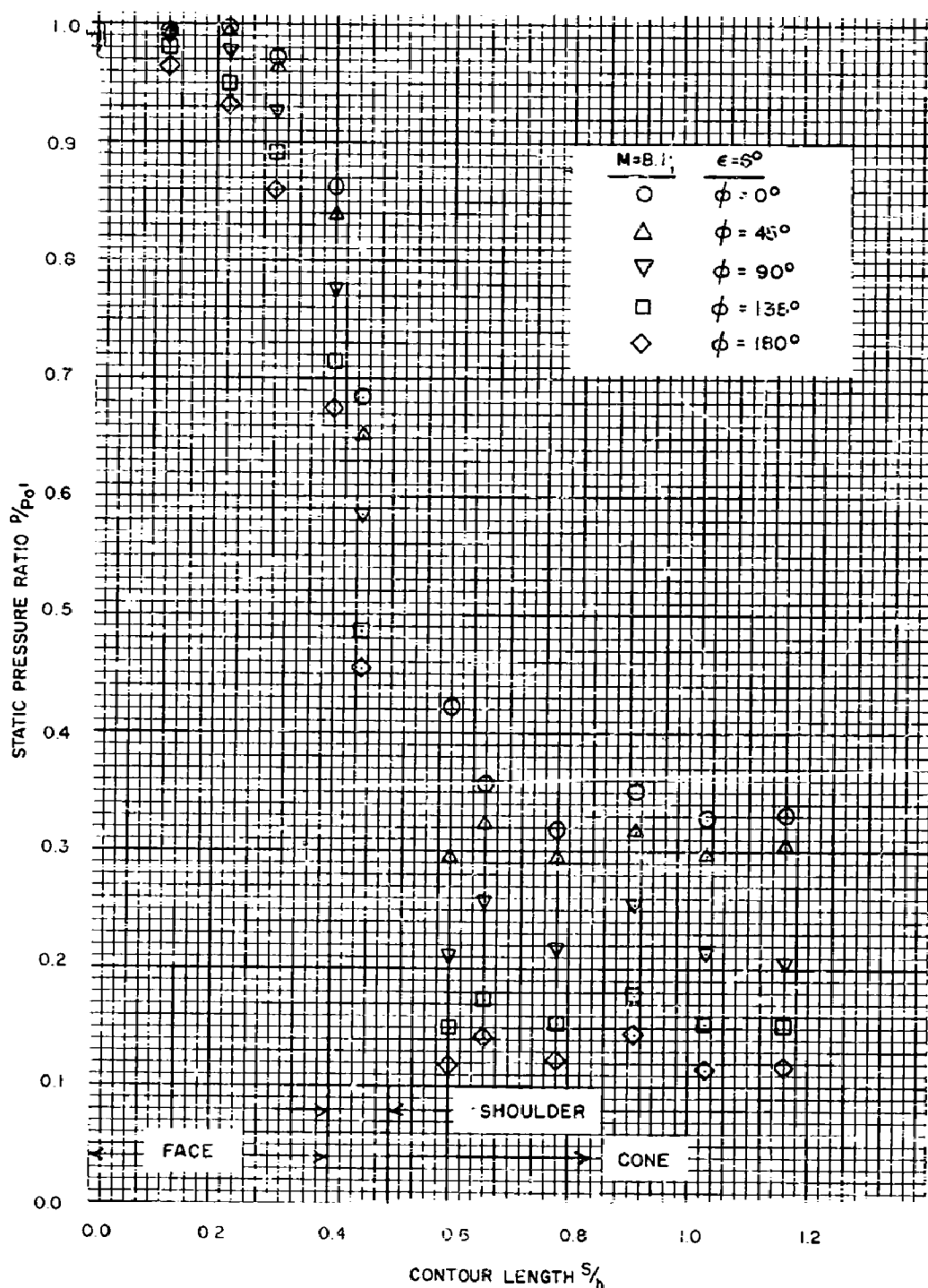


FIG.37 THE STATIC PRESSURE DISTRIBUTION ON BODY # 6

AT  $M=8.1$ ,  $\epsilon = 6^\circ$

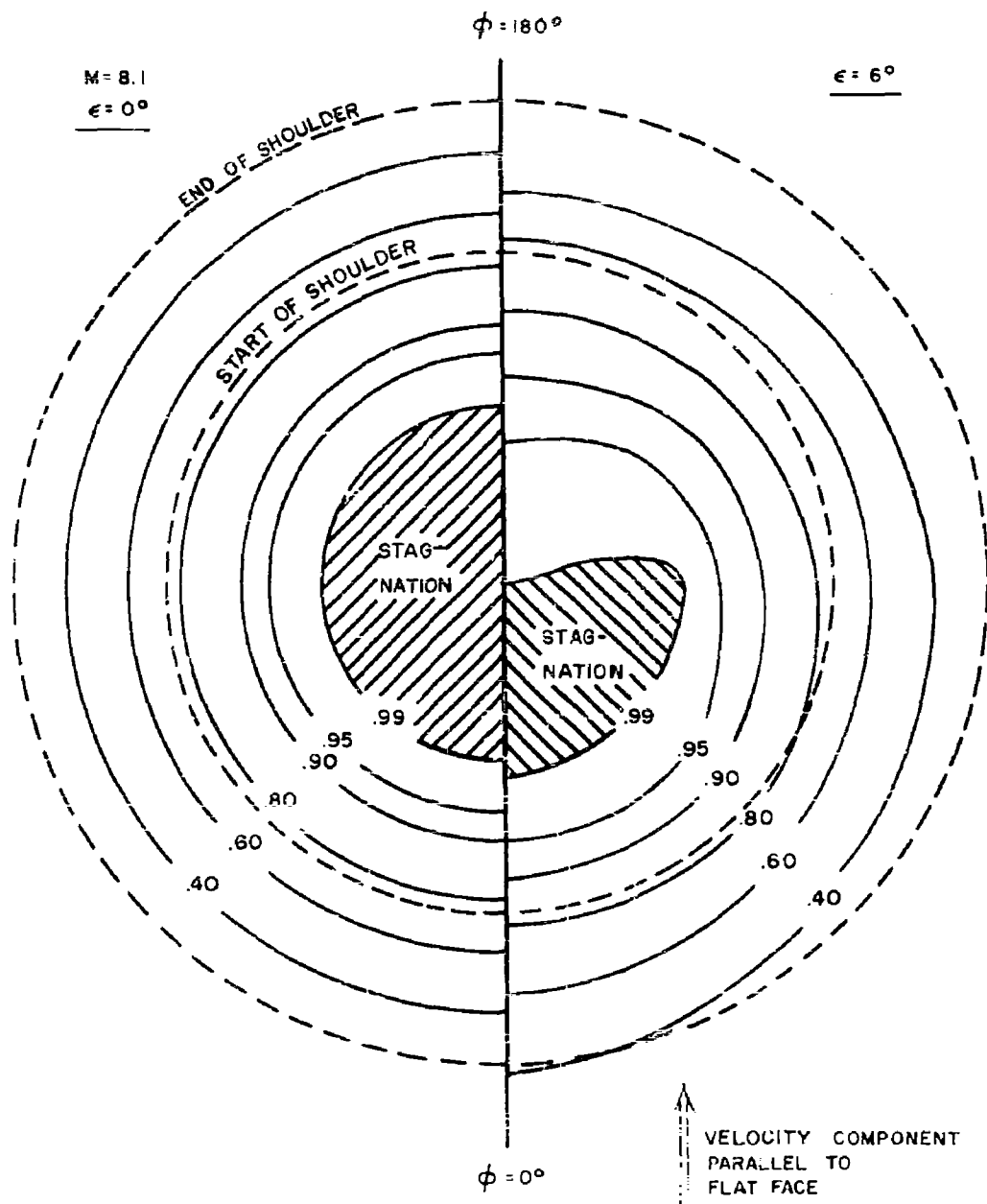


FIG. 38 PRESSURE CONTOURS ( $p/P_o'$ ) ON THE FACE AND SHOULDER OF BODY #6 AT  $M = 8.1$ ,  $\epsilon = 0$  &  $6^\circ$

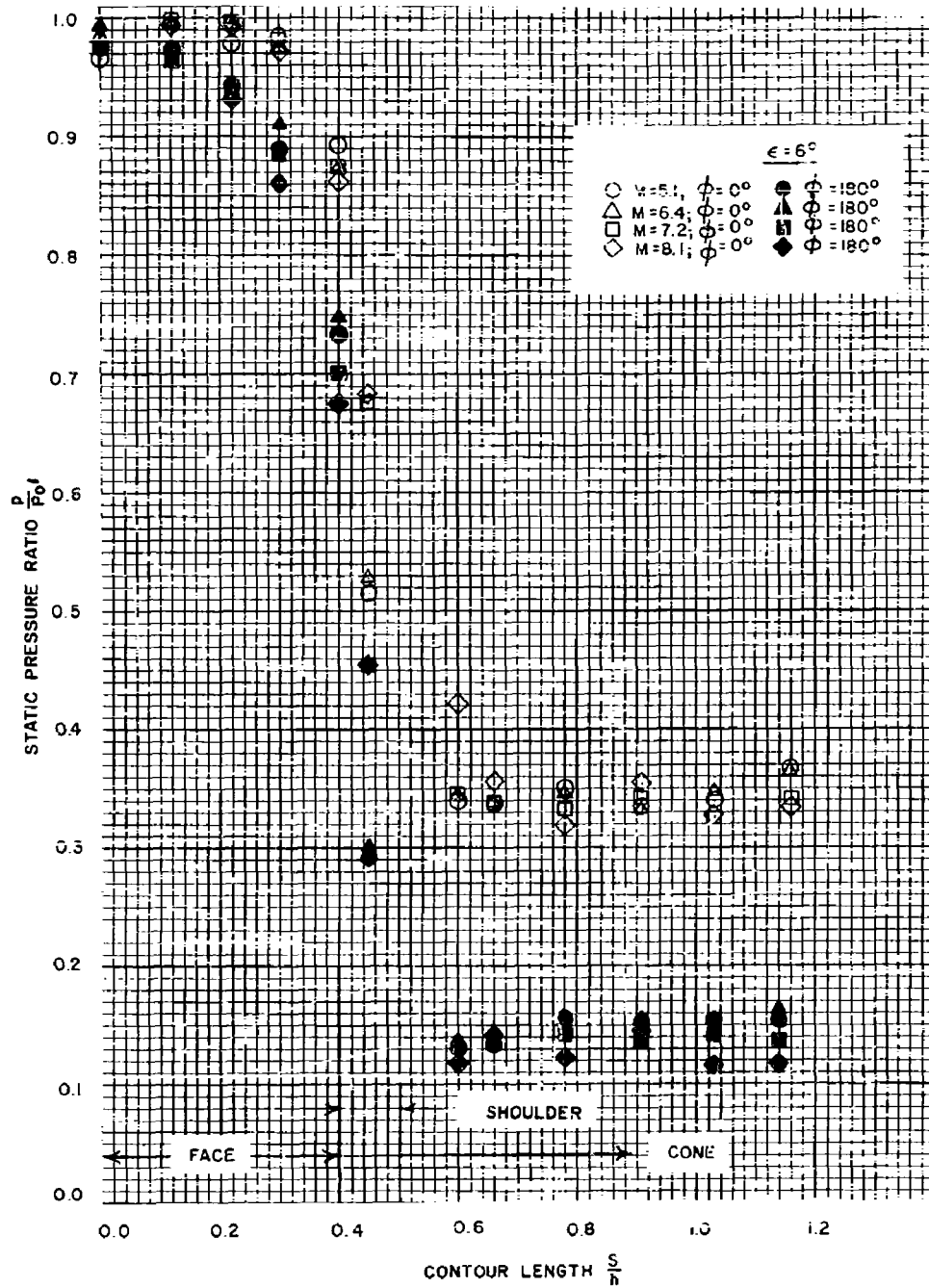


FIG. 39 THE EFFECT OF MACH NUMBER ON THE PRESSURE DISTRIBUTION ON BODY #6 AT  $\epsilon = 6^\circ$

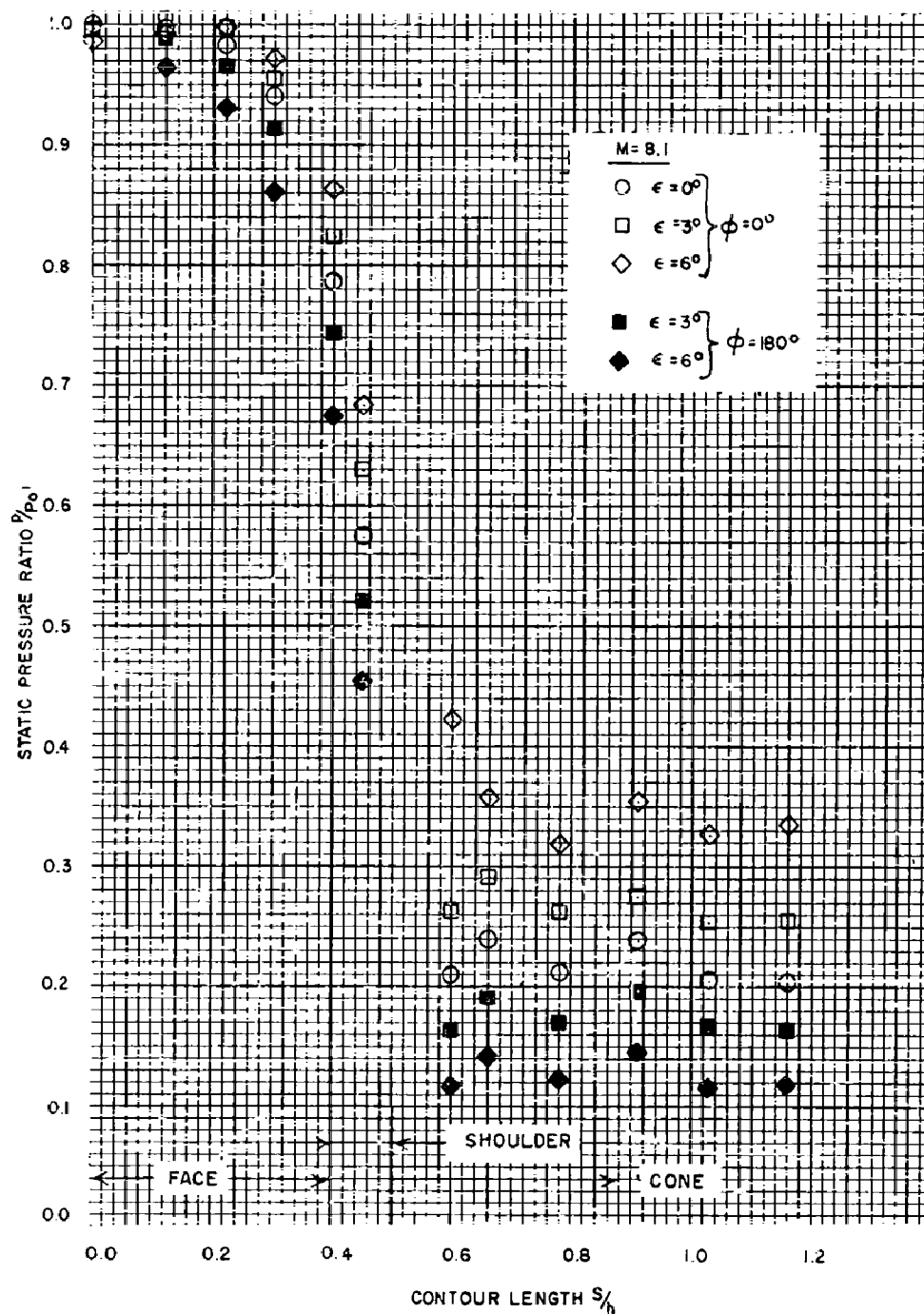


FIG.40 THE EFFECT OF YAW ON THE PRESSURE DISTRIBUTION ON BODY #6 AT  $M=8.1$



FIG. 41 SHADOWGRAPH OF BODY # 3 AT  $M=1.79$  WITH ROUGHNESS AT STAGNATION POINT

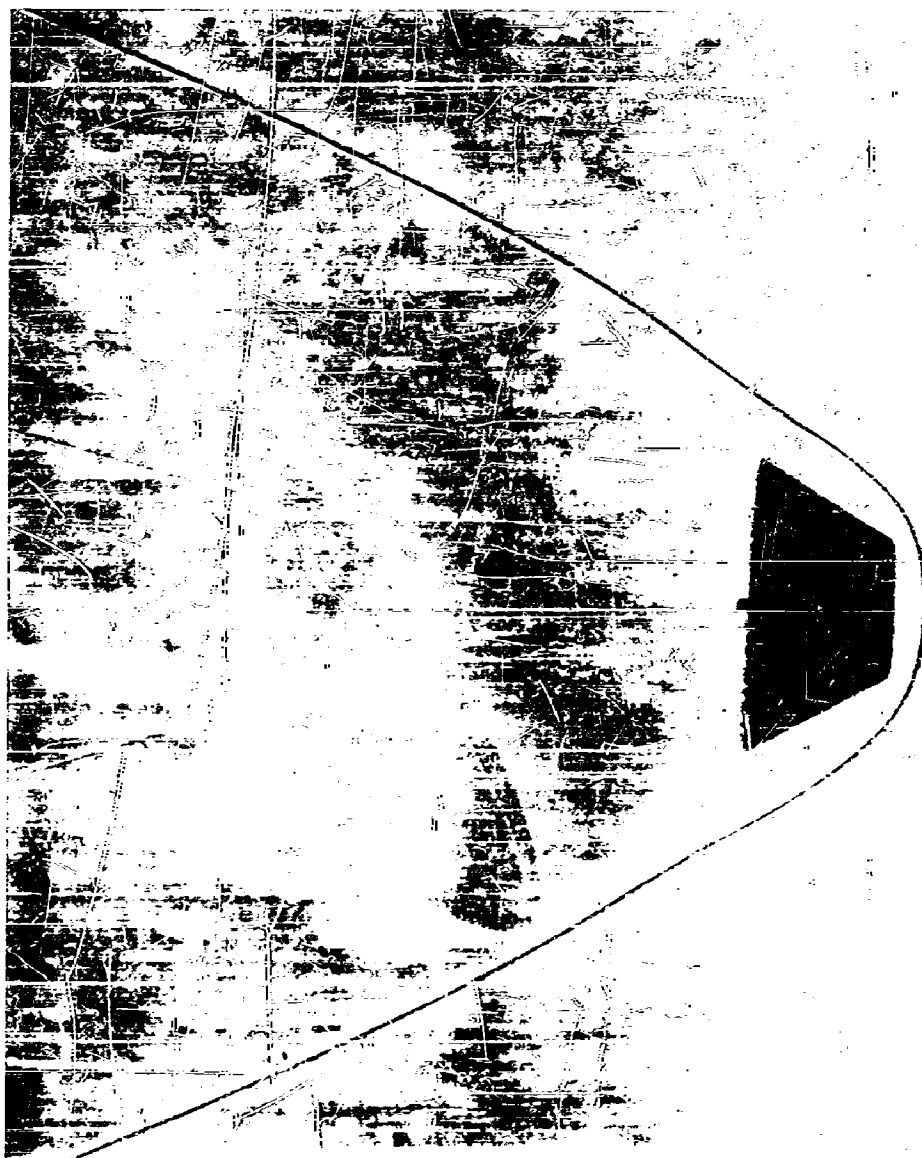


FIG. 42 SHADOWGRAPH OF BODY #7 AT  $M = 3.85$

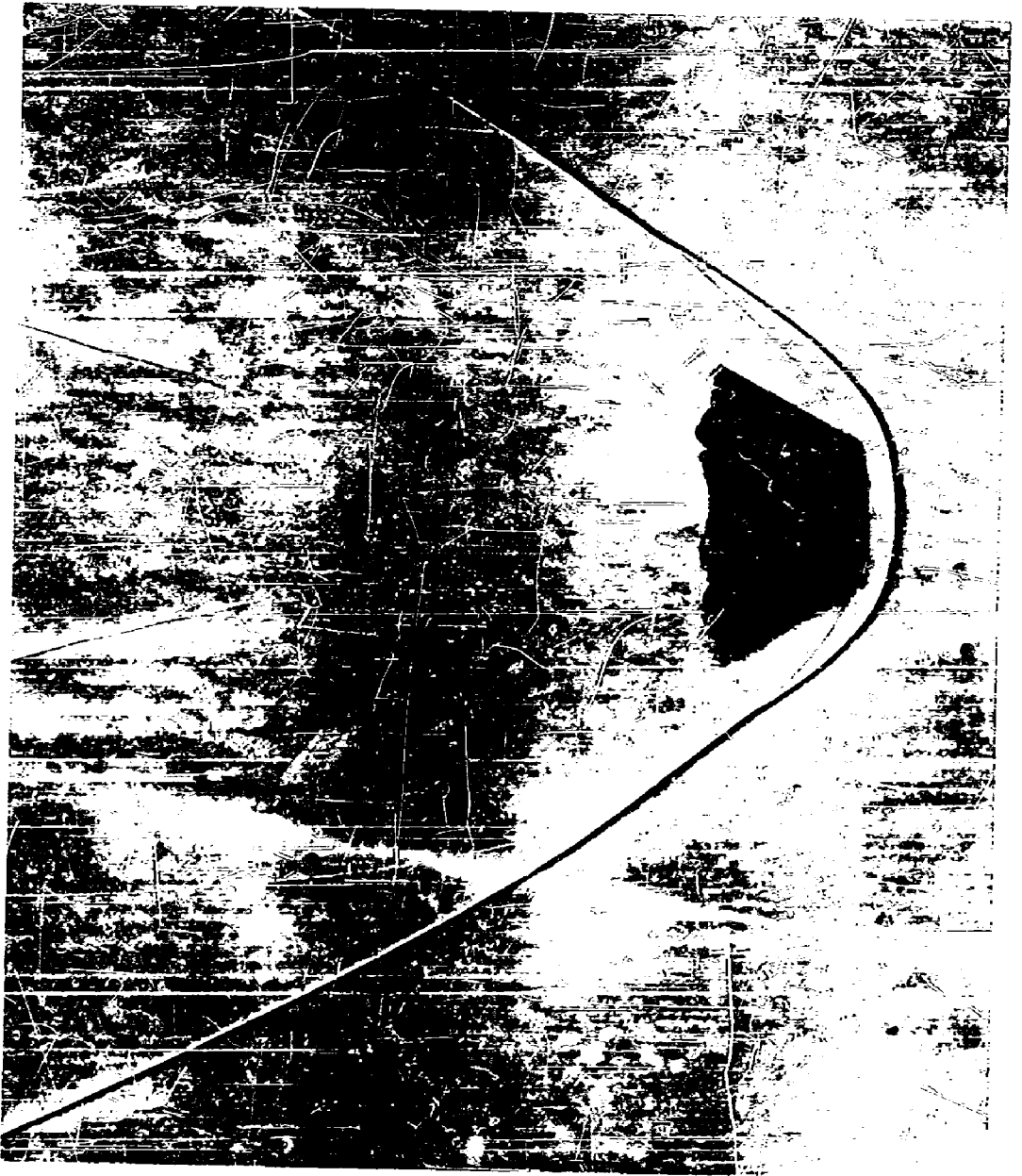


FIG. 43 SHADOWGRAPH OF BODY #7 AT  $M = 3.19$

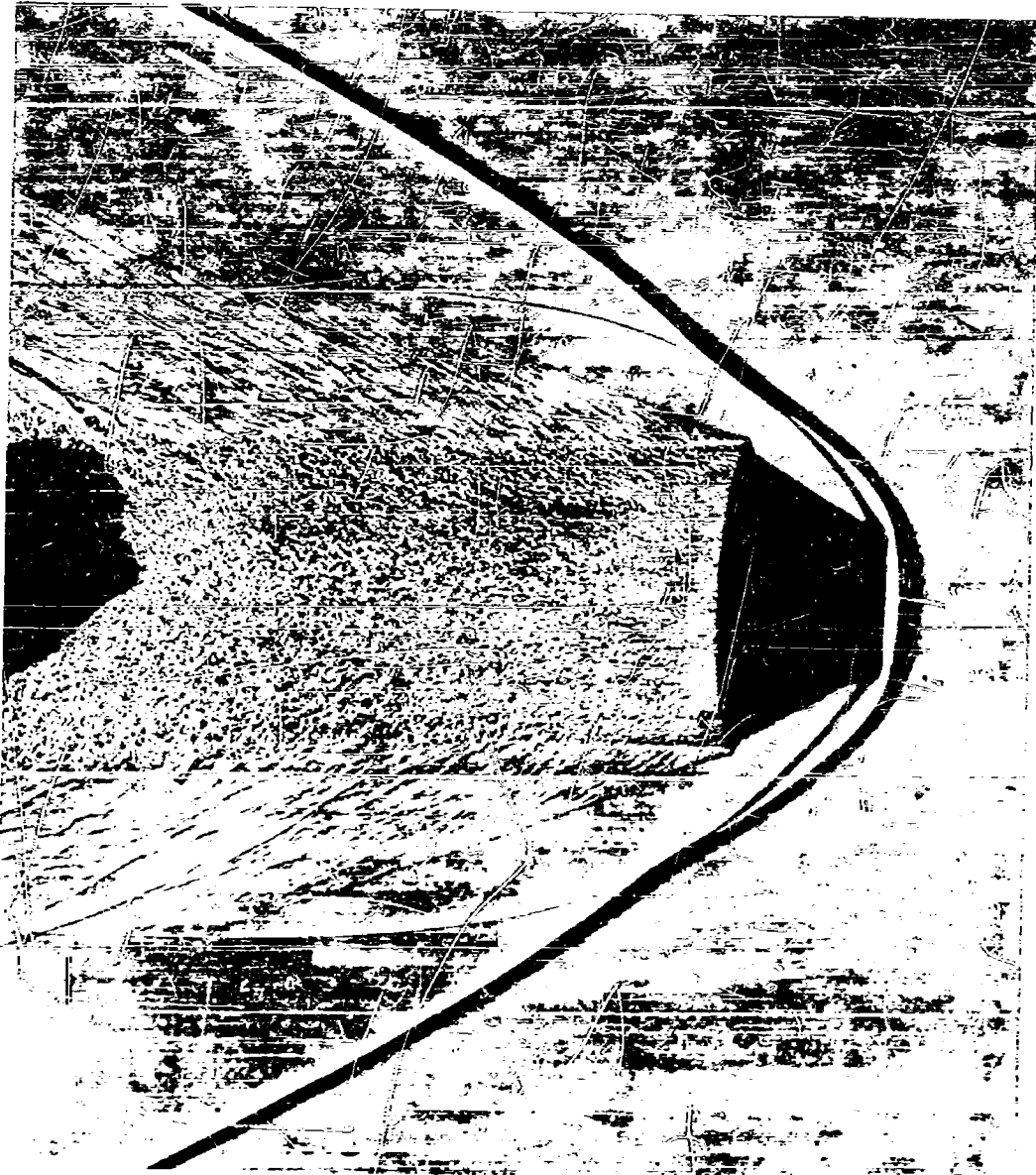


FIG. 44 SHADOWGRAPH OF BODY #7 AT  $M = 2.92$



FIG. 45 SHADOWGRAPH OF BODY #7 AT  $M = 2.78$

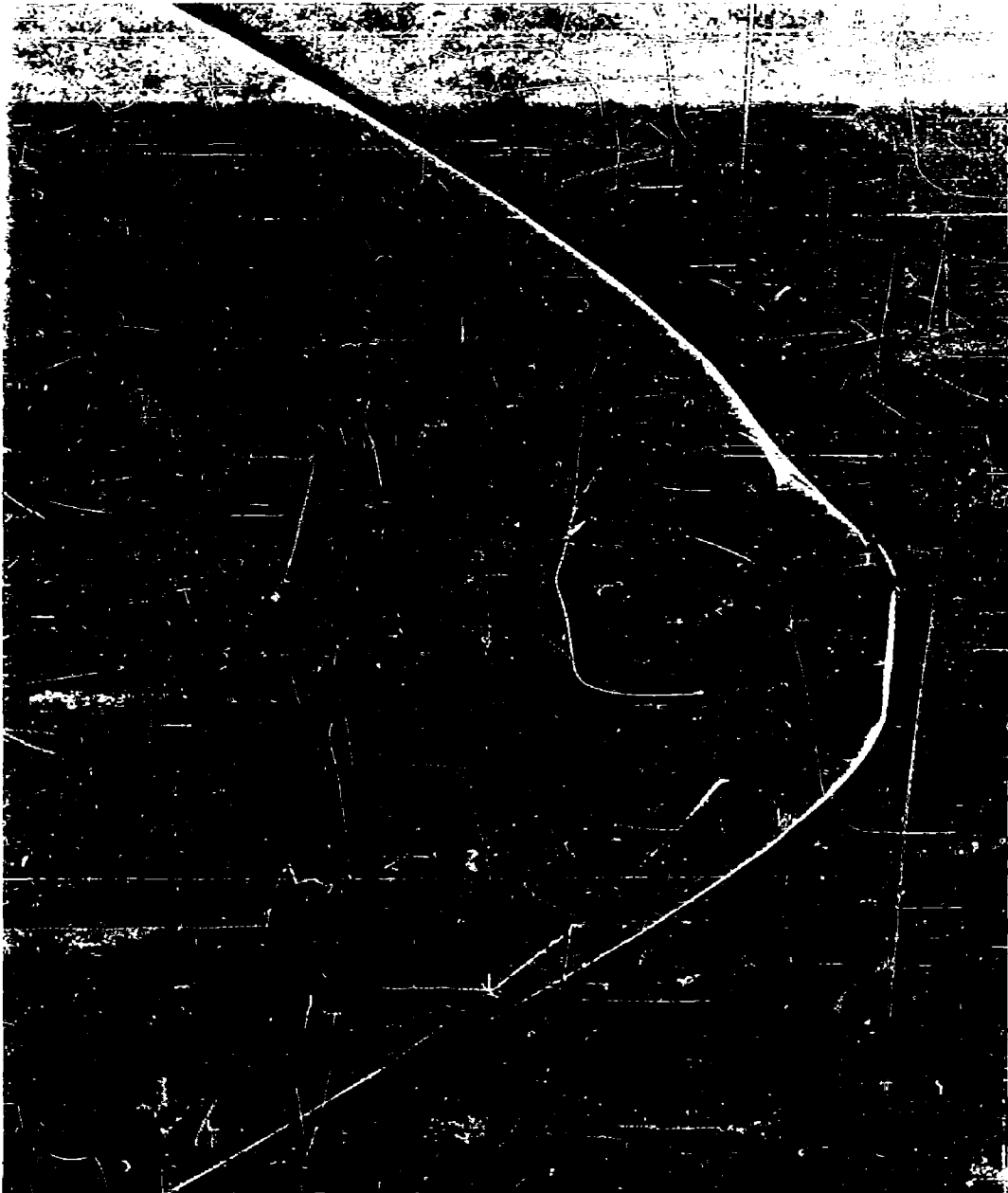


FIG. 46 SHADOWGRAPH OF BODY #7 AT  $M = 2.73$

# UNCLASSIFIED

# AD

# 156 190

Reproduced

## Armed Services Technical Information Agency

ARLINGTON HALL STATION; ARLINGTON 12 VIRGINIA

**NOTICE: WHEN GOVERNMENT OR OTHER DRAWINGS, SPECIFICATIONS OR OTHER DATA ARE USED FOR ANY PURPOSE OTHER THAN IN CONNECTION WITH A DEFINITELY RELATED GOVERNMENT PROCUREMENT OPERATION THE U. S. GOVERNMENT THEREBY INCURS NO RESPONSIBILITY, NOR ANY OBLIGATION WHATSOEVER; AND THE FACT THAT THE GOVERNMENT MAY HAVE FORMULATED, FURNISHED, OR IN ANY WAY SUPPLIED THE SAID DRAWINGS, SPECIFICATIONS, OR OTHER DATA IS NOT TO BE REGARDED BY IMPLICATION OR OTHERWISE AS IN ANY MANNER LICENSING THE HOLDER OR ANY OTHER PERSON OR CORPORATION, OR CONVEYING ANY RIGHTS OR PERMISSION TO MANUFACTURE, USE OR SELL ANY PATENTED INVENTION THAT MAY IN ANY WAY BE RELATED THERETO.**

# UNCLASSIFIED